THE UNIVERSITY *of* EDINBURGH

THE ASSESSMENT OF AORTIC STENOSIS USING MODERN NON-INVASIVE IMAGING TECHNIQUES

Dr Marc Richard Dweck BSc (hons) MBChB MRCP

A thesis presented for the degree of Doctor of Philosophy at the University of Edinburgh March 2012

To Carrie, Tom & Eva

ABSTRACT

Introduction. Aortic stenosis is characterised both by progressive narrowing of the valve and the hypertrophic response of the left ventricle. The purpose of this thesis was to study the contribution of inflammation and calcification to valve narrowing using Positron Emission and Computed Tomography (PET/CT) and to investigate the hypertrophic response using cardiovascular magnetic resonance (CMR).

Methods. *PET/CT studies.* Patients with aortic sclerosis and mild, moderate and severe stenosis were prospectively compared to matched control subjects. Aortic valve severity was determined by echocardiography. Calcification and inflammation in the aortic valve and coronary arteries were assessed by sodium 18-fluoride (18F-NaF) and 18-fluorodeoxyglucose (18F-FDG) uptake using PET.

CMR studies. Consecutive patients with moderate or severe aortic stenosis undergoing CMR were enrolled into a registry. Patients who received gadolinium contrast were categorised into absent, mid-wall or infarct patterns of late gadolinium enhancement (LGE) by blinded independent observers. Patients follow-up was completed using patient questionnaires, source record data and the National Strategic Tracing Scheme. After excluding those patients with concomitant triggers to LV remodeling, the extent and patterns of hypertrophy were investigated based upon measurements of indexed LV mass, indexed LV volume and the relative wall mass.

Results. *PET/CT studies.* 121 subjects (20 controls; 20 aortic sclerosis; 25 mild, 33 moderate and 23 severe aortic stenosis) were studied. Quantification of tracer uptake within the valve demonstrated excellent inter-observer reproducibility with no biases and limits of agreement of ±0.21 (18F-NaF) and ±0.13 (18F-FDG) for maximum tissue-to-background ratios (TBR). Activity of both tracers was higher in patients with aortic stenosis than control subjects (18F-NaF: 2.87±0.82 *vs* 1.55±0.17; 18F-FDG: 1.58±0.21 *vs* 1.30±0.13; both P<0.001). 18F-NaF uptake displayed a progressive rise with valve severity (r^2=0.540, P<0.001) with a more modest increase observed for 18F-FDG (r^2=0.218; P<0.001). Amongst patients with aortic stenosis, 91% had increased 18F-NaF (>1.97) and 35% increased 18F-FDG (>1.63) uptake. Increased 18F-NaF uptake was also observed in the coronary arteries in a subset of patients with atherosclerosis. These patients (n=40) had higher rates of prior cardiovascular events (p=0.016) and angina (p=0.023), and higher Framingham risk scores (p=0.011).

CMR studies. 143 patients (aged 68±14 years; 97 male) were followed up for 2.0±1.4 years and 27 died. Compared to those with no LGE (n=49), univariate analysis revealed that patients with mid-wall fibrosis (n=54) had an eight-fold increase in all-cause mortality despite similar aortic stenosis severity and coronary artery disease burden. Patients with an infarct pattern (n=40) had a six-fold increase. Mid-wall fibrosis (HR 5.35 [95% CI 1.16-24.56]; P=0.03) emerged as an independent predictor of all cause mortality by multivariate analysis. The pattern of LV remodelling was studied in 91 patients (61±21 years; 57 male) and displayed wide variation comprising normal ventricular geometry (n=11), concentric remodelling (n=11), asymmetric remodelling (n=11), concentric hypertrophy (n=34), asymmetric hypertrophy (n=14) and LV decompensation (n=10). The magnitude of the hypertrophic response was unrelated to the severity of aortic valve narrowing.

Conclusions. Modern imaging techniques have provided important insights in to the pathology underlying aortic stenosis and suggest that valvular calcification and myocardial fibrosis have a key role. Both represent important potential targets for future therapeutic interventions.

CONTENTS

Figures Index

Tables Index

DECLARATION

This thesis represents research undertaken in the Centre for Cardiovascular Sciences, University of Edinburgh, the Clinical Research Imaging Centre, the Royal Infirmary of Edinburgh, and the Cardiovascular Magnetic Resonance Unit The Royal Brompton Hospital, London between March 2009 and March 2012.

The study was sponsored by a British Heart Foundation Clinical PhD Training Fellowship FS/10/026 and an extension to that fellowship FS/10/026. All PET/CT scans were performed at the Clinical Research Imaging Centre, University of Edinburgh and I was personally involved in the recruitment, acquisition and analysis for all scans. Cardiovascular Magnetic Resonance scans in Chapters 5 & 6 were performed at the Royal Brompton Hospital between 2003 and 2009 as part of an ongoing and successful collaboration. I was personally involved with interpretation and analysis of all these scans and in the collection of all clinical and follow-up data. I am extremely grateful for the assistance in this work provided by my colleagues Dr Sanjiv Joshi and Dr Timothy Murigu under the supervision of Dr Sanjay Prasad.

Chapters 1, 3, 4, and 5 have all been published in major peer-reviewed scientific journals. I have sought and obtained copyright permission for inclusion of the printed journal manuscripts within this thesis. This thesis has not been accepted in any previous applications for a degree and all sources of information have been acknowledged. All studies were undertaken in accordance with Declaration of Helsinki of the World Medical Association and the regulations of the South East Scotland Ethics Committee and the local ethics committee of the Royal Brompton Hospital.

Marc Dweck 13th February 2012

ACKNOWLEDGEMENTS

The research was conducted under the supervision of Professor David Newby (Professor of Cardiology and Consultant Cardiologist) and Dr Nicholas Boon (Honorary Reader and Consultant Cardiologist) at the University of Edinburgh. I am extremely grateful for their vision in establishing the project and their constant guidance and support both on a professional and personal level throughout my thesis. They have inspired me to pursue an academic career and I am very much looking forward to working with them both in the future.

In addition I would like to thank Dr James Rudd (University of Cambridge) who trained me in the conduct of vascular Positron Emission Tomography and provided a constant source of advice and guidance throughout the project. Without his expertise we would not have been able to perform a vascular PET study of this nature in Edinburgh. Indeed great credit should go to the Clinical Research Imaging Centre, for delivering this project, which was the first of its kind at this new institution. In particular I would like to thank the centre's director Prof Edwin van Beek in addition to Dr Alison Fletcher and Hamish Richardson for their expertise and guidance through the somewhat daunting world of PET physics, David Brian (head radiographer) for accommodating the research studies, and all the other radiographers in the department for their expertise in performing the scans.

I would like to thank Audrey White for her dedication in performing all of the echocardiograms in Edinburgh often arranged at short notice and the Clinical Research Facility at the Royal Infirmary of Edinburgh for providing us with the facilities to do so.

For the cardiovascular magnetic resonance study I would like to thank the CMR unit at the Royal Brompton Hospital for the opportunity to use their aortic stenosis registry to study the prognostic role of late gadolinium enhancement in this condition and for training me in cardiovascular magnetic resonance as part of my fellowship. In particular I would like to thank Prof Dudley Pennell for facilitating that fellowship and Dr Sanjay Prasad for helping to supervise my CMR research. I am also indebted to many of the doctors and fellows in the department for their help in data collection in particular Dr Sanjiv Joshi, Dr Timothy Murigu, Dr Ankur Gulati and Dr Andrew Jabbour. Without their hard work, tenacity and friendship I would not have been able to complete this work especially given the geographical distance separating our institutions. Also I am indebted to Winston Banya for his help with the statistical analysis of these data.

Most important of all I am indebted to my wife Caroline and my family whose support, understanding and love have provided me with countless opportunities in life and allowed me to complete this thesis.

Abbreviations

18F-FDG	18F-fluorodeoxyglycose
18F-NaF	18F-sodium fluoride
ACE	Angiotensin converting enzyme
ARB	Aldosterone receptor blocker
AS	Aortic stenosis
BMI	Body mass index
BMP	Bone morphogenic protein
CABG	Coronary artery bypass graft
CAC	Coronary artery calcium scoring
CAD	Coronary artery Disease
CHD	Coronary heart disease
CMR	Cardiovascular magnetic resonance
CT	Computed tomography
CVA	Cerebrovascular accident
CVD	Cardiovascular disease
DTPA	Diethylentriamene pentaacetate
HCM	Hypertrophic cardiomyopathy
ICC	Intra-class correlation coefficient
Il	Interleukin
LDL	Low density lipoprotein
LVEDV	Left ventricular end-diastolic volume
LVH	Left ventricular hypertrophy
MACE	Major adverse cardiovascular events
MMP	Matrix metalloproteinases
MI	Myocardial infarction
MRI	Magnetic resonance Imaging
PCI	Percutaneous coronary intervention
OPG	Osteoprotegerin
PET/CT	Combined positron emission tomography and computed tomography
RANK	Receptor activator of nuclear factor kappa B
ROI	Region of interest
SUV	Standard uptake value
TIA	Transient ischemic attack
TBR	Tissue-to-background ratio
TGF	Transforming growth factor
TIMP	Tissue inhibitor of metalloproteinases
TNF	Tumor necrosis factor
TGF	Transforming growth factor
VIC	Valve interstitial cells

Introduction

1.0 OVERVIEW

Calcific aortic stenosis (AS) is the most common form of valve disease in the western world and represents a major healthcare burden. Over the last decade, the number of aortic valve replacements performed in the United States of America has doubled and, with an increasingly elderly population, the prevalence of AS is likely to double again in the next 20 years.[1] However, the underlying pathophysiology of AS remains incompletely defined, and there are currently no effective medical treatments capable of altering its course. Furthermore we lack reliable markers that can predict disease progression, the future need for surgery, or mortality. There is therefore a pressing need to re-evaluate the underlying pathophysiological processes involved.[2]

Aortic stenosis is characterized by progressive narrowing of the aortic valve that increases the pressure afterload on the left ventricle. Myocytes enlarge and wall thickness increases in a hypertrophic response that initially restores wall stress but ultimately proves maladaptive. The rate at which patients with aortic stenosis move towards symptoms, adverse events and the need for surgery is determined both by the severity of the valve narrowing and by the myocardial hypertrophic response.[3, 4] Both processes are of clinical importance and, whilst linked, they are under the influence of different pathological factors.

With advances in technology and motion correction, modern non-invasive imaging techniques such as cardiovascular magnetic resonance (CMR) and positron emission tomography (PET) have become applicable to the heart. This has afforded the opportunity to improve our understanding of the

pathogenesis underlying aortic stenosis in a non-invasive manner. Specifically combined PET and computed tomography (PET/CT) allow processes such as inflammation and calcification to be investigated within small anatomical structures such as the aortic valve, whilst cardiovascular magnetic resonance (CMR) allows for the assessment of left ventricular remodelling and for the identification of replacement myocardial fibrosis.

The purpose of this thesis was to use these imaging techniques to gain insights in to pathophysiology of aortic stenosis

1.1 NARROWING OF THE AORTIC VALVE

ANATOMY OF THE NORMAL VALVE

Normal aortic valves are made up of three cusps (Figure 1.1), the arrangement of which results in even distribution of mechanical stress to the valve ring and the aorta.[5] Each cusp is <1 mm thick and appears smooth, thin and opalescent, with very few cells and the following clearly defined tissue layers. On the aortic and ventricular aspects of the valve is the endothelium, which is continuous with that of the aortic endothelium and left ventricular endocardium. Moving into the valve, the fibrosa consists of fibrous tissue with fibroblasts and collagen fibers arranged concentrically. The ventricularis on the ventricular side of the leaflet is composed of elastin rich fibers arranged radially, perpendicular to the collagen fibers in the fibrosa.[6] A further layer, the spongiosa, can be found at the base of the valve between the fibrosa and the ventricularis. It is a layer of loose connective tissue containing mucopolysaccharides, mesenchymal cells and fibroblasts, whose function is to resist compressive forces within the cusps (Figure 1.1). At their base the valve leaflets are attached to a dense collagenous network, called the annulus, which facilitates their attachment to the aortic root and the dissipation of mechanical force (Figure 1.1).

Figure 1.1 Normal structure of the tri-leaflet aortic valve

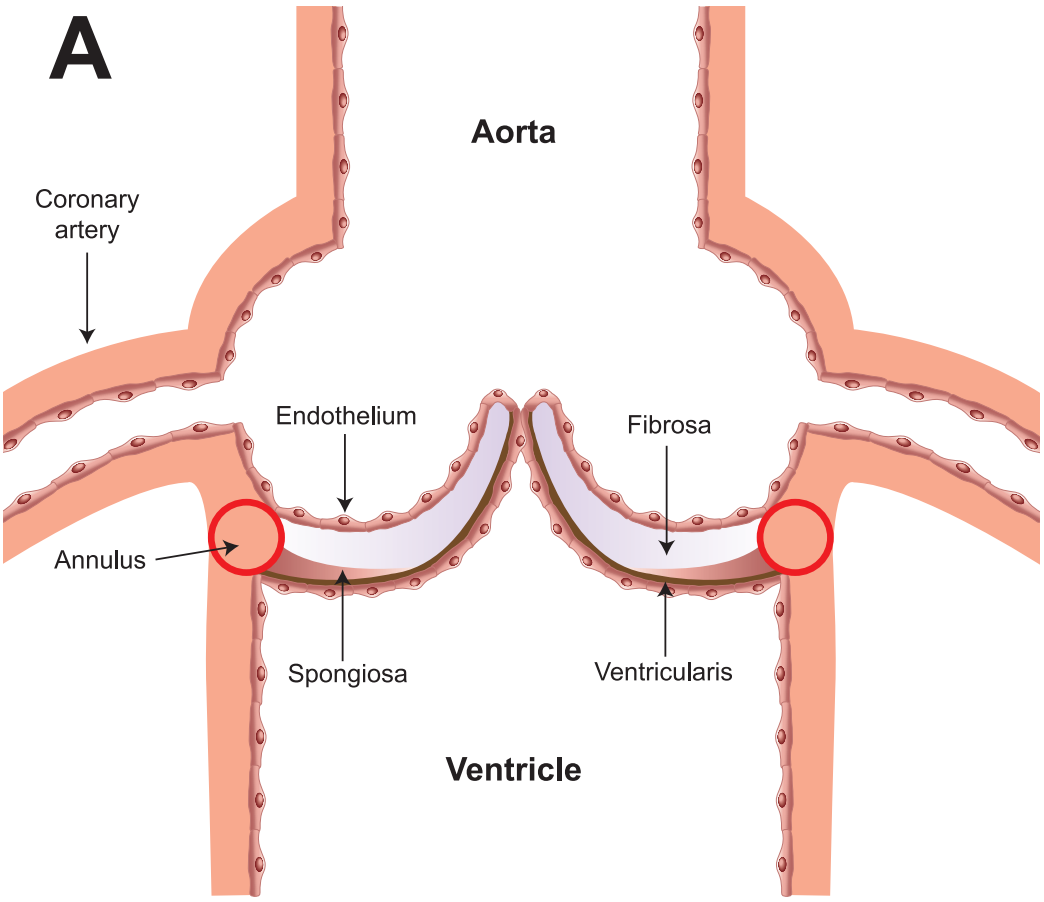

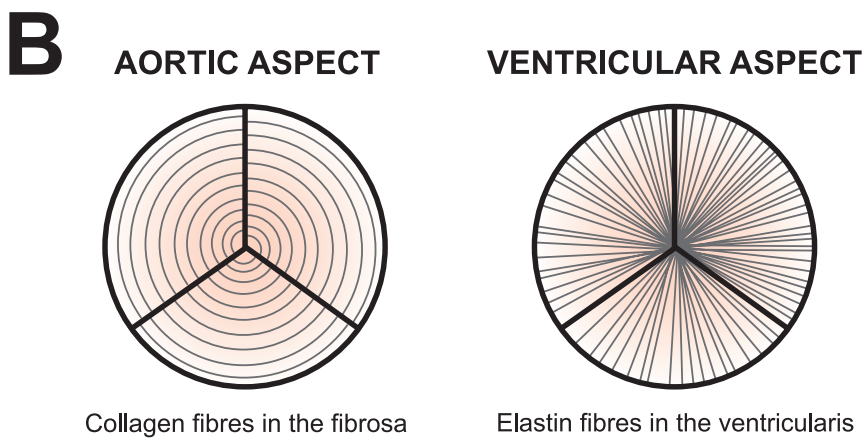

A) Long-axis view of the aortic valve showing the left and right coronary cusps. The valve cusps have a four-layered structure. On the aortic aspect of the valve the endothelium is continuous with that of the aorta and the coronary arteries, which arise above the valve in the coronary sinuses. Moving towards the ventricular aspect of the valve is the fibrosa, which consists of fibroblasts and collagen fibers. The spongiosa is predominantly found at the base of the leaflets and contains proteoglycans, which absorb compressive forces within the valve. Finally the ventricularis is found on the ventricular aspect of the valve and contains elastin fibers orientated perpendicularly to the collagen.
B) Short-axis views of the right, left and non-coronary cusps of the aortic valve. Aortic aspect of the valve displays the concentric arrangement of collagen fibers in the fibrosa layer of the valve. Ventricular aspect showing the radial arrangement of elastin fibers in the ventricularis layer of the valve.

PATHOLOGY

In calcific aortic stenosis, the valve cusps become progressively thickened, fibrosed and calcified. This results in increased valve stiffness, reduced cusp excursion, and progressive valve orifice narrowing that contrasts with the cusp fusion seen with rheumatic heart disease. Historically, calcific aortic stenosis has been attributed to prolonged "wear and tear" and age-associated valvular degeneration. However, recent evidence suggests that it is instead the result of active inflammatory processes involving biochemical, humoral and genetic factors (Figure 1.2).

Mechanical Stress & Endothelial Damage

The early stages of aortic stenosis are in many ways similar to atherosclerosis. Like atherosclerosis, the initiating event is believed to be endothelial damage resulting from increased mechanical stress and reduced shear stress. This results in a characteristic distribution of lesions within the stenotic valve. Shear stress is highest in the cusps adjacent to the coronary ostia due to the influence of coronary artery flow. Consequently the non-coronary cusp has lower shear stress and is most frequently involved in aortic stenosis. Mechanical tissue stress is highest around the flexion areas of the cusps near their attachment to the aortic root and 50% of lesions can also be observed in this region.[7] However, the bicuspid aortic valve perhaps best illustrates the role of mechanical stress in the pathogenesis of aortic stenosis. This common congenital abnormality is characterized by a two-cusp structure that results in a less efficient distribution and concentration of mechanical forces within the valve such that aortic stenosis develops almost invariably in these patients and on average two decades earlier than in those with a tri-leaflet valve. [8, 9]

Figure 1.2. Summary of the pathological processes occurring within the valve during aortic stenosis

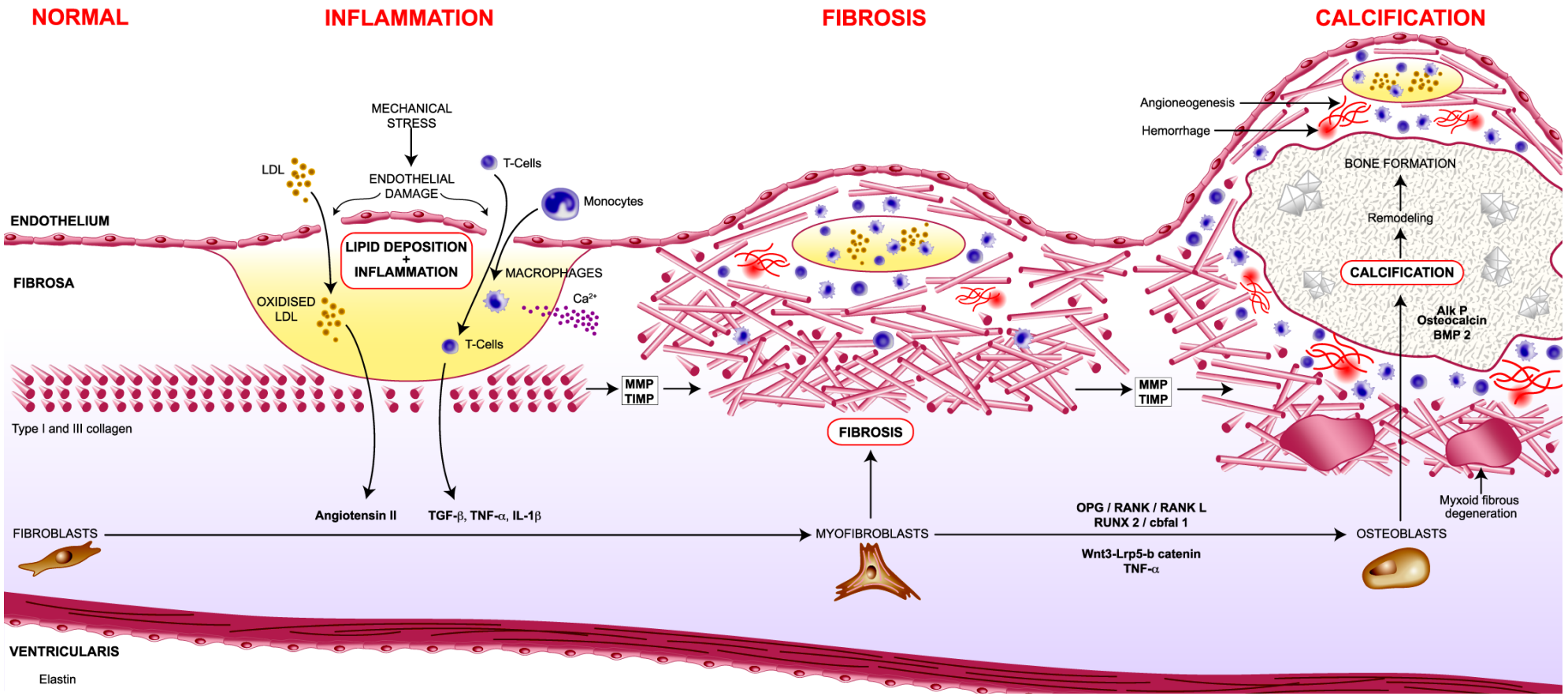

Mechanical stress results in endothelial damage that allows infiltration of lipid and inflammatory cells in to the valve to form lipid plaques. Lipid oxidization further increases inflammatory activity within these lesions and the secretion of pro-inflammatory and pro-fibrotic cytokines. The latter drives the differentiation of fibroblasts in to myofibroblasts that secrete increased amounts of collagen I and III under the influence of angiotensin. In addition matrix metallopoteineases (MMP) and tissue inhibitors of metalloproteinases (TIMP) have a complex role in disrupting the existing circumferential arrangement of these fibers. The result is an accumulation of disorganized fibrous tissue within the valve, and Myxoid fibrous degeneration resulting in thickening and increased cusp stiffness. The calcification process begins in the early stages of the disease driven by the secretion of micro-vesicles by macrophages, which act as a subsequent nidus for calcification. However, acceleration of this process is stimulated by the differentiation of myofibroblasts into osteoblasts under the influence of pro-calcific pathways including osteoprotegerin/RANK/RANKL, Runx 2-cbfal 2, Wnt3-Lrp5-b catenin, and TNFα. Osteoblasts subsequently coordinate calcification of the valve as part of a highly regulated process akin to skeletal bone formation, with expression of many of the same mediators such as osteocalcin, alkaline phosphatase (Alk P) and bone morphogenic protein (BMP) 2. With time maturation of valvular calcification occurs so that by the end stages of the disease lamellar bone, microfractures and hemopoeitic tissue can all be observed with the valve. These pathogenic processes are sustained in the thickened valve by angioneogenesis, with new vessels localising, in particular, to regions of inflammation surrounding calcific deposits. Haemorrhage has also been demonstrated in severe disease and may have a role in driving disease progression.

Inflammation

Endothelial injury or disruption may allow lipids to penetrate the valvular endothelium and accumulate in areas of inflammation.[10, 11] The lipoproteins implicated in atherogenesis, including low-density lipoprotein (LDL) and lipoprotein (a), are present in early aortic valve lesions [10] and undergo oxidative modification.[11] These oxidised lipoproteins are highly cytotoxic and capable of stimulating intense inflammatory activity and subsequent mineralization (Figure 1.2).[12]

A combination of endothelial damage and lipid deposition triggers inflammation within the valve. Expression of adhesion molecules allows infiltration of the endothelial layer by monocytes that differentiate into macrophages,[13] and T cells that release pro-inflammatory cytokines including transforming growth factor (TGF)-β1,[14] tumor necrosis factor (TNF)-α and interleukin (IL)-1β.[15] These inflammatory cells and cytokines ultimately help to stimulate and establish the subsequent fibrotic and calcific processes that drive increasing valve stiffness (Figure 1.2).

An inflammatory basis for aortic stenosis is supported by studies demonstrating increased C-reactive protein concentrations in the valves and systemic circulation of patients with aortic stenosis,[16, 17] increased temperature in stenotic aortic valve cusps [18] and more recently by non-invasive imaging studies using combined positron emission tomography and computed tomography (PET/CT). 18F-Fluorodeoxyglycose (18F-FDG) is a PET ligand that serves as a marker of macrophage activity, and has become an established means of measuring inflammation in aortic and carotid atheroma.[19] A recent study has now used this technique to examine inflammation in the aortic valve and demonstrated an increased in valvular 18F-FDG activity in patients with aortic stenosis compared to controls.[20]

Angioneogenesis and Valve Hemorrhage

Further histological studies have suggested that the inflammatory processes within the valve are sustained by angioneogenesis. Thin neovessels are commonly observed in regions of intense inflammation surrounding calcific deposits and demonstrate a positive correlation with T lymphocyte density. Furthermore both intercellular adhesion molecule (ICAM)-1 and vascular cell adhesion molecule (VCAM)-1 expression is increased in these vessels suggesting that they act as an important portal of entry for inflammatory cells.[21, 22] In addition hemorrhage related to these vessels has emerged as a potentially important pathological mechanism, being present in 78% of patients with severe aortic stenosis and associated with neovascularization, macrophage infiltration and more rapid rates of disease progression (Figure 1.2).[23]

Fibrosis

The stenotic aortic valve is characterized by extensive thickening due to accumulation of fibrous tissue and remodelling of the extracellular matrix. In all three layers of the valve, abundant fibroblast-like cells are found. They contain vimentin and are commonly referred to as valve interstitial cells (VICs). A sub-population of these cells become activated by the inflammatory activity within the valve and differentiate into myofibroblasts.[24] Whilst fibroblasts control the synthesis of collagen in the normal valve, myofibroblasts are believed to be responsible for the accelerated fibrosis observed in pathological states.[25] In addition, matrix metalloproteinases are secreted by myofibroblasts and inflammatory cells, and have an important and complex role in the restructuring of the valve leaflet matrix (Figure 1.2).[15, 26, 27]

The renin-angiotensin system is thought to modify this fibrotic process. Tissue angiotensin-converting enzyme (ACE) and angiotensin II are both up regulated in stenotic aortic valves, and angiotensin receptors have been identified on valve myofibroblasts.[28] Angiotensin directly stimulates

myofibroblast proliferation and collagen synthesis via these receptors but also has indirect effects via the increased expression of pro-fibrotic factors such as TGF-β.[29]

Calcification

Valve calcification plays a key role in the development of aortic stenosis and can be quantified using computed tomography. The degree of valvular calcification correlates with valve severity, [30] disease progression[31] and the development of symptoms and adverse events.[32] Moreover disorders of mineral metabolism including Paget's disease,[33] osteoporosis,[34] vitamin D polymorphisms [35] and hemodialysis [36] are all associated with an increased prevalence of aortic stenosis and more rapid progression of calcification within the valve.[34]

Although other processes predominate, microscopic areas of calcification can be observed in the early stages of aortic sclerosis and these co-localize to areas of lipid deposition and inflammation. In a sixth of patients with sclerosis, the calcification process accelerates, hemodynamic obstruction ensues and the valve becomes stenotic.[37] This progression is thought to be driven by the differentiation of myofibroblasts into osteoblasts [38, 39] under the influence of the Wnt3-Lrp5-β catenin signaling pathway,[40] the osteoprotegerin (OPG)/Receptor Activator of Nuclear factor Kappa B (RANK)/RANK ligand (RANKL) pathway [41] and increased levels of TNF-α (Figure 2).[42] Osteoblasts subsequently co-ordinate calcification as part of a highly regulated process, akin to new bone formation[43, 44] with the local production of many factors more commonly associated with skeletal bone metabolism including osteopontin, osteocalcin, bone sialoprotein and bone morphogenic protein 2 (BMP-2).[44-47] In addition serum concentrations of Fetuin A, an inhibitor of calcification, are reduced in patients with aortic stenosis.[48] Interestingly a reduction in this protein is commonly

observed in patients with severe renal dysfunction and may provide an explanation for the accelerated vascular and valvular calcification associated with this condition.[49,50]

As aortic sclerosis progresses to mild aortic stenosis, calcification is comprised of nodules containing hydroxyapatite deposited on a bone-like matrix of collagen, osteopontin and other bone matrix proteins.[45, 46, 51] Remodelling of this calcification occurs as aortic stenosis progresses until by the later stages of disease, lamellar bone, microfractures and hemopoeitic tissue can all be identified within the valve.[46]

1.3 LEFT VENTRICULAR HYPERTROPHY

Aortic stenosis causes an increase in pressure afterload and ventricular wall stress that stimulates hypertrophy of the left ventricular myocardium. Myocytes enlarge and wall thickness increases in a response that initially restores wall stress and preserves left ventricular function.[52, 53] However, evidence is accumulating that increasing levels of hypertrophy may in fact be maladaptive.[54] The landmark Framingham studies first linked increasing hypertrophy with the progression to heart failure,[55] and left ventricular hypertrophy is now considered a marker of an adverse prognosis across a number of cardiac conditions.[56-59] Furthermore animal studies have suggested that the development of cardiac hypertrophy and normalization of wall stress may not be necessary to preserve cardiac function.[60]

In aortic stenosis, patients display a marked variation in the magnitude of their hypertrophic response. This has recently been demonstrated to be of prognostic importance[4] and might explain the marked heterogeneity between symptom onset and the severity of valve narrowing that is observed.

VARIATION IN THE DEGREE OF LEFT VENTRICULAR HYPERTROPHY

It is perhaps surprising that echocardiographic studies have only suggested a weak correlation between the degree of left ventricular hypertrophy and the severity of valve obstruction.[54, 61, 62] Instead the magnitude of the hypertrophic response appears to be more closely associated with other factors such as advanced age, male sex and obesity.[61, 63-65] Genetic factors modulate the degree of hypertrophy in response to a wide range of physiological and pathological triggers[66-68] and also play a role in aortic stenosis. In particular, polymorphisms of the ACE I/D gene have been

associated with different degrees of hypertrophy [69] and reverse remodelling after valve replacement.[70]

Other contributors to an increased afterload frequently co-exist in patients with aortic stenosis and are likely to modulate the hypertrophic response. Hypertension is common in this patient group and an analysis of participants in the Simvastatin and Ezetimibe in Aortic Stenosis (SEAS) trial showed that co-existent hypertension was associated with an increased left ventricular mass and higher prevalence of hypertrophy.[71] Increased arterial stiffness is also frequently observed due to a combination of advanced age, co-existent atherosclerosis, diabetes and high blood pressure. The resultant loss of arterial compliance means that the heart has to pump even harder to fill the vasculature with blood and also changes the timing of the pulse wave reflection so that it arrives in systole rather than diastole. Both these effects result in an increase in left ventricular afterload and contribute to the development of left ventricular dysfunction in aortic stenosis.[72] On this basis, a global measure of afterload, Z_{VA}, has been proposed that is derived from both the mean valve gradient and the systemic arterial compliance. This variable has been shown to predict an adverse prognosis in patients with moderate and severe aortic stenosis, and has been proposed as a means of improving risk stratification and clinical decision-making.[73]

The variation in the hypertrophic response has important clinical consequences. In a study of 218 patients with asymptomatic severe disease, Cioffi and colleagues demonstrated that subjects with inappropriately high left ventricular mass had an increased mortality compared to patients with comparable valve narrowing but more moderate hypertrophy.[4] The mechanism for this adverse prognosis is likely to relate to premature decompensation of the hypertrophic process.

FROM HYPERTROPHY TO HEART FAILURE

The transition from hypertrophy to heart failure marks the tipping point where the left ventricle fails in the face of an increased pressure afterload and is no longer able to maintain forward flow through the valve. This heralds the onset of symptoms, adverse events and a poor prognosis. Hein and colleagues established that this key progression is associated with increased myocyte apoptosis and fibrosis, and postulated that these two processes were responsible for the transition (Figure 1.3).[74]

Myocyte Apoptosis

The rate of apoptosis in the hypertrophied myocardium has been estimated at 5-10% of myocytes per year.[75] Apoptosis is usually balanced by myocyte regeneration but in hypertrophy there appears to be a net loss of cells. Increased apoptotic rates may simply be a response to the direct mechanical forces associated with an increased afterload.[76, 77] However, angiotensin II has also been implicated and angiotensin receptor blockers reduce apoptosis in patients with hypertension, even at doses that do not reduce blood pressure.[78, 79] Ischemia may also be important. In aortic stenosis, myocardial oxygen demand is increased by a combination of the elevated myocardial mass and increased afterload. In contrast to physiological hypertrophy, the density of the coronary capillary network does not expand sufficiently to meet this demand and coronary flow reserve is impaired (Figure 1.3).[80] Galiuto and colleagues demonstrated impaired myocardial perfusion in patients with severe aortic stenosis and normal coronary arteries, and that this was associated with increased cardiomyocyte apoptosis.[81] Impaired coronary flow reserved in aortic stenosis has also been confirmed in two more recent studies.[82, 83]

Figure 1.3. The development and subsequent decompensation of left ventricular hypertrophy in response to aortic stenosis

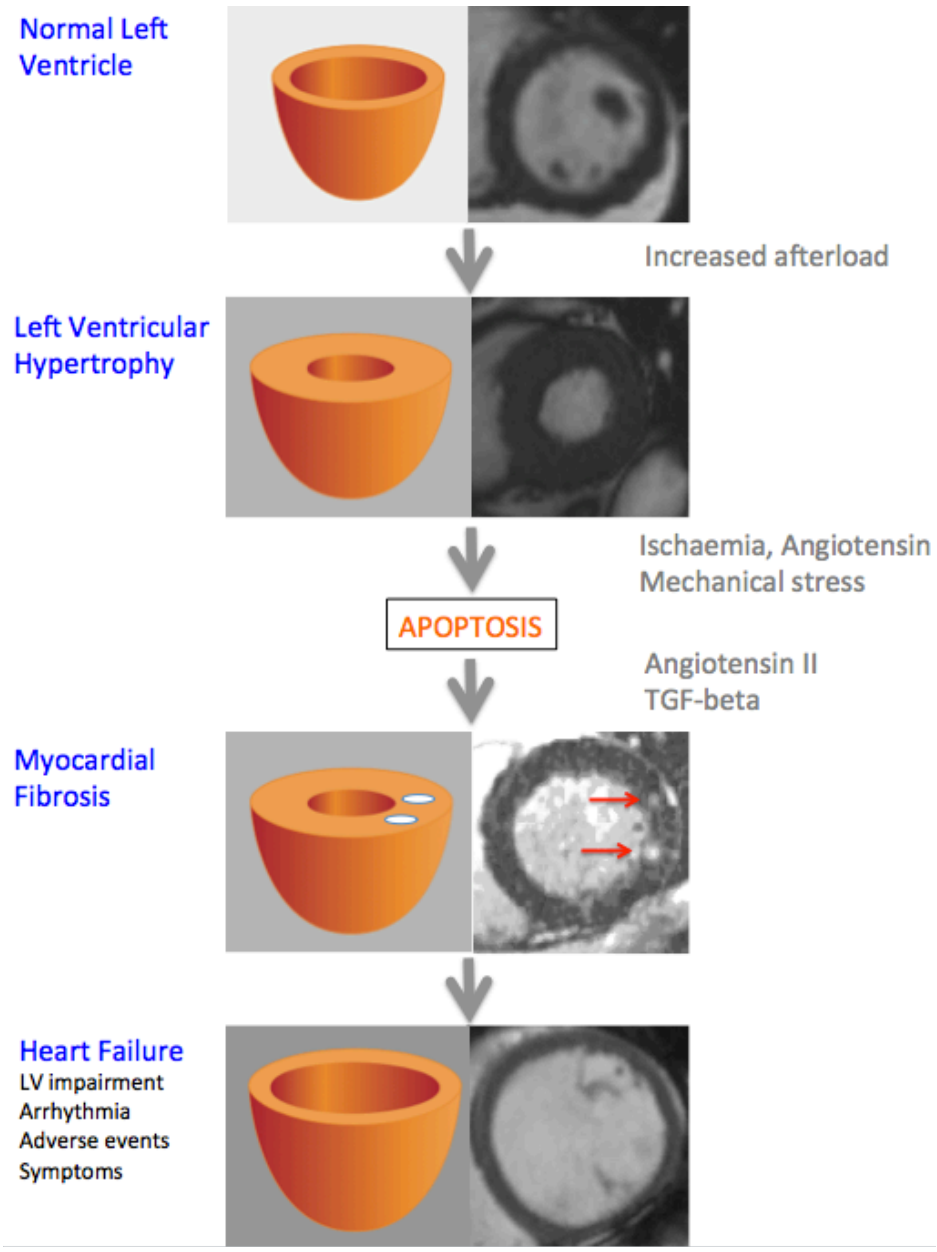

Progression of the left ventricular adaptive response is illustrated in cartoon format and using short-axis cardiovascular magnetic resonance images of the left ventricle in end-diastole. Aortic valve narrowing imposes an increased afterload and wall stress on the left ventricle. This stimulates a hypertrophic response, which initially restores wall stress and maintains cardiac performance. However this process ultimately becomes decompensated. Myocyte apoptosis is triggered by a combination of myocardial ischemia, direct mechanical forces and the actions of angiotensin. This triggers a fibrotic response in the myocardium under the influence of pro-fibrotic mediators such as angiotensin and TGF-β, which can be visualized using the late gadolinium enhancement technique (red arrows show regions of mid-wall fibrosis in the lateral wall of the ventricle). Increasing myocardial fibrosis leads to progressive systolic and diastolic impairment and the progression to heart failure. Symptoms and adverse events ensue perhaps in part due to an increased tendency to arrhythmia.

Fibrosis

Histopathological studies have confirmed fibrosis to be an integral part of the hypertrophic process.[84, 85] Myofibroblasts infiltrate the myocardium and secrete extracellular matrix proteins including collagen types I and III.[86] Areas of fibrosis are observed to co-localize with areas of myocyte apoptosis [87] and it has been suggested that fibrosis occurs as a form of scarring after myocyte death and injury. As with fibrosis in the valve, the renin-angiotensin system, TGF-beta and an imbalance in MMP/TIMP activity have all been implicated in this process (Figure 1.3).[88, 89-90]

1.4 SIMILARITIES BETWEEN AORTIC STENOSIS AND ATHEROSCLEROSIS

Atherosclerosis and aortic stenosis share many common risk factors and are both characterized by endothelial damage, lipid deposition, angioneogenesis, calcification and inflammation (Table 1.1). Both are prevalent in an elderly population and frequently co-exist. This provides the opportunity to study coronary pathology alongside valve disease in a population of patients with aortic stenosis. In addition the similarities in pathophysiology led to the hypothesis that statins might delay the progressive valve narrowing observed in aortic stenosis. However this strategy has proven disappointing with three major prospective randomized control trials having failed to demonstrate any impact on disease progression or clinical outcome.[91-93] These results probably reflect important pathophysiological differences between the development and progression of aortic stenosis and atherosclerosis (Table 1.1). In atherosclerosis, inflammation and lipid deposition are key components in both the development of arterial plaque and its stability. Adverse events are predominantly related to plaque rupture and much of the benefit from statin therapy is due to plaque stabilization and a thickening of the fibrous cap. By contrast in aortic stenosis, adverse events are related to

progressive narrowing of the aortic valve. This is predominantly driven by increasing calcification, a process that statins have consistently failed to impact on, even in the context of coronary atherosclerosis.[94-96]

Table 1.1 Comparisons between the pathological processes underlying aortic stenosis and atherosclerosis

	AORTIC STENOSIS	**ATHEROSCLEROSIS**
Initiating event	Increased mechanical stress and reduced shear stress causing endothelial damage	Increased mechanical stress and reduced shear stress causing endothelial damage.
Predominant Cell Types	Macrophages and T helper cells Valve Interstitial Cells Myofibroblasts Osteoblasts	Macrophages and T helper cells Foam cells Vascular smooth muscle cells
Early pathology	Oxidized lipid deposition, inflammation	Oxidized lipid deposition, inflammation, foam cells
Later pathology	Calcification and fibrosis predominate Neovascularization and hemorrhage	Lipid deposition and pools, Inflammation and calcification Neovascularization and hemorrhage
Disease Progression	Fibrosis, calcification and hemorrhage	Lipid deposition and pools, inflammation plaque rupture and thrombosis
Mechanism of adverse events	Progressive valve rigidity due to calcification and fibrosis Decompensation of the hypertrophic response	Plaque rupture due to lipid rich pool, inflammatory infiltrate and thin fibrous cap. Intravascular thrombosis.

1.5 Positron Emission Tomography

Physics

Positron Emission Tomography is a non-invasive imaging technique, which provides information regarding the activity of specific biochemical processes within the body. The positron or anti-electron is the antiparticle of the electron, having the same mass but a positive electric charge. PET tracers consist of a positron emitter, such as 18F-fluoride, 15O-oxygen or 11C-carbon, attached to a molecular vehicle that targets the biochemical process of interest. [97]

18F-Fluoride is the most commonly used positron emitter because its relatively long half-life allows for commercial production and distribution. In the nuclei of these molecules, protons decay to neutrons (beta decay) resulting in emission of a positron and a neutrino. After a time, collision between the positron and an electron results in annihilation of both particles and the release of two photons, with a specific energy (511keV), at 180 degrees to one another. Detection of these photons provides the basis for PET scanning.

PET imaging uses a dedicated PET camera system, which involves multiple rings of detectors completely surrounding the patient. These detectors are made up of scintillation crystals (bismuth gernmanium oxide (BGO) gadolinium oxyorthosilicate (GSO) or lutetium oxyorthosilicate) coupled with photomultiplier tubes. When photons hit the scintillator an energetic electron is produced. This excites other surrounding electrons, which release light as they decay back to the ground state. This light is then detected by a photomultiplier tube and converted in to an electrical signal. PET imaging utilises the concept that two 511keV photons detected in close temporal proximity (6-12 nanoseconds) by two opposed detectors in the ring are likely to have originated from a single

annihilation event in the body somewhere in a line between them (the line of response). Such simultaneous detections are termed coincidences and these events are used to build up the PET image of activity and the sites where tracer accumulation has occurred. [97]

The resultant images provide detailed functional data regarding the biochemical process being studied, however PET scans are limited by a lack of spatial resolution. Recently this issue has addressed using combined positron emission tomography and computed tomography, which combines the functional PET data with the high-resolution data provided by CT scanning. PET/CT scanners incorporate both PET and CT within the same gantry. Patients lie in the same position for both scans, which allows the PET and CT scans to be superimposed upon one another. This serves two purposes: firstly the CT can be used to perform accurate attenuation correction of the PET image; and secondly co-registration allows precise localisation of tracer uptake within small structures such as the aortic valve.

18F-Flurodeoxyglucose

Tracer development has largely been driven by oncology studies, in which PET has become a widely available clinical tool. The most commonly used tracer is 18F-flurodeoxyglucose (18F-FDG), which is a glucose analogue that is taken up into cells by glucose transport proteins and enters the glycolytic metabolic pathway. Following the initial hexokinase step, 18F-FDG-6-phosphate cannot be metabolized further and becomes trapped within cells that have high metabolic requirements. Increased uptake is therefore observed in malignant cells but also by arterial macrophages, which have increased metabolic requirements compared to other cells in the vasculature. This has been the

basis for vascular PET imaging using 18F-FDG, which has become an established means of quantifying vascular inflammation in both the aorta and carotid arteries.[98, 99]

Rudd and colleagues first established that 18F-FDG uptake was increased in symptomatic carotid plaque following TIA compared to contralateral lesions.[99] Subsequently the level of 18F-FDG activity has been shown to correlate with plaque macrophage burden[100] although preclinical studies have suggested that uptake may also relate to plaque hypoxia. [101] Arterial uptake of 18F-FDG has now been extended to the aorta, femoral and iliac vessels displaying excellent reproducibility[102,103] as well as the aortic valve in a small observational study of oncology patients.[20] It is hoped that vascular 18-FDG scanning may provide useful prognostic information. Several small observational studies have linked increased uptake to an increased incidence of cardiovascular events [104, 105] although the results of a large-scale prospective study, The High Risk Plaque Initiative, are still awaited. In this study prognostic information from non-invasive cardiac imaging, including FDG-PET, will be compared against traditional risk factors.

Finally FDG PET holds promise as means of assessing novel anti-inflammatory atherosclerotic agents. Tahara and colleagues demonstrated that simvastatin significantly reduced carotid 18F-FDG uptake after 3 months of treatment. More recently 18F-FDG has been used to study a novel cholesteryl ester transfer protein (CETP) inhibitor, Dalcetrapib, that appeared to result in a reduction in the carotid plaque signal.[19]

Advances in our knowledge regarding 18F-FDG uptake in the major arteries of the body has led to hope that this technique might also be applicable to the coronary arteries. Acute plaque rupture is the most common cause of acute coronary syndromes and a major cause of morbidity and mortality.

Such events are related to increased plaque inflammation leading to the hope that 18F-FDG might be able to identify vulnerable coronary plaque. Whilst several reports have shown some promise,[106] this technique has been hampered by the problems caused by cardiac motion and myocardial uptake. However potential solutions to these problems exist in the form of ECG/respiratory gating and the use a high fat, low carbohydrate diet prior to the scan (aimed at switching the myocardium from a glucose to fat-based metabolism).[107, 108]

18F- Sodium Fluoride (18F-NaF)

18F-sodium fluoride (18 F-NaF) is an alternative PET tracer that is thought to detect areas of novel calcification and regions of calcium remodelling. It is used clinically for the detection of primary osteoblastic tumours, bone metastases and conditions associated with high bone turnover such as Paget's disease.[109, 110] More recently studies have described 18F-NaF uptake as a marker of calcification within carotid and aortic atheroma,[111, 112] and demonstrated an association between activity and cardiovascular risk factors.[112] However to date this tracer has not been used to study patients with aortic stenosis nor coronary atheroma.

18F-sodium fluoride is thought to directly incorporate in to bone crystals via an exchange with hydroxyl groups in the hydroxyapatite crystal of bone (Ca10(PO4)6OH2) to form fluoroapatite (Ca10(PO4)6F2). This process can be divided into four stages as originally described by Blau and colleagues.[113] In steps 1 and 2, fluoride moves from the blood through the extracellular space to the shell of bound water around exposed crystals, a process which occurs within minutes of exposure. Step 3 is travelling of the tracer on to the crystal surface and probably occurs in hours, whilst in step 4 Fluoride is incorporated into the bone crystal, which takes days or weeks. Uptake in bone is therefore

thought to reflect two processes: firstly increased blood flow and secondly processes that increase the exposed bone crystal surface. The former should be broadly constant within aortic valve tissue whilst the latter has been shown to correlate with osteoblast and osteoclast activity,[113-115] which increase the surface area to which 18F-NaF can bind.[116]

Limitations to PET

The primary limitations to this technique related to its cost (£1,000 per scan in our centre), and it's relative lack of availability, although with the growing role of PET in the assessment of oncology patients this is becoming less of an issue. Furthermore there is a relative lack of clinically approved radiotracers so that only a limited number of pathological processes can be studied at this time. However in principle a tracer can be designed to any biochemical process so that this technique holds great future promise as a means of studying cardiovascular pathology. Finally the scans are associated with a dose of radiation. This is generally small (about 5mSv for each PET scan in our centre) which equates roughly to a CT coronary angiogram. However this needs to taken in to consideration especially in young patients and those likely to undergo multiple investigations which themselves involve ionising radiation. Furthermore it limits the role of PET in longitudinal studies requiring scans at multiple time points.

1.6 Cardiovascular Magnetic Resonance

Magnetic Resonance Imaging (MRI) uses the body's natural magnetic properties to provide detailed anatomical and functional images of the body. Clinical scans use the hydrogen nucleus (a single proton), which is found in abundance in both fat and water. Each of the many protons present within each cell has a positive charge and is spinning in a random manner that creates multiple tiny and opposing magnetic fields. When a patient is placed within a high-field magnet, these magnetic forces align along the magnet's long-axis. The MRI scanner then sends a radiofrequency excitation pulse into the patient at the same frequency as the precessing hydrogen nucleus. This energy excites the protons causing a deflection in the orientation of their magnetic field. Protons are unstable at this higher energy state and will ultimately relax and return to their stable baseline position. In so doing, they will release energy back in the form of a radiowave, which can be detected by the scanners body surface coils. Different tissues have different proton densities and different molecular configurations, which result in variable relaxation properties (T1 reflecting the exchange of energy from protons to their local surrounding environment; and T2 reflecting exchange of energy from one nucleus to another). They will therefore result in the emission of different radiowaves during relaxation that allows the MRI scanner to generate an image of the body's internal structures.[117]

MRI was first developed in in the 1950's but was not immediately applicable with respect to the heart due to problems related to cardiac and respiratory motion. However, with the development of rapid sequence imaging and ECG-gating, cardiovascular magnetic resonance (CMR) has become a widely adopted research and clinical tool. CMR images provide excellent contrast between the myocardium and the blood pool and affords more detailed assessment of left ventricular structure. It has therefore become the gold-standard method for the assessment of left ventricular volume, mass

and ejection fraction.[118] In addition the late gadolinium enhancement technique allows for the non-invasive visualization of replacement fibrosis and scar tissue within the myocardium.

Late Gadolinium Enhancement

Gadolinium is a paramagnetic contrast agent, which reduces the T1 relaxation time in regions of uptake. In its free ion form, gadolinium is highly toxic but safe when chelated to cyclic carrier molecules such as Diethylentriamene pentaacetate (DTPA). After chelation, gadolinium contrast agents have a large molecular size that prevents them from crossing cell membranes, and causes them to accumulate in areas of increased extracellular water or within cells that have lost their membrane integrity. Regions of fibrosis display marked expansion of the extracellular compartment and therefore accumulate gadolinium readily. Similarly gadolinium is able to penetrate necrotic myocytes within regions of myocardial infarction. Indeed differences in gadolinium pharmacokinetics between different types of myocardial tissue form the basis of the late gadolinium enhancement technique (Figure 1.4).

In regions of normal myocardium gadolinium washes rapidly in and out of the tissue due to an uncompromised blood supply and a low volume of distribution respectively. In areas of ischaemic myocardium, gadolinium moves in slowly due to restricted blood flow (providing the basis for CMR perfusion imaging) but again washes out rapidly. Finally in infarcted myocardium there is once more a delay in gadolinium entering these regions, however once it has arrived gadolinium will persist in this tissue and washout slowly due to the high volume of distribution. Consequently between 10 and 20 minutes after administration of gadolinium, a concentration gradient exists between regions of normal and fibrotic or infarcted myocardium that provides the basis for late gadolinium enhancement. Inversion recovery sequences are used to excite the protons, which then decay to

their baseline state after passing through the null point. Decay is dependent on their T1 relaxation times and therefore the concentration of gadolinium within the tissue. The time to inversion (TI) reflects the time between excitation and imaging and can be manipulated so that the normal myocardium is nulled and appears black, whilst tissue containing gadolinium contrast will provide comparatively infinite signal and appear bright.[117]

Figure 1.4. Pharmacokinetics of gadolinium contrast into different tissues after bolus administration

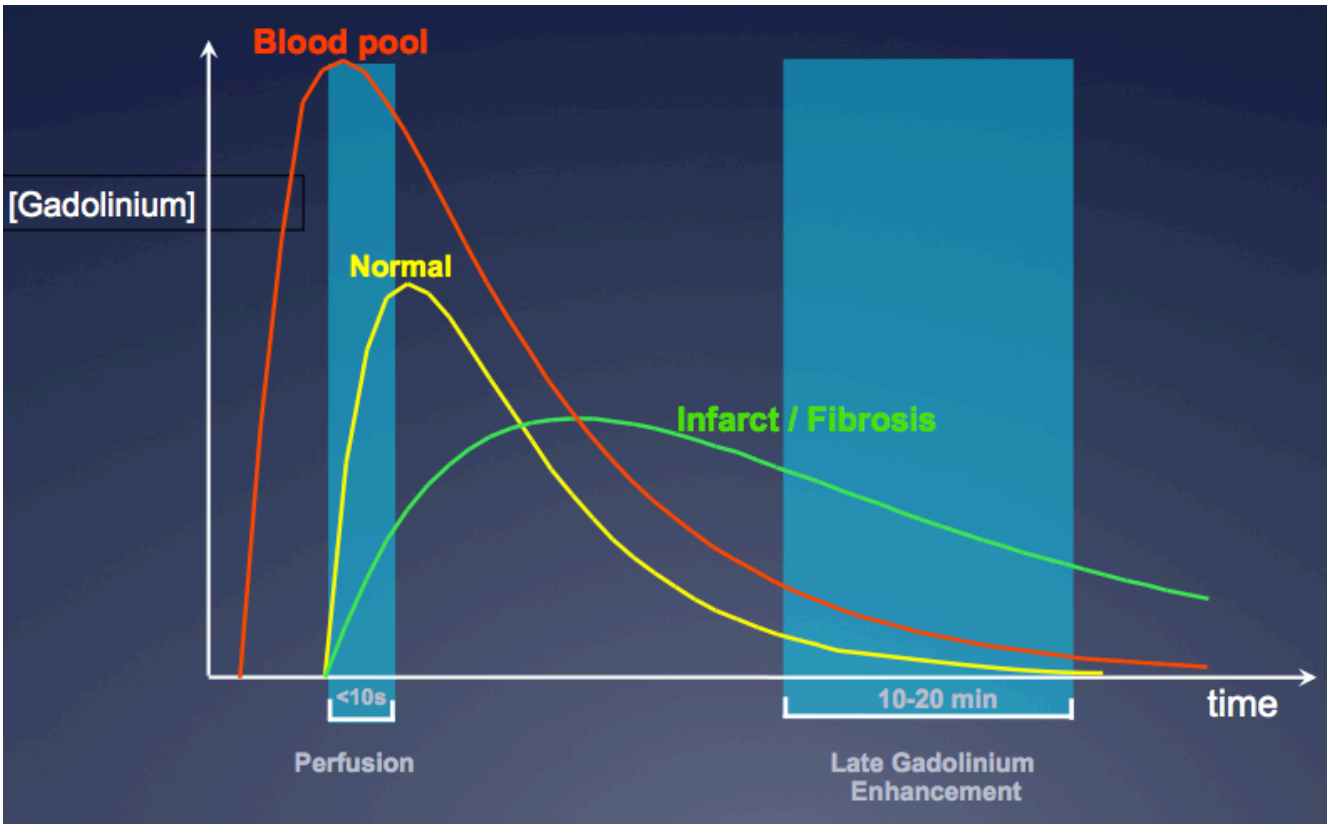

Gadolinium concentrations within different tissues following its bolus administration are shown against time. Blood washes quickly in and out of the myocardium and normal cardiac tissue. Gadolinium is slow to wash into areas of infarct due to a compromised blood supply. This can be detected as a difference in first pass perfusion immediately following gadolinium administration. In addition washout is slower in regions of infarct than in normal tissue because of an increased volume of distribution. Therefore between 10 and 20 minutes after administration a differential concentration of gadolinium exists in these issues, which can be detected using the late gadolinium enhancement technique.
Based on an image provided by the Royal Brompton Hospital, CMR course.

CMR Studies in Aortic Stenosis

Cardiovascular Magnetic Resonance has been used in previous studies to assess patients with aortic stenosis. In addition to accurate measurement of wall thickness, left ventricular mass, volumes and ejection fraction accurate planimetry of the aortic valve area is possible. Short axis cine images can be obtained at the level of the tips of the aortic valve. The aortic valve area can then be planimetered during systole, a technique that has demonstrated good correlation with measurements made during transoesophageal echocardiography.[119]

Recent studies have demonstrated a mid-wall pattern of enhancement in patients with aortic stenosis in the absence of coronary artery disease.[120, 121] Its presence has been shown to predict less symptomatic benefit following surgery[122] and has been associated with low-gradient, severe aortic stenosis.[123] However whilst the presence of LGE is associated with an adverse prognosis in other cardiac conditions,[124-128] this has not been assessed in aortic stenosis.

Limitation to CMR

Whilst CMR has the considerable advantage of not involving ionizing radiation there are several limitations. Firstly there is the cost (roughly £500 per scan), which makes clinical research studies expensive. Secondly there is availability of the technique: acquiring interpretable pictures requires considerable training and experience, which is not widely available. Thirdly not all patients can undergo CMR, for example patients with permanent pacemakers and ICDs, which limits the use of this modality in this important group of cardiovascular patients. The issue of nephrogenic systemic fibrosis has received much attention but is now only considered a problem in patients with renal failure of on dialysis, in whom CMR is generally contraindicated.

1.7 Aims

Our aim was to investigate the pathophysiology of aortic stenosis using modern non-invasive imaging techniques. Specifically we sought to assess the role of calcification and inflammation in progressive valve narrowing using PET/CT and to investigate the LV hypertrophic response including the role of myocardial fibrosis using CMR.

Positron Emission Tomography

1) To examine the feasibility of assessing aortic valve inflammation with 18F-FDG and calcification with 18F-NaF using PET/CT.

2) To examine the reproducibility of this approach.

3) To use this technique to assess the relative importance of inflammation and calcification at different stages of the disease.

4) To assess uptake of 18F-FDG and 18F-NaF in the coronary arteries of our aortic stenosis patients undergoing PET/CT scanning.

Cardiovascular Magnetic Resonance

1) To establish the prevalence of infarct and mid-wall patterns of late gadolinium enhancement in patients with moderate and severe aortic stenosis

2) To establish the prognostic significance of mid-wall and infarct patterns of late gadolinium enhancement in patients with moderate and severe aortic stenosis both in terms of all cause and cardiac mortality.

3) To establish the relationship between aortic stenosis severity and the degree of hypertrophy using CMR.

4) To investigate and categorise the different patterns of remodelling and hypertrophy that occur in response to aortic stenosis using CMR

1.8 Hypotheses

Positron Emission Tomography

We hypothesized the following:

1) PET/CT using 18F-FDG and 18F-NaF would prove to be both a feasible and repeatable approach to the assessment of inflammation and calcification within the aortic valve (Chapter 3).

2) Both 18F-NaF and 18F-FDG uptake in the aortic valve would be higher in patients with aortic sclerosis and stenosis than in control subjects and increase with increasing disease severity (Chapter 3).

3) That uptake of 18F-NaF in the aortic valve would exceed that of 18F-FDG reflecting the relative importance of calcification and inflammation in the pathogenesis of aortic stenosis (Chapter 3).

4) That uptake of 18F-NaF and 18F-FDG might be feasible in the coronary arteries and demonstrate high risk plaque by identifying microcalcification and inflammation respectively. (Chapter 4).

Cardiovascular Magnetic Resonance

We hypothesized the following:

1) That mid-wall and infarct patterns of late gadolinium enhancement would be prevalent in patients with moderate and severe aortic stenosis (Chapter 5).

2) That mid-wall patterns and infarct patterns of late enhancement would be associated with an increase in all-cause and cardiac mortality compared to patients with no late gadolinium enhancement (Chapter 5).

3) The degree of left ventricular hypertrophy would be poorly related to the severity of valve narrowing in aortic stenosis (Chapter 6).

4) That CMR could be used to categorise the patterns of left ventricular remodelling and hypertrophy observed in aortic stenosis (Chapter 6).

Methods

2.1 Patient Populations

This thesis was based upon the study of two populations with aortic stenosis. Positron-emission tomography studies were conducted in a prospective cohort of patients recruited from the Royal Infirmary of Edinburgh. Cardiovascular magnetic resonance studies were based upon a registry of patients who underwent clinical CMR scans at the Royal Brompton Hospital London.

Positron Emission Tomography Studies

Consecutive patients over 50 years of age with aortic sclerosis and mild, moderate and severe aortic stenosis attending the outpatient department of the Royal Infirmary of Edinburgh were considered for participation in this study. Exclusion criteria included insulin-dependent diabetes mellitus, blood glucose >200 mg/dL, planned aortic valve surgery (and therefore symptoms attributed by their physician to their valve disease) and inability to undergo PET/CT scanning. Patients were not approached if they fulfilled any of the exclusion criteria or if their clinician felt participation was not appropriate. Of the patients approached, 52% agreed to take part in the trial. These patients were then compared to age- and sex-matched control subjects with a normal aortic valve and a similar range of co-morbidity. The studies were conducted with the written informed consent of all patients.

Cardiovascular Magnetic Resonance Imaging

Consecutive patients with moderate and severe aortic stenosis (based upon Doppler echocardiographic demonstration of peak aortic valve pressure gradient >36 mmHg and peak trans-valvular velocity >3 m/s, according to American Heart Association/American College of Cardiology

criteria [129]) who attended the Royal Brompton Hospital between January 2003 and October 2009 for CMR were recruited in to a registry prospectively. Ethical approval was granted in 2003. Royal Brompton Hospital guidelines recommend CMR for all patients with severe aortic stenosis. Other reasons for referral included diagnostic evaluation, clarification of disease severity, pre-operative evaluation, and assessment of the hypertrophic response.

Patients who received gadolinium contrast were followed up in order to determine the prognostic role of late gadolinium enhancement. Exclusion criteria for this part of the study were disseminated malignancy; moderate or severe aortic regurgitation, mitral regurgitation or mitral stenosis; contraindications to CMR including pacemaker and defibrillator implantation; and an estimated glomerular filtration rate (Cockcroft-Gault equation) of <30 mL/min. Clinical and follow up data was assimilated at the end of the study in 2009.

For the studies examining the patterns of remodelling and hypertrophy the same registry of aortic stenosis patients were used but different inclusion and exclusion criteria employed. Firstly it was not necessary for patients to have been administered gadolinium during their CMR scan, therefore patients who had only had cine imaging of their ventricle were also included. Secondly in order to study the effects of aortic stenosis on the ventricle in isolation the patient group was carefully selected to avoid those with confounding drivers of left ventricular remodelling. Exclusion criteria therefore included those with prior myocardial infarction, severe hypertension >180/120, significant valve disease other than aortic stenosis (moderate or severe mitral, tricuspid or pulmonary valve disease and moderate or severe aortic regurgitation), a clinical diagnosis of co-existent cardiomyopathy including hypertrophic cardiomyopathy, amyloidosis, disseminated malignancy and severe renal failure (estimated glomerular filtration rate <30 mL/min). Given the prevalence of

hypertension in elderly patients we were not able to exclude all patients with this condition. However hypertension also increases the LV afterload and so can be expected to have similar effects on the left ventricle. Coronary artery disease was excluded by invasive coronary angiography (84% of the cohort), computed tomography coronary angiography (8%) or stress perfusion imaging (2%). In patients under 40 years, it was excluded in the absence of symptoms or risk factors (6%).

2.2 Ethical Considerations

All studies gained ethical approval from the South East Scotland Research Ethics Committee, and local research ethics committee of the Royal Brompton Hospital and were conducted in accordance with the Declaration of Helsinki of the World Medical Association. The studies were registered on www.clinicaltrials.gov (reference numbers NCT01358513 and NCT00930735). For the PET study written informed consent was obtained for all patients. This was not required under the ethical approval for the MRI studies.

2.3 Positron Emission Tomography and Computed Tomography

For each patient enrolled in to the PET/CT studies combined PET/CT scans of the aortic valve were performed on two occasions in close succession using a hybrid scanner (Biograph mCT, Siemens Medical Systems, Erlangen, Germany).

Upon arrival the patients height and weight were measured on a consistent set of scales, calibrated to the PET scanner. Blood pressure and pulse rates were recorded and an intravenous cannula inserted. Thirty mls of blood was then taken. A 12-lead electrocardiogram was performed and bloods were sent for measurement of the full blood count, urea and electrolytes, serum calcium, phosphate

and alkaline phosphatase. The remainder was centrifuged at room temperature (10 minutes, 3000rpm) to provide serum samples, which were stored in case of future use at -70 degrees Celsius. Patients were then transferred to the lead lined uptake room. This is monitored using video surveillance, patients rested on a couch. A toilet with restricted access to the general public and other staff members was in close proximity and patients were encouraged to bring reading material with them.

18F-NaF had been ordered from a commercial producer the day before the scans (Erigal Ltd, Keele) pre-specifying the amount of activity required for injection of patients at specific times. This information allowed the supplier to calculate the amount of tracer that needed to be made that same morning based upon its decay characteristics. Three scans were performed in an afternoon in order to maximize the cost effectiveness with regard to delivery charges. On the first occasion we aimed to administer a target dose of 125 MBq 18F-NaF. Activity was drawn up in to a syringe using a semi-automatic system in order to minimize radiation exposure to the operator. The activity of the tracer drawn up in to the syringe was then measured and the time of measurement recorded. Adjustments were made as necessary in order to ensure the target dose would be achieved. The tracer was then injected in to the patient via the cannula and flushed with 10mls of saline. The time of injection was recorded. The intravenous cannula was then removed. Activity in the empty syringe that had contained the 18F-NaF was then measured to ensure that there was no significant residual and in order to calculate the exact activity that had been injected. Patients subsequently rested in the quiet environment of the uptake room for 60-minutes. After this time patients were transferred on to the PET scanner. Patients lay on their back with their hands above their head and were connected to a 3-lead ECG monitor, which allowed ECG gating of the subsequent CT calcium score. Patients then moved in to the scanner feet first. An attenuation correction CT scan (non-enhanced

low-dose 120 kV and 50 mAs, pitch 0.8, field of view 780mm, 5mm slice thickness, 3mm increment, B19f LowDose kernel, standard filtered back projection reconstruction algorithm) was then performed followed by PET imaging covering two bed positions centred over the valve in 3-dimensional mode for 10 min. Finally an ECG-gated, breath-hold CT scan (non enhanced, 40 mAs/rot [CareDose], 100 kV, Pitch 0.24, field of view 210mm, 3mm slice thickness, 1.5mm increment, B35f kernel, standard filtered back projection reconstruction algorithm) was performed of the aortic valve immediately after the 18F-NaF PET/CT scan for calculation of the aortic valve and coronary calcium scores. Patients were then removed from the scanner and allowed to leave the department with instructions not to have close physical contact with babies or pregnant females for the rest of the day.

On the second occasion, 18F-FDG was ordered and the patients were prepared in a similar manner as for the 18F-NaF scan. A target dose of 200 MBq 18F-FDG was injected. Patients rested in the uptake room for 90 min. They were asked to refrain from significant physical activity in order to reduce muscle uptake of 18F-FDG. Towards the end of the uptake time they were asked to urinate in order to expel the tracer (which is renally excreted) from the bladder. Patients were then transferred on to the PET scanner. They again lay flat on the scanner but because this scan did not require ECG gating, they were moved in to the scanner head first. Combined PET/CT imaging was then performed as described for the 18F-NaF scan but using a 15-min bed time. Tracer circulation times for the two tracers were based on previous studies using 18F-FDG and 18F-NaF in atherosclerosis[99, 111, 112] and aimed to allow for optimal contrast between the aortic wall, aortic valve and the blood pool.

The PET data were reconstructed using the Siemens Ultra-HD (time of flight +True X) reconstruction algorithm. Corrections were applied for attenuation, dead time, scatter and random coincidences. All

image analysis was performed on fused PET/CT data sets. Field of view was 780mm and a 512 matrix size was used for reconstructions so the voxel size was 1.5 × 1.5 × 3.0mm.

Dietary Restrictions

Intense uptake of 18F-FDG by the left ventricle leads to difficulties in discriminating between activity in the aortic valve and the myocardium. All patients in the PET cohort were asked to observe a carbohydrate-free diet for 24 h prior to their 18F-FDG scan because this suppresses myocardial uptake as the heart switches from a glucose to free-fatty acid metabolism.[107, 108, 130] Patients were provided with a list of food and drink to avoid (milk, bread, pasta, rice, potatoes, chips, crisps, chocolate, sugar, fruit, fruit juice, alcohol) and reminded of these restrictions the day before their scan by means of a telephone call. Clear fluids including black tea and coffee were acceptable and patients were encouraged to consume steak and a salad the night before, and to have bacon, eggs, sausages, black pudding for breakfast the morning of the scan. Dietary diaries were recorded and patients were categorized into dietary compliance or non-compliance. Myocardial tracer uptake was assessed by recording the maximum standardized uptake value (SUV) in the left ventricular septal myocardium. The SUV is the decay-corrected tissue uptake divided by the injected dose per body weight and is a semiquantitative dimensionless unit that is a widely used and validated measure of tissue 18F-FDG and 18F-NaF uptake.[99, 111, 131] High myocardial 18F-FDG uptake was pre-specified as an SUV value ≥5.0 whilst low uptake, indicating successful myocardial suppression, was defined by measurements <5.0.[108]

2.4 Cardiovascular Magnetic Resonance

For each patient enrolled in to the CMR study, CMR was performed using a 1.5T scanner (Magnetom Sonata or Avanto, Siemens, Erlangen, Germany) at the Royal Brompton Hospital. Upon arrival patients were changed in to a gown. They were asked to complete an MRI safety questionnaire to ensure that they had no contraindication to MRI (presence of a permanent cardiac pacemaker, severe claustrophobia, intracardiac defibrillator, cerebral aneurysm clip, cochlear implant, ventriculoperitoneal shunt or metal fragments in the eye). Orbital x-rays were preformed in patients who had worked with metalwork in whom there was a concern that fragments may have entered the eye. Their height and weight were recorded using a standard set of scales calibrated to the MRI machine. Blood pressure measurements were recorded and the patient's most recent eGFR checked to ensure that it was >30mls/min (to allow for the administration of gadolinium contrast, which is relatively contraindicated below this cut off due to the risk of nephrogenic systemic fibrosis). After checking that they did not have metal on their person (including dentures, dental plates, hearing aids, wigs, piercings) and that they were not wearing analgesic, human replacement therapy or nicotine patches, patients were transferred to the MRI scanner. Patients lay supine with their arms lying comfortably by their side. They were attached to an MRI compatible infusion pump (containing the gadolinium contrast). Earphones were placed to reduce the noise made by the scanner and a body coil positioned on the patient's chest. Patients were then put in to the centre of the MRI scanner and given an emergency buzzer in case of problems. Communication between the radiographer and patient was possible at all times via the headphones.

A standardised imaging protocol with stable study parameters was then followed. Localiser scans were performed to ascertain the position of the heart, followed by HASTE black blood imaging in the form of an axial and coronal stack (in addition to a sagittal oblique stack if aortic assessment was also

required on clinical grounds). These stacks were used to plan long-axis steady state free precession (SSFP) cine views of the heart as follows. The two chamber view was obtained by positioning the imaging slice through the anterior and inferior walls of the left ventricle on scout short-axis views and also through the apex of the left ventricle and the left atrium. The four-chamber view of the heart was planned on a scout short-axis view through the left and right ventricles, the LV apex, left and right atria, whilst missing the left ventricular outflow tract (LVOT). Three-chamber views were planned through the LVOT, apex of the left ventricle and the left atrium. Finally an LVOT view was performed by placing the imaging position through the aortic vale and aortic root perpendicular to the 3=chamber view. Subsequently a short-axis cine stack of the left and right ventricles was performed from the mitral valve down to the left ventricular apex. Starting basally on the atrial side of the mitral valve the plane of imaging was placed across the left and right ventricle on the 4-chamber view, perpendicular to the septum. Eight mm short-axis slices were then acquired from bases to apex with 2mm gaps so that each slice was 10mm further towards the apex than its predecessor. Temporal resolution was less than 45ms between phases and parallel imaging was used as available.

SSFP cine imaging of the vale was performed next. Short-axis views were obtained by placing the imaging slice perpendicular to the aortic root and left ventricular outflow tract on the 3-chamber and LVOT views at the level of the tips of the valve during systole. The imaging position was altered as necessary based on this initial image to ensure that the minimum aortic valve area was obtained.
This was followed by an assessment of the peak velocity through the aortic valve. Flow images were obtained in the 3-chamber view, with the velocity encoding parameter adjusted to prevent aliasing. The resulting image was used to generate further velocity maps perpendicular to the aortic jet at the level of the peak velocity seen on the 3-chamber velocity flow map.

After cine imaging a proportion of patients received Gadolinium contrast so that the late gadolinium enhancement technique could be performed as an assessment of myocardial infarction and fibrosis. An injection of 0.1mmol/kg gadolinium contrast agent (Gd-DTPA; Schering, Germany) was administered using an MR–compatible pump injector at 3mls/second, followed by a 20ml flush of saline at the same injection rate. Prior to 2007 a dose of 0.2mmol/kg was used because this was the dose used in initial validation studies. However concern regarding the risk of nephrogenic systemic fibrosis led to calls for the reduced dose of 0.1mmol/kg to be used from that time on. Patients were then left to rest inside the scanner. Ten to fifteen minutes following the injection inversion-recovery prepared spoiled gradient echo images were acquired in the same the 4-chamber, 2-chamber and short-axis views used for cine imaging to detect areas of late gadolinium enhancement. This technique relies on the successful nulling of the left ventricular myocardium. This requires continuous alteration of the inversion time (the Ti) so that the myocardium has no T1 signal and appears black. By contrast regions of fibrosis that have accumulated gadolinium contrast will have comparatively infinite signal and will appear bright.[125] The operator did not move on to the next image until the optimal Ti had been achieved.

All images were repeated in two separate phase-encoding directions to exclude artifact (artifacts usually move in the direction of the phase encoding direction and so will be shifted by changing its orientation). In those cases where great difficulty was had in nulling the myocardium phase sensitive inversion recovery (PSIR) sequences were used which are less sensitive to variations in the inversion time.

2.5 Echocardiography

Each patient participating in the PET/CT study underwent echocardiography on the day of one of their PET/CT scans. This was performed by a dedicated research sonographer using a standardised protocol.

On arrival patients were asked to remove clothing from the waist up and if necessary asked to put on a gown. ECG electrodes were placed on the chest and the patients connected to the dedicated echo machine (Phillips Medical Systems, Best, the Netherlands). Echocardiograms were performed by a single dedicated research ultrasonographer in the same room on the same bed to ensure consistency of conditions. A formal protocol was employed[30, 92] using an S51 pure wave transducer (Phillips Medical Systems, Best, the Netherlands) for 2-dimensional, M-mode, and pulsed and continuous wave Doppler studies.

Patients were placed in the left lateral position. Two-dimensional images were obtained in the parasternal position to provide long and short-axis view views of the heart. Switching to the apical position, 4-chamber, 5-chamber and 2-chamber views were obtained. These images allowed for assessment of left ventricular systolic function and valve function. In the 5-chamber view pulsed wave Doppler was used to obtain pre-valve velocities in the left ventricular out flow tract just below the level of the valve. Continuous wave Doppler was then used to calculate the peak post valve velocity. This was confirmed using a D2 CWC transducer (Phillips, Netherlands) from the apex, right sternal edge and supra-sternal notch. Measurements were determined on line and averaged from three cardiac cycles or five if the patient was in atrial fibrillation.

Aortic sclerosis was defined as a thickened aortic valve on echocardiography in the absence of accelerated flow though the valve (peak jet velocity <2 m/s). The severity of aortic stenosis was graded according to American Heart Association and American College of Cardiology criteria using the peak transvalvular aortic valve velocity, and the mean and maximum aortic valve pressure gradients, the time velocity integral (TVI), the dimensionless index and the aortic valve area, calculated using the continuity equation.[129] Mild aortic stenosis was defined as a peak velocity of 2-3m/s, a mean gradient of less than 25mmHg and an aortic valve area >1.5cm^2: moderate aortic stenosis, peak velocity of 3-4m/s, a mean gradient of 25-40mmHg, aortic valve area 1.0-1.5cm^2: severe aortic stenosis, peak velocity >4m/s, mean gradient >40mmHg, aortic valve area <1.0cm^2. In our clinical laboratory, we have previously demonstrated a co-efficient of reproducibility of 0.32 m/s for the Doppler measurement of peak aortic valve velocity in patients with aortic stenosis.[30]

For patients participating in the CMR studies the results of echocardiograms performed within 6 months of their CMR scan were identified. These were conducted at a variety of different hospital however standard assessments of aortic stenosis severity were employed at all sites according to British Society of Echocardiography guidelines (http://www.bsecho.org/education/guidelines-and-protocols/). Furthermore the presence and severity of aortic regurgitation, mitral vale disease and tricuspid valve disease was assessed according to those same guidelines.

2.7 Image Analysis

Positron Emission Tomography

Regions of interest were drawn around the aortic valve, and the ascending and descending aortae on adjacent slices until their entire volume of each structure had been covered (Figure 2.1). Exact methods are discussed below. Mean and maximum SUV values were calculated for each slice and then for the tissue as a whole after averaging these values. However, SUV measurements in vascular structures are influenced by variation in 18F-FDG and 18F-NaF activity in the blood-pool. Therefore SUV measurements were divided by an averaged mean SUV value derived from 5 circular ROIs drawn in the central blood-pool of the superior vena cava. This provided mean and maximum tissue-to-background ratios (TBRs).[100, 103] Regions of interest were also drawn in the left main stem and the proximal portions of the left anterior descending, circumflex and right coronary arteries and maximum SUV and TBR values recorded.

Quantification of tracer uptake in the aortic valve

PET image quantification is usually performed in the axial, coronal or sagittal planes. However, the aortic valve is a complex 3-dimensional structure that does not align perfectly with any of these orthogonal planes, making accurate identification of the boundaries of the valve difficult using standard techniques. To try to overcome this, the PET and CT images were fused and analysed using a workstation (OsiriX version 3.5.1 64-bit; OsiriX Imaging Software, Geneva, Switzerland) that allows for rotation of the plane of view into the true axis of the valve. This is the first time such a technique has been described and it facilitated the more accurate delineation of regions of interest (ROI) around the valve as described below.

18F-NaF Analysis

The fused PET/CT image was rotated in a 3-dimensional multi-planar reconstruction (MPR) mode to provide a co-axial short-axis view of the aortic valve (Figure 2.1). Starting superiorly, a circular region of interest (ROI) was drawn around the aortic valve on 3-mm slices guided by anatomical information provided by CT and any obvious valvular calcification (Figure 2.2). Further ROIs were drawn on adjacent slices until the whole valve had been examined.

18F-FDG Analysis

The co-axial short-axis method was performed for 18F-FDG as described above. Whilst the pre-scan dietary restrictions aimed to minimize the difficulties cause by myocardial 18F-FDG uptake, we also explored two further image analysis approaches to define better and to assess more specifically the valvular uptake (Figure 2.1). In the long-axis technique, images were reoriented into a modified coronal view where it was hoped the boundaries of myocardial uptake would be more clearly observed and therefore avoided. In the center-valve technique, ROIs were again drawn on the co-axial short-axis view but in the center of the valve, thereby excluding the base of the valve leaflets and any potential incorporation of myocardial or aortic wall uptake.[132] For all techniques, measurements were taken on adjacent 3-mm slices, and mean and maximum SUV and TBR values calculated for the valve.

Quantification of tracer uptake in the aorta

For the aorta, circular ROIs were drawn around the ascending and descending aorta on adjacent 3-mm axial slices, from the arch down to the right pulmonary artery and diaphragm respectively. This provided mean and maximum SUV and TBR values. Uptake from surrounding

tissue spilling in to the aorta was avoided (Figure 2.2). Most commonly this was in the form activity in the thoracic vertebral column spilling in to the descending aorta. Uptake was not quantified in the aortic arch as that has previously been shown to be poorly reproducible.[102]

Quantification of tracer uptake in the coronary arteries

For 18F-NaF uptake, the coronary arteries were visually identified and regions of interest drawn around areas of maximal uptake in the left main stem, left anterior descending artery, circumflex artery and the right coronary artery (Figure 2.2). The maximum SUV value was recorded from these regions. It was not possible to determine the mean SUV values given the difficulty in identifying the exact borders of the coronary arteries on the non-contrast enhanced scans. SUV values were used to calculate the maximum TBR. Quantification of 18F-FDG uptake was performed as for 18F-NaF but restricted to the proximal and mid-portions of the coronary vessels.[106] Difficulties were still encountered as a result of the pervasive myocardial uptake observed with this tracer and coronary activity was only quantified in areas where myocardial uptake could be confidently avoided.

Figure 2.1. Method for the quantification of 18F-NaF and 18F-FDG uptake in the aortic valve.

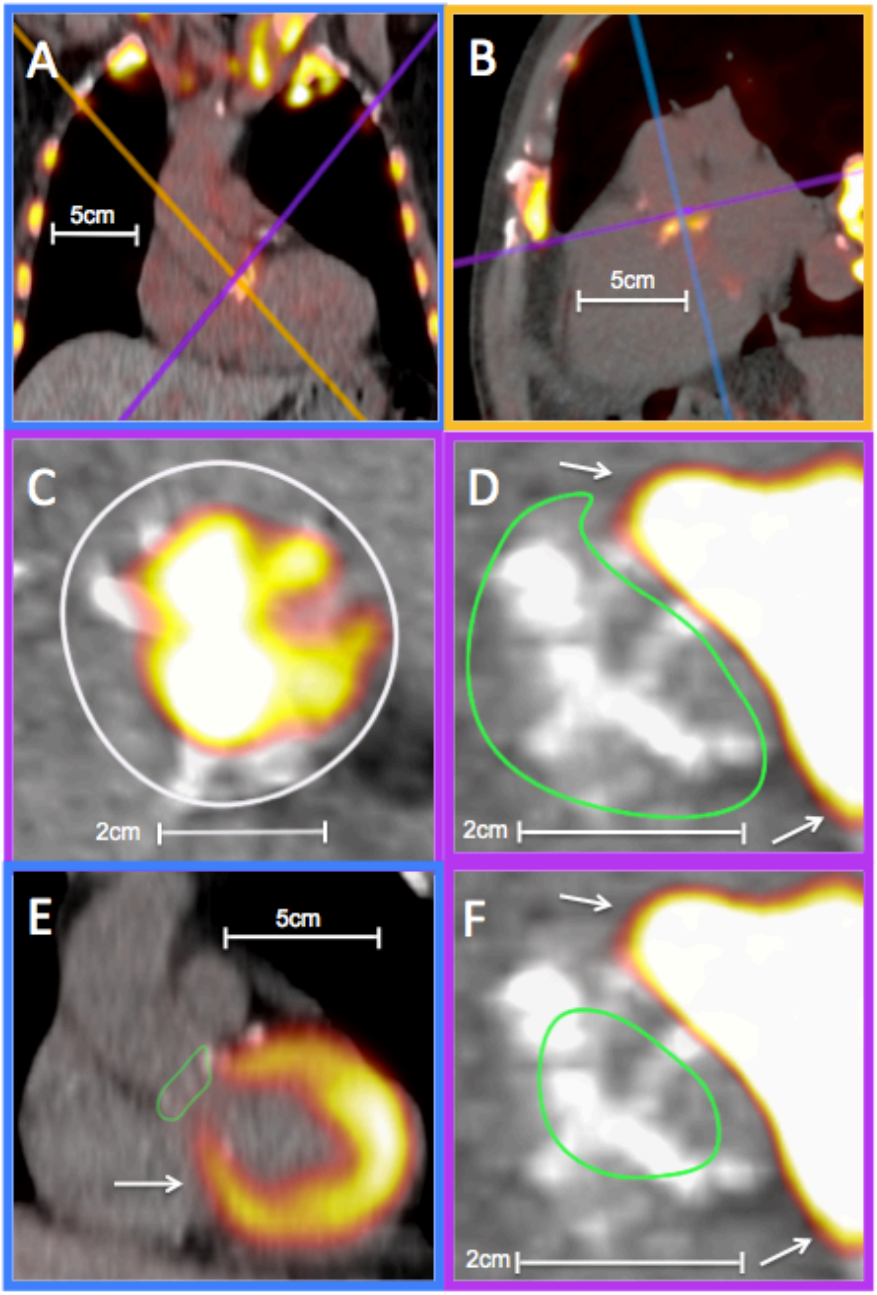

18F-NaF A. Coronal view (blue axis) of the thorax: note the intense 18F-NaF uptake (white, red and yellow areas) in the calcified aortic valve as well as in the ribs, clavicles and arch of the aorta. The purple axis has been rotated so that it lies perpendicular to the aorta and parallel to the aortic valve. **B.** Modified sagittal view of the valve (yellow axis). The purple axis has again been rotated so that it lies perpendicular to the aorta and parallel to the aortic valve. **C.** A co-axial short axis view of the aortic valve is now obtained along the purple axis. White areas denote areas of existing calcium whilst yellow/red region denote areas of increased 18F-NaF uptake. A region of interest has been drawn around the valve (green lines).

18F-FDG D. *Short-axis technique.* The imaging plane has been reorientated as described for 18F-NaF to provide the co-axial short axis view shown. This patient has intense myocardial 18F-FDG uptake, which appears to spill in to the aortic valve (white arrows) and makes appreciation of the less intense activity in the valve difficult. In the short-axis technique the green ROI has been drawn to include as much of the valve as possible whilst avoiding the myocardial activity.

E. *Centre-valve technique.* In the same patient the ROI has been drawn in the centre of the valve well away from myocardial uptake around the periphery. **F** *Long-axis technique:* an ROI has been drawn on the modified coronal images attempting to avoid the myocardial uptake.

Figure 2.2. Regions of interest in different tissues on fused PET/CT scans
A. Circular regions of interest drawn around the aortic valve using the short axis technique for the assessment of 18F-NaF activity
B. Regions of interest drawn around the ascending and descending aortae and the left anterior descending coronary artery for the assessment of 18F-NaF activity

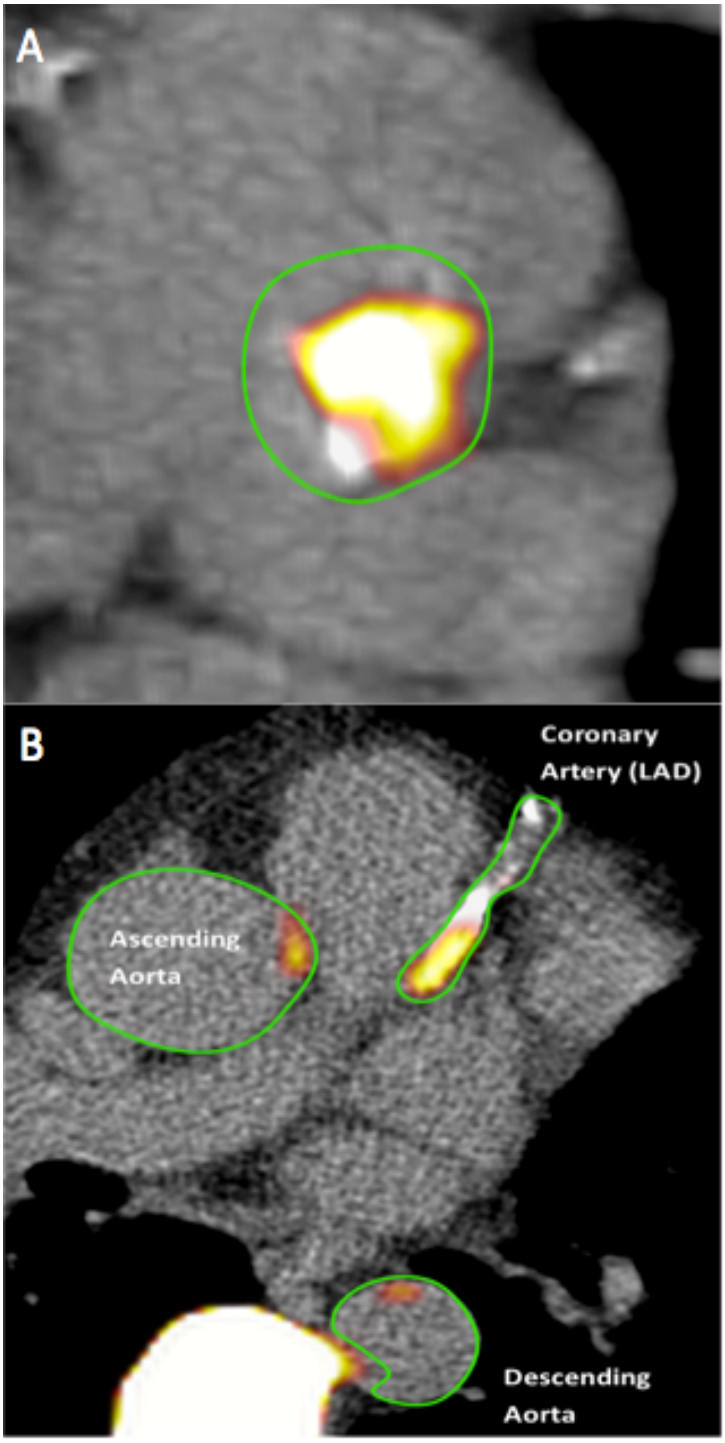

Quantification of Aortic Valve and Coronary Calcium Scoring

Evaluation of the calcium score was performed using calcium score analysis software (VScore, Vital Images, Minnetonka, USA). Vessel specific and total Agatston calcium scores were calculated as described previously. [133] Coronary calcium was defined as an area greater than or equal to 1 mm^2 in the axial plane in the course of a coronary artery with an attenuation threshold-value of greater than or equal to 130 Hounsfield units. Regions of interest were defined in each vessel (left main stem, left anterior descending artery, circumflex artery, right coronary artery) on each slice by one trained observer. The Agatston score was calculated in Agatston units (AU) by multiplying the area of a region of interest by a weighting factor selected dependent on the peak signal within the region of interest. Vessel and total scores were obtained by summing the weighted scores.

For the aortic valve regions of interest were drawn around areas of calcification in the valve on adjacent slices. Care was taken to avoid calcium in the aorta and mitral valve annulus. Agatston scores were calculated as above for the valve as a whole on the basis of these regions.

Cardiovascular Magnetic Resonance

For quantification of LV function and volumes, the endocardial and epicardial contours were semi-automatically applied in end-systole and end-diastole using dedicated software (CMR Tools, Cardiovascular Imaging Solutions, London). LV mass was calculated from the total end-diastolic myocardial volume multiplied by the specific gravity of the myocardium (1.05 g/mL). LV mass and volumes were indexed to body surface area, age and gender, and were considered abnormal if they were outside the 95thpercentile of the normal range published by Maceira and colleagues.[134] Ejection fractions were calculated and considered impaired if below the 95th percentile of the normal range

published by Maceira et al.[134] This quantification was performed by multiple different experienced operators over the course of the six years that the scans were performed. However all operators underwent a standardized period of training and used the same analysis technique. Each operator underwent an initial period of validation before analyzing scans independently. We did not examine our inter-scan or inter observer measures of reproducibility or validate our volumes against other measures such as stroke volume calculated on velocity mapping. This is a limitation of our study.

Maximal wall thickness was measured by observers from short-axis views of the LV in end diastole, and its position with reference to the 17-segment model of the LV recorded.[135] Measurements were made so that they were perpendicular to the compacted myocardium with right and left ventricular trabeculations excluded from the measurements. Aortic stenosis severity was assessed using CMR-derived planimetry of aortic valve area by one experienced operator (MD). This technique has been validated against echocardiographic measures of aortic stenosis severity.[136] In accordance with American Heart Association/American College of Cardiology guidelines, aortic stenosis was graded using the aortic valve area as follows: mild, >1.5 cm^2; moderate, 1.5-1.0 cm^2; and severe, <1.0 cm.[129]

The presence and pattern of LGE was assessed by two independent observers (Francisco Alpendurado and Raad Mohiaddin) who were blinded to the clinical data including valve severity, coronary anatomy and outcomes. A third blinded observer adjudicated where there was a disparity between the initial two observers (Sanjay Prasad). Patients with a mixed pattern of LGE were categorized according to the predominant pattern of fibrosis. LGE mass was calculated semi-automatically by a single operator using MRI-mass software (Qmass ,Medis, Leiden Netherlands). The endocardial and epicardial borders were traced for each short-axis slice. A region of interest averaging 50 mm^2 was defined within normal remote myocardium in an area with uniform

myocardial suppression free of artifacts. A multi-pass region-growing algorithm was used to identify the fibrotic boundaries based on the "full width half maximum" technique and fibrosis was expressed as present or absent, and its extent was quantified as a percentage of total LV mass (% LGE mass). It has been pointed out that the algorithm used by the Medis software may not actually represent the full width half maximum technique as it is also based on the signal in the nulled myocardium. Nevertheless the same software was used for all studies to ensure consistency in this measurement.

2.6 Statistics

Continuous variables were expressed as mean ± SD and compared using unpaired Student's *t*-test or one-way analysis of variance where appropriate. Categorical variables were expressed as percentages and analyzed using the χ^2-test**.** Correlations between normally distributed data were performed using Pearson's correlation, whilst Spearman's correlation was used for non-parametric data. A two-sided $P<0.05$ was regarded as statistically significant.

Reproducibility Studies

Measures of reproducibility for the PET studies in this thesis are based on the operators analyzing the same scans on different occasions. They effectively represent inter and intra observer variation in conducting the measurements. PET scans were not themselves repeated so we have not assessed the test/retest repeatability. Reproducibility measures are not presented for the CMR studies. The 95% normal range for differences between sets of SUV and TBR measurements (the limits of agreement) were estimated by multiplying the standard deviation of the mean difference by 1.96.[137] Intra-class correlation coefficients with 95% confidence intervals were calculated for intra-observer and inter-observer variation. Statistical analysis was performed using SPSS version 18 (SPSS Inc, Chicago, Illinois) unless stated. A two-sided $P<0.05$ was regarded as statistically significant.

CHAPTER 3

Assessment of valvular calcification and inflammation by positron emission tomography in patients with aortic stenosis

Published by **Dweck MR**, Jones C, Joshi N, Fletcher AM, Richardson H, White A, Marsden M, Pessotto R, Clark JC, Wallace WA, Salter DM, McKillop G, van Beek EJR, Boon NA, Rudd JHF, Newby DE. **Circulation** 2012;125(1):76-86.

3.1 Summary

Background.

The pathophysiology of aortic stenosis is incompletely understood and the relative contributions of valvular calcification and inflammation to disease progression are unknown.

Methods.

Patients with aortic sclerosis and mild, moderate and severe stenosis were prospectively compared to age and sex-matched control subjects. Aortic valve severity was determined by echocardiography. Calcification and inflammation in the aortic valve were assessed by sodium 18-fluoride (18F-NaF) and 18-fluorodeoxyglucose (18F-FDG) uptake using positron emission tomography.

Results.

One hundred and twenty one subjects (20 controls; 20 aortic sclerosis; 25 mild, 33 moderate and 23 severe aortic stenosis) were administered both 18F-NaF and 18F-FDG. Quantification of tracer uptake within the valve demonstrated excellent inter-observer reproducibility with no fixed or proportional biases and limits of agreement of ±0.21 (18F-NaF) and ±0.13 (18F-FDG) for maximum tissue-to-background ratios (TBR). Activity of both tracers was higher in patients with aortic stenosis than control subjects (18F-NaF: 2.87±0.82 *vs* 1.55±0.17; 18F-FDG: 1.58±0.21 *vs* 1.30±0.13; both P<0.001). 18F-NaF uptake displayed a progressive rise with valve severity (r^2=0.540, P<0.001) with a more modest increase observed for 18F-FDG (r^2=0.218; P<0.001). Amongst patients with aortic stenosis, 91% had increased 18F-NaF (>1.97) and 35% increased 18F-FDG (>1.63) uptake. A weak correlation between the activities of these tracers was observed (r^2= 0.174, P<0.001).

Conclusions.

Positron emission tomography is a novel, feasible and repeatable approach to the evaluation of valvular calcification and inflammation in patients with aortic stenosis. The frequency and magnitude of increased tracer activity correlates with disease severity, and is strongest for 18F-NaF.

3.2 Introduction

Calcific aortic stenosis is the commonest form of valvular heart disease in the western world and represents a major healthcare burden that is projected to increase with an ageing population.[131] However, the underlying pathophysiology remains incompletely defined, and there are currently no effective medical treatments capable of altering its course.[2] Unfortunately histological studies are limited by the availability of valve tissue from patients with advanced disease and do not lend themselves to the longitudinal study of disease progression. Alternative techniques are therefore required to investigate the pathogenesis and progression of this condition.

Positron emission tomography (PET) combined with computed tomography (CT) is a non-invasive imaging technique that allows the identification and quantification of specific biochemical processes within small anatomic structures, such as the aortic valve. Furthermore two common PET tracers target calcification and inflammation, which are believed to play a key role in the development of the disease. PET/CT therefore holds considerable promise as a means of investigating the pathophysiology of aortic stenosis.

18F-Flurodeoxyglucose (18F-FDG) is a glucose analogue that is taken up into cells by glucose transport proteins and enters the glycolytic metabolic pathway. Following the initial hexokinase step, 18F-FDG-6-phosphate cannot be metabolized further and becomes trapped within cells that have high metabolic requirements, such as macrophages. PET imaging using 18F-FDG has become an established means of quantifying vascular inflammation in both the aorta and carotid arteries,[98, 99] correlating with plaque macrophage burden,[100] and symptomatic status.[99] 18F-sodium fluoride (18 F-NaF) is an alternative PET tracer that is directly incorporated into exposed bone crystal (hydroxyapatite) via an exchange mechanism with hydroxyl groups.[113] It is therefore thought to

detect areas of novel calcification and regions of calcium remodelling, and is used clinically for the detection of primary osteoblastic tumours and bone metastases.[110] More recently studies have described 18F-NaF uptake as a marker of calcification within atherosclerotic plaque,[111, 112] however to date this tracer has not been used to study patients with aortic stenosis.

In this PET study we investigated 18F-NaF and 18F-FDG uptake in the valves of patients with aortic stenosis, with three major aims: to examine the feasibility of this approach, to establish its reproducibility, and to assess the relative importance of inflammation and calcification at different stages of the disease.

3.3 Methods

As described in Chapter 2 patients over 50 years of age with aortic sclerosis and mild, moderate and severe aortic stenosis were recruited prospectively from the outpatient department of the Royal Infirmary of Edinburgh and compared to age- and sex-matched control subjects with a normal aortic valve and similar range of co-morbidity.

Echocardiography

Valve disease severity was assessed using echocardiography in all patients by a single dedicated research ultrasonographer on a dedicated machine as described in Chapter 2. Aortic sclerosis was defined as a thickened aortic valve on echocardiography in the absence of accelerated flow though the valve (peak jet velocity <2 m/s). The severity of aortic stenosis was graded according to American Heart Association and American College of Cardiology criteria using the peak transvalvular aortic valve velocity, and the mean and maximum aortic valve pressure gradients.[129] Aortic stenosis severity was also assessed using the time velocity integral (TVI), the dimensionless index and the aortic valve area, calculated using the continuity equation.

Positron Emission Tomography and Computed Tomography

As described in Chapter 2 combined PET/CT scans of the aortic valve were performed using 18F-FDG and 18F-NaF on two occasions in close succession using a hybrid scanner. Dietary restrictions were applied prior to the 18F-FDG scan and myocardial uptake measured. Patients were then categorised in to dietary compliance and non-compliance and to high and low myocardial 18F-FDG uptake (Chapter 2).

Quantification of tracer uptake in the aortic valve

PET image quantification was performed as described in Chapter 2. Breifly the short-axis method was used for 18F-NaF and 18F-FDG. Whilst the pre-scan dietary restrictions aimed to minimize the difficulties cause by myocardial 18F-FDG uptake, we also explored two further image analysis approaches to define better and to assess more specifically the valvular uptake: the long axis and centre-valve techniqes (Chapter 2, Figure 2.1). For all techniques, measurements were taken on adjacent 3-mm slices, and mean and maximum SUV and TBR values calculated for the valve.

Reproducibility studies

Twenty-five patients with a range of aortic valve disease were selected at random from the cohort. Having established the aortic valve image analysis methodology, all scans from these patients were analyzed independently by two trained observers (MD, CJ). For each technique, this provided measures of inter-observer reproducibility for mean and maximum SUV and TBR values. In order to assess intra-observer variation, both observers repeated the analyses at least two weeks later to minimize recall bias.

***Ex-vivo* studies**

One patient underwent an aortic valve replacement 3 months after their PET scans. The valve was harvested and incubated with 18F-FDG, Dulbecco's modified eagle medium (Invitrogen, Paisley, UK) and 10% fetal calf serum for 90 min before PET/CT imaging using the same protocol as the *in vivo* clinical scans. The next day, PET/CT imaging was repeated after incubation with 18F-NaF for 60 min. Finally the valve was fixed in formalin and decalcified using ethylene diamine tetracetic acid before immunohistochemistry was performed to examine for macrophage accumulation (CD68) and active calcification (osteocalcin).

Statistical Methods

Continuous variables were expressed as mean ± standard deviation (SD) and compared using unpaired Student's t -test or one-way analysis of variance where appropriate. All continuous variables were tested for normal distribution using the Shapiro-Wilk test. Where data were not normally distributed, they were presented as the median ± interquartile range. Categorical variables were expressed as percentages and analyzed using the χ^2-test**.** Correlations between normally distributed data were performed using Pearson's correlation, and presented as r^2 values. Spearman's correlation was used for non-parametric data. Differences between sets of SUV and TBR measurements were calculated along with limits of agreement and Intra-class correlation coefficients to provide measures of intra and inter-observer variation.

3.4 Results

Patient Population

A total of 121 patients were recruited (age 72±8 years, 69% male, peak aortic valve velocity 2.8±1.2 m/s) and had both 18F-NaF (66±7 min after 124±10 MBq) and 18F-FDG (94±7 min after 197±14 MBq) scans of their aortic valve less than one month apart. This cohort comprised 20 control subjects, 20 patients with aortic sclerosis, and 25 patients with mild, 33 with moderate and 23 with severe aortic stenosis. Patients were well-matched for age, sex and co-morbidity (Table 3.1).

Dietary Restrictions & Blood Pool Uptake

Average myocardial SUV across the entire cohort was 4.6±3.6 and dietary restrictions effectively suppressed 18F-FDG myocardial uptake (SUV<5) in 67% of patients, similar to that observed in previous studies.[106] Based on dietary diaries, 61% of patients complied with the dietary restrictions and had lower myocardial 18F-FDG uptake than non-compliers (SUV 3.2±2.3 *vs* 6.7±4.2; P<0.001). Across the cohort blood-pool uptake in the SVC was 0.99±0.18 for 18F-NaF and 1.26±0.20 for 18F-FDG.

Table 3.1. Baseline subject characteristics.

	Control	Aortic Sclerosis	Aortic Stenosis			P Value
			Mild	*Moderate*	*Severe*	
Number	20	20	25	33	23	-
Age (years)	70 ±8	71 ±9	73 ±8	72 ±7	73 ±11	0.726
Male Sex (%)	65	75	60	76	65	0.687
Body Mass Index (kg/m^2)	26 ±3	29 ±6	27 ±3	29 ±5	28 ±4	0.051
Ischemic Heart Disease (%)	35	40	48	36	22	0.445
Cardiovascular Disease (%)	35	45	48	39	22	0.373
Smoking (%)	50	35	48	52	61	0.566
Diabetes Mellitus (%)	10	15	20	13	17	0.886
Hypertension (%)	40	55	64	73	61	0.203
Chronic kidney disease Stage 3 and above (%)	20	20	20	24	30	0.927
Creatinine (mg/dL)	0.91 ±0.20	0.99 ±0.26	0.97 ±0.32	1.05 ±0.26	1.09 ±0.41	0.314
Urea (BUN) (mg/dL)	20.2 ±5.1	19.0 ±6.8	20.5 ±10.4	21.0 ±4.6	22.3 ±7.8	0.651
Calcium (mg/dL)	9.2 ±0.2	9.2 ±0.7	9.2 ±0.5	9.3 ±0.4	9.5 ±0.9	0.228
Phosphate (mg/dL)	3.7 ±0.5	3.6 ±0.6	3.6 ±0.5	3.6 ±1.5	3.6 ±0.4	0.973
Alkaline Phosphatase (U/L)	75 ±19	85 ±30	79 ±21	82 ±22	102 ±89	0.314
Total Cholesterol (mg/dL)	191 ±42	194 ±53	210 ±59	171 ±41	203 ±52	0.040*
LDL Cholesterol (mg/dL)	98 ±44	101 ±41	121 ±47	89 ±37	119 ±48	0.036*
HDL Cholesterol (mg/dL)	58 ±15	60 ±35	57 ±19	49 ±11	49 ±13	0.165
Triglycerides (mg/dL)	63 ±35	72 ±33	69 ±41	77 ±52	82 ±45	0.613
Statin therapy (%)	35	50	52	67	57	0.262
ACE inhibitor therapy (%)	35	40	52	36	30	0.604

Mean ±SD. BUN- Blood urea nitrogen, AU- Agatston unit, LDL- low density lipoprotein, HDL- high density lipoprotein, ACE- angiotensin converting enzyme.
*There was no correlation between peak aortic valve velocity and either serum total cholesterol (Pearson's correlation, r^2= 0.000; p= 0.976) or LDL cholesterol (r^2 = 0.007, p= 0.36) concentrations.

Reproducibility Studies

18F-Sodium Fluoride

Amongst the 25 patients selected (age 74±10 years, 64% male, aortic valve peak velocity 3.8±1.1 m/s), aortic valve 18F-NaF uptake showed excellent inter-observer reproducibility for the mean and maximum SUV and TBR values. There were no fixed or proportional biases, and the majority of data fell within narrow limits of agreement: ±0.20 for mean and ±0.21 for maximum TBR measurements (Table 3.2, Figure 3.1). Limits of agreement for intra-observer measurements were similarly good whilst intra-class coefficients for inter and intra-observer reproducibility were all >0.95 indicating excellent agreement (Table 4).

18F-Fluorodeoxyglucose

Avoiding myocardial uptake was difficult using the short and long-axis techniques, particularly for the latter. Reproducibility statistics reflected this and demonstrated that the variability was much greater than for 18F-NaF. The inter-observer limits of agreement for the short-axis technique were ±0.28 and ±0.72 for the mean and maximum TBR values respectively, and were ±0.78 and ±1.18 using the long-axis approach (Table 3.2, Figure 3.1). The intra-class coefficients for the short-axis technique were 0.76 and 0.59 for the mean and maximum TBR values respectively, and were 0.39 and 0.52 using the long-axis approach (Table 3.3). Intra-observer reproducibility measures were similarly poor. The reason for better measures on reproducibility for CJ than MD using the long-axis technique is not clear.

The centre-valve analysis was more reproducible. There were no fixed or proportional biases in the differences between inter-observer measurements and the data fell within narrow limits of

agreement: ±0.11 for mean and ±0.13 for maximum TBR values (Table 3.2, Figure 3.1). Intra-observer reproducibility was similarly good whilst intra-class coefficients were all >0.90 indicating excellent agreement (Tables 3.2 & 3.3).

There were concerns that the centre-valve technique might underestimate 18F-FDG activity in the valve by excluding the valve ring. However, there was no difference between mean uptake values calculated using the centre-valve technique and the short-axis method (centre-valve TBR: 1.43±0.17; short-axis: 1.47±0.45; P=0.473). Maximum TBR values were lower using the former approach (centre-valve: 1.60±0.20 *vs* short-axis: 1.80±0.45; P=0.041). However, this difference was no longer apparent when patients with high myocardial uptake (n=11) were excluded from the analysis (centre-valve 1.56±0.18 *vs* short-axis 1.64±0.20; P=0.245) reflecting the wide limits of agreement (±1.05) for the short-axis technique when myocardial suppression was poor. By contrast, limits of agreement for the centre-valve technique were equally good in patients with low and high myocardial uptake (±0.13 *vs* ±0.14 respectively; P=0.919). Given this and other advantages, subsequent analysis of the entire cohort was performed using the centre-valve method for 18F-FDG.

Table 3.2 Inter and intra-observer reproducibility statistics for 18F-NaF and 18F-FDG quantification in the aortic valve

	Mean Difference between Aortic Valve SUV & TBR measurements		
	Inter-observer	Intra-observer	
		(MD)	(CJ)
Mean SUV			
18F-NaF short-axis	0.04 (-0.12 to 0.20)	0.02 (-0.10 to 0.14)	0.05 (-0.14 to 0.24)
18F-FDG short-axis	0.02 (-0.18 to 0.20)	-0.01 (-0.10 to 0.12)	-0.02 (-0.19 to 0.15)
18F-FDG long-axis	0.05 (-0.57 to 0.67)	0.05 (-0.37 to 0.47)	0.00 (-0.14 to 0.14)
18F-FDG centre-valve	0.01 (-0.05 to 0.07)	0.01 (-0.05 to 0.07)	-0.02 (-0.16 to 0.12)
Maximum SUV			
18F-NaF short-axis	0.02 (-0.16 to 0.20)	0.04 (-0.11 to 0.19)	0.00 (-0.19 to 0.19)
18F-FDG short-axis	0.02 (-0.80 to 0.84)	-0.11 (-0.64 to 0.42)	-0.09 (-0.89 to 0.72)
18F-FDG long-axis	-0.03 (-1.06 to 1.00)	0.12 (-0.44 to 0.68)	0.10 (-0.41 to 0.61)
18F-FDG centre-valve	0.03 (-0.07 to 0.13)	0.02 (-0.13 to 0.17)	-0.06 (-0.26 to 0.14)
Mean TBR			
18F-NaF short-axis	0.07 (-0.13 to 0.27)	-0.01 (-0.15 to 0.17)	0.05 (-0.17 to 0.27)
18F-FDG short-axis	0.06 (-0.22 to 0.34)	0.00 (-0.15 to 0.15)	0.01 (-0.12 to 0.14)
18F-FDG long-axis	0.06 (-0.72 to 0.84)	0.07 (-0.50 to 0.64)	0.02 (-0.22 to 0.26)
18F-FDG centre-valve	-0.01 (-0.12 to 0.10)	0.02 (-0.06 to 0.10)	-0.01 (-0.07 to 0.05)
Maximum TBR			
18F-NaF short-axis	0.02 (-0.19 to 0.23)	-0.04 (-0.16 to 0.24)	0.00 (-0.21 to 0.21)
18F-FDG short-axis	0.06 (-0.66 to 0.78)	-0.09 (-0.39 to 0.57)	0.07 (-0.06 to 0.20)
18F-FDG long-axis	0.01 (-1.17 to 1.19)	0.12 (-0.50 to 0.74)	0.06 (-0.33 to 0.39)
18F-FDG centre-valve	-0.02 (-0.15 to 0.11)	0.02 (-0.11 to 0.15)	-0.05 (-0.14 to 0.04)

Mean difference between standard uptake value (SUV) and tissue-to-background ratio (TBR) measurements for 18F-NaF valve uptake using the short-axis technique and 18F-FDG uptake using the short-axis, centre-valve and long-axis techniques (95% confidence intervals in brackets). The short-axis technique for 18F-NaF and the centre-valve technique for 18F-FDG display no fixed proportional bias with narrow limits of agreement.

Table 3.3. Intra-class coefficient values for 18F-NaF and 18F-FDG quantification in the aortic valve

	ICC Values comparing Aortic Valve SUV and TBR measurements		
	Inter-observer	Intra-observer	
		MD	CJ
Mean SUV			
18F-NaF short-axis	0.98 (0.96-0.99)	0.99 (0.98-1.00)	0.98 (0.94-0.99)
18F-FDG short-axis	0.95 (0.88-0.98)	0.98 (0.96-0.99)	0.96 (0.91-0.98)
18F-FDG long-axis	0.58 (0.24-0.79)	0.68 (0.39-0.84)	0.96 (0.91-0.98)
18F-FDG centre-valve	0.99 (0.97-0.99)	1.00 (0.99-1.00)	0.99 (0.98-1.00)
Maximum SUV			
18F-NaF short-axis	0.99 (0.99-1.00)	1.00 (0.99-1.00)	0.99 (0.98-1.00)
18F-FDG short-axis	0.62 (0.30-0.81)	0.88 (0.75-0.95)	0.58 (0.24-0.79)
18F-FDG long-axis	0.53 (0.18-0.76)	0.77 (0.54-0.89)	0.80 (0.60-0.91)
18F-FDG centre-valve	0.98 (0.94-0.99)	0.98 (0.95-0.99)	0.96 (0.90-0.98)
Mean TBR			
18F-NaF short-axis	0.98 (0.96-0.99)	0.99 (0.97-0.99)	0.97 (0.93-0.99)
18F-FDG short-axis	0.76 (0.52-0.89)	0.94 (0.86-0.97)	0.94 (0.87-0.97)
18F-FDG long-axis	0.39 (0.01-0.68)	0.56 (0.22-0.78)	0.93 (0.85-0.97)
18F-FDG centre-valve	0.96 (0.90-0.98)	0.97 (0.93-0.99)	0.84 (0.66-0.92)
Maximum TBR			
18F-NaF short-axis	0.99 (0.99-1.00)	0.99 (0.99-1.00)	0.99 (0.99-1.00)
18F-FDG short-axis	0.59 (0.26-0.80)	0.89 (0.76-0.95)	0.71 (0.44-0.86)
18F-FDG long-axis	0.52 (0.17-0.76)	0.85 (0.69-0.93)	0.92 (0.83-0.97)
18F-FDG centre-valve	0.92 (0.83-0.97)	0.94 (0.87-0.97)	0.91 (0.80-0.96)

Intra-class correlation coefficient (ICC) values (95% confidence intervals in parentheses) for the short-axis 18F-NaF technique and the centre-valve 18F-FDG method. SUV, standard uptake value; TBR, tissue-to-background ratio.

Figure 3.1 Bland-Altman plots of inter-observer variability

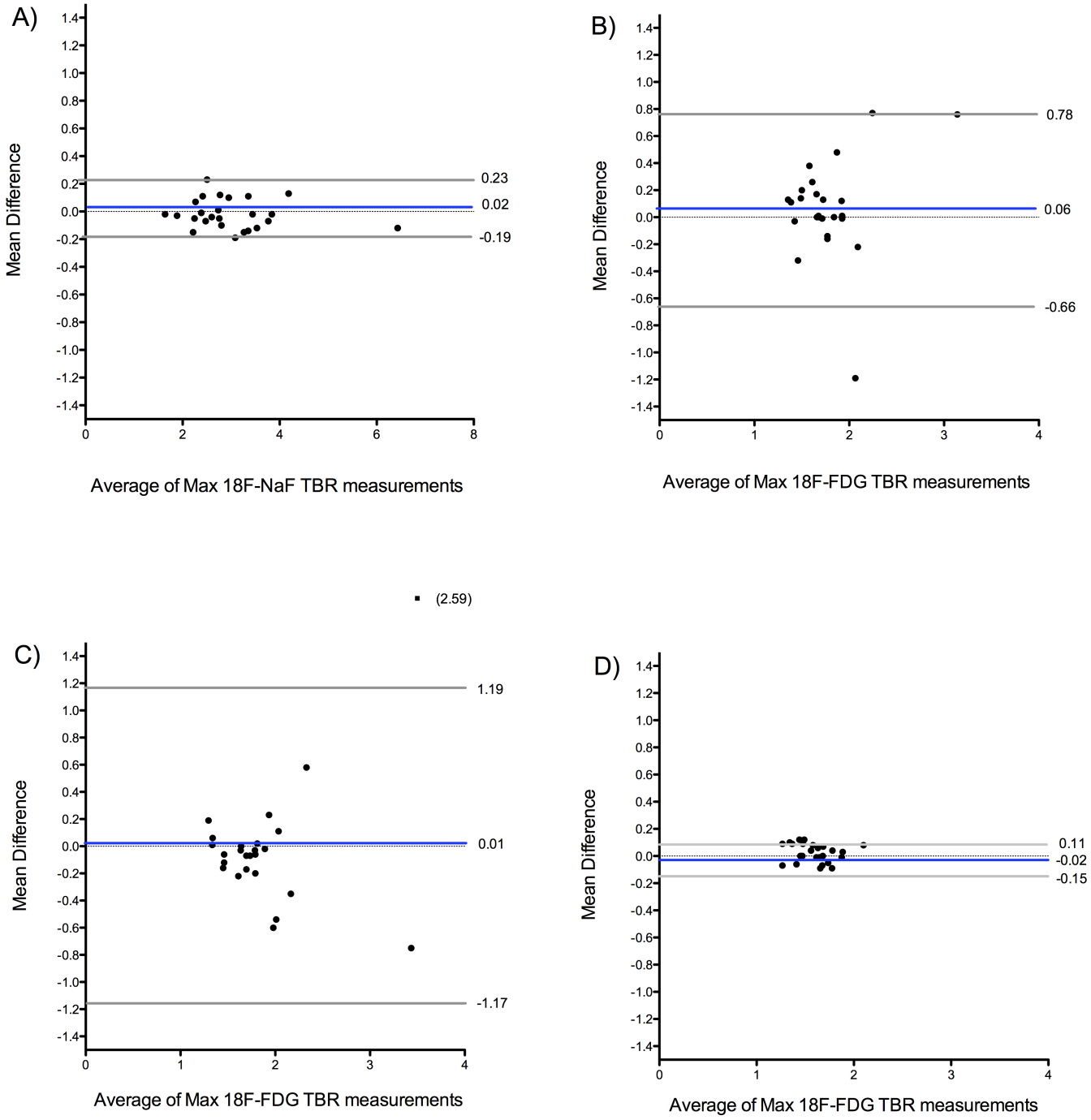

A) Maximum 18F-NaF tissue-to-background ratio (TBR) values using the short-axis technique. The central line is the mean difference between the two analyses, which does not show any fixed or proportional biases. The dotted lines show the limits of agreement (mean of the differences ± 1.96 × SD), which are narrow.
Maximum 18F-FDG values using the short-axis **(B),** long-axis **(C)** and centre-valve techniques **(D).** Note the wide limits of agreement for the short-axis and long axis 18F-FDG techniques but the excellent measures of reproducibility for the centre-valve technique. Also note there is a single outlier not plotted on the long-axis graph (C): the mean difference for this patient is given in brackets.

Aortic Valve Uptake

Sodium 18Fluoride

Focal 18F-NaF uptake was observed in the valves of patients with calcific aortic valve disease in areas overlying, adjacent to and remote from existing calcification. Areas of established calcium were also frequently observed in the absence of increased 18F-NaF activity (Figure 3.2). Compared to control subjects, valvular 18F-NaF uptake was higher in patients with both aortic sclerosis (max TBR: 1.55±0.17 vs 1.92±0.31; p<0.001) and aortic stenosis (max TBR: 1.55±0.17 *vs* 2.87±0.82; P<0.001). The highest maximum TBR value in the control group was 1.97, which was used to divide patients with aortic valve disease into those with increased 18F-NaF uptake (>1.97) and those without (≤1.97). Overall 45% of patients with aortic sclerosis and 91% of those with aortic stenosis had increased uptake. The proportion of patients with increased activity rose sharply with increasing disease severity such that 100% of patients with severe disease had increased uptake (Table 3.4).

All measures of 18F-NaF uptake displayed a progressive rise with increasing aortic jet velocity (max TBR: r^2=0.540, P<0.001; Table 3.4, Figure 3.3), the aortic valve calcium score (r^2= 0.641, P<0.001) and other echocardiographic measures of aortic stenosis severity (time-velocity integral: r^2= 0.546, p<0.001; aortic valve area: r^2= 0.387, p<0.001; dimensionless index: r^2=0.527, p<0.001).

18Fluorodeoxyglucose

18F-FDG showed a more diffuse pattern of activity within the valve (Figure 3.2) and compared to control subjects, uptake was increased in patients with aortic sclerosis (max TBR: 1.30±0.13 *vs* 1.47±0.15; P<0.001) and aortic stenosis (max TBR: 1.30±0.13 *vs* 1.58±0.21; P<0.001). The highest maximum TBR value in the control group was 1.63, which was used to divide patients with aortic valve disease into those with increased 18F-FDG uptake (>1.63) and those without (≤1.63). Overall

20% of patients with aortic sclerosis and 35% of patients with aortic stenosis had increased uptake. The proportion of patients with increased activity in the valve again rose with increasing aortic valve disease, however this rise was more gradual than for 18F-NaF with only 52% of patients with severe disease demonstrating increased activity (Table 3.4).

All measures of 18F-FDG activity displayed a progressive rise with increasing aortic jet velocity (max TBR: r^2=0.218, P<0.001; Table 3.4, Figure 3.3), the aortic valve Agatston score (r^2= 0.138, p<0.001) and other echocardiographic measures of aortic stenosis (time-velocity integral: r^2= 0.246, p<0.001; aortic valve area: r^2= 0.184, p<0.001; dimensionless index: r^2= 0.229; p<0.001). These correlations were weaker and more modest than for 18F-NaF. A modest correlation was also observed between valvular 18F-NaF and 18F-FDG activities (max TBR: r^2= 0.174, P<0.001).

Figure 3.2 18F-NaF and 18F-FDG uptake in patients with aortic stenosis.

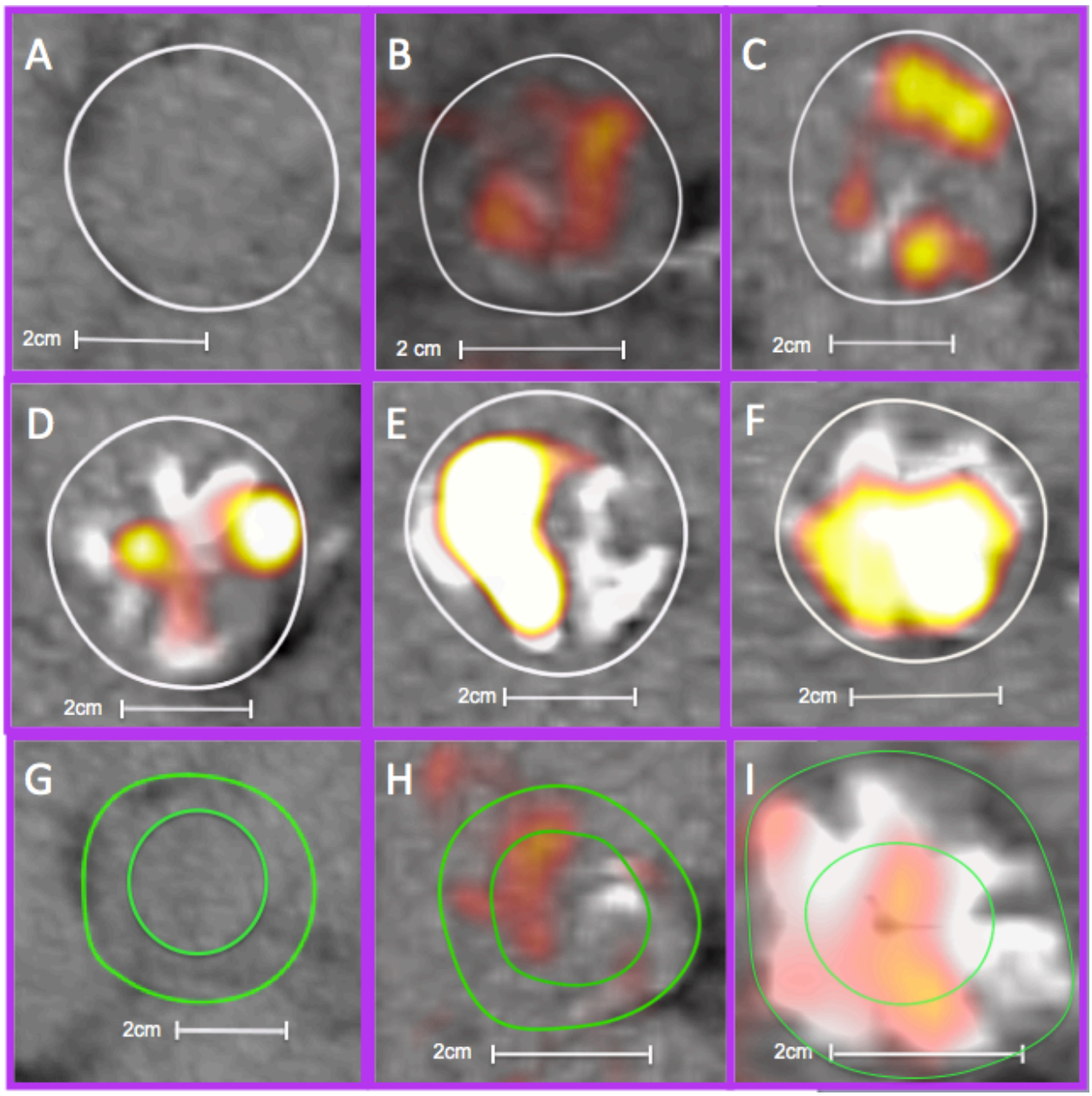

18F-NaF. Fused PET/CT scans demonstrating uptake of 18F-NaF on co-axial short axis views of the aortic valve in patients with a normal aortic valve **(A),** aortic sclerosis **(B)**, and mild **(C)**, moderate **(D)** and severe aortic stenosis **(E & F)**. White areas show regions of existing calcium whilst yellow and red areas show areas of 18F-NaF uptake. Focal areas of uptake are observed in areas overlying existing calcium as well as in areas remote from it. Furthermore areas of existing calcification are observed in the absence of overlying 18F-NaF uptake. Note the increased activity with increasing severity of valve disease. Regions of interest have been drawn around the periphery of the valve (white lines) using the short-axis technique.
18F-FDG Fused PET/CT scans demonstrating uptake of 18F-FDG on co-axial short axis views of the aortic valve in patients with a normal aortic valve **(G),** mild aortic stenosis **(H)**, and severe aortic stenosis **(I)**. Patients all have excellent myocardial suppression allowing uptake to be visualized in the patients with aortic valve disease. Regions of interest have been drawn using both the short-axis and centre-valve techniques (green lines).

Figure 3.3 Uptake of 18F-FDG and 18F-NaF according to the severity of aortic stenosis

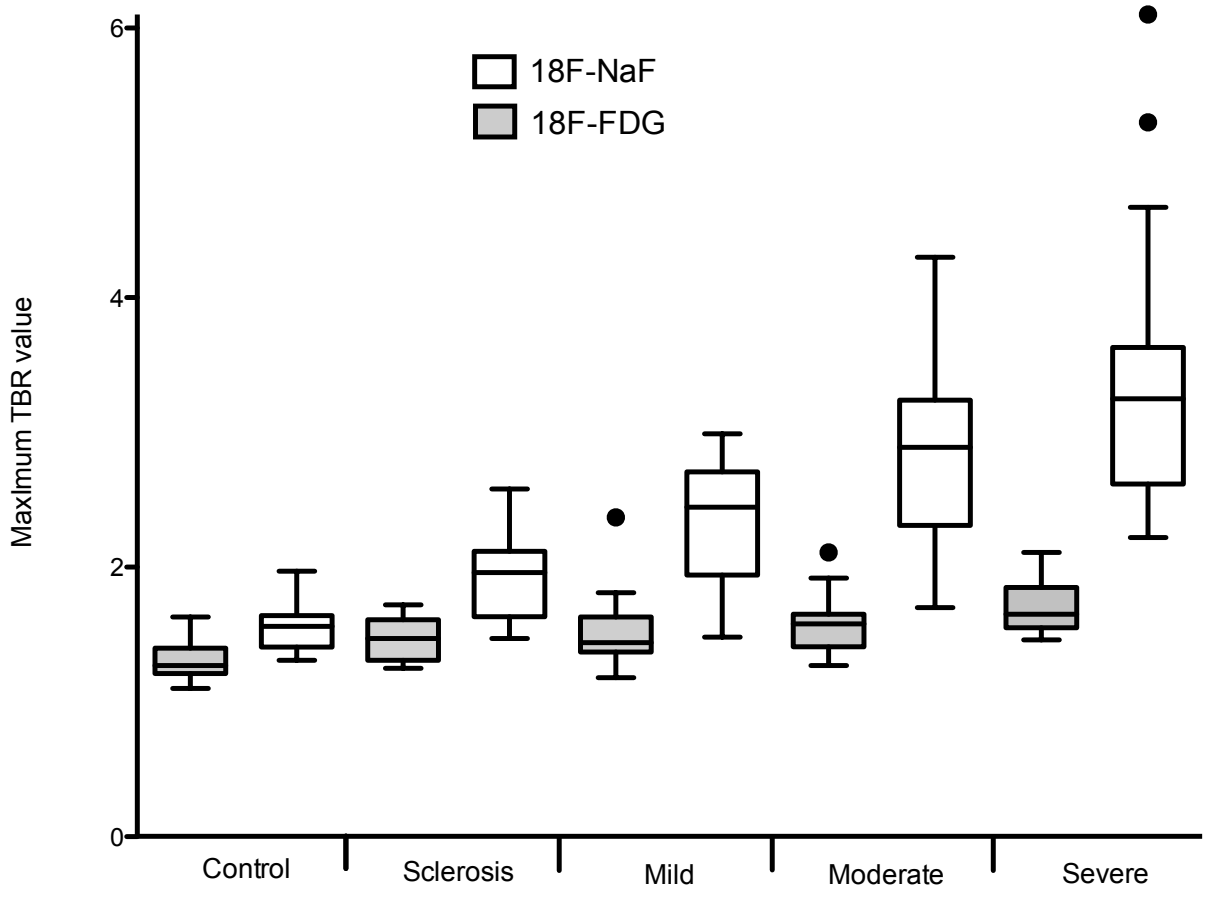

Box-plots show the median and interquartile ranges of the tissue-to-background ratios (TBR) for 18F-NaF (white boxes) and 18F-FDG (grey boxes) with whiskers to 1.5 x interquartile range.

Table 3.4. Correlation between aortic stenosis severity and radiotracer uptake

	Control	Aortic Sclerosis	Aortic Stenosis			Correlation with peak aortic-jet velocity	
			Mild	*Moderate*	*Severe*		
						r^2 value	P value
18F-NaF							
Mean SUV	1.20 (1.10-1.55)	1.35 (1.24-1.59)	1.59 (1.38-1.73)	1.82 (1.67-2.05)	2.10 (1.78-2.51)	0.461	<0.001
Mean TBR	1.23 (1.20-1.36)	1.53 (1.34-1.59)	1.73 (1.45-1.92)	2.03 (1.71-2.28)	2.17 (1.82-2.36)	0.534	<0.001
Max SUV	1.54 (1.33-1.86)	1.77 (1.58-2.09)	2.21 (1.84-2.45)	2.57 (2.27-2.99)	3.25 (2.47-4.42)	0.551	<0.001
Max TBR	1.56 (1.41-1.64)	1.96 (1.63-2.11)	2.45 (1.94-2.71)	2.89 (2.31-3.24)	3.25 (2.62-3.63)	0.540	<0.001
Patients with increased uptake %	0	45	76	95	100	-	-
18F-FDG							
Mean SUV	1.49 (1.33-1.56)	1.73 (1.46-1.88)	1.66 (1.53-1.88)	1.71 (1.61-1.91)	1.76 (1.61-2.18)	0.142	<0.001
Mean TBR	1.18 (1.09-1.26)	1.35 (1.19-1.44)	1.29 (1.21-1.45)	1.33 (1.26-1.47)	1.42 (1.36-1.62)	0.203	<0.001
Max SUV	1.62 (1.47-1.68)	1.91 (1.64-2.07)	1.85 (1.72-2.07)	1.95 (1.81-2.18)	2.07 (1.88-2.25)	0.213	<0.001
Max TBR	1.27 (1.21-1.40)	1.47 (1.31-1.61)	1.44 (1.37-1.63)	1.58 (1.41-1.65)	1.65 (1.55-1.85)	0.218	<0.001
Patients with increased uptake %	0	20	24	30	52	-	-

SUV, standard uptake value; TBR, tissue-to-background ratio. Median ±interquartile range. Pearson's correlation.

***Ex-vivo* studies**

18F-NaF uptake was consistent on both the *in vivo* and *ex vivo* PET/CT scans. Furthermore uptake co-localized with the distribution of osteocalcin staining on histology, extending beyond the boundaries of existing macroscopic calcification (Figure 3.4). The pattern of valvular 18F-FDG uptake was again consistent between *in-vivo* and *ex-vivo* PET/CT scans. Furthermore activity mapped closely to areas of increased macrophage density on immunohistochemistry (Figure 3.5).

Figure 3.4

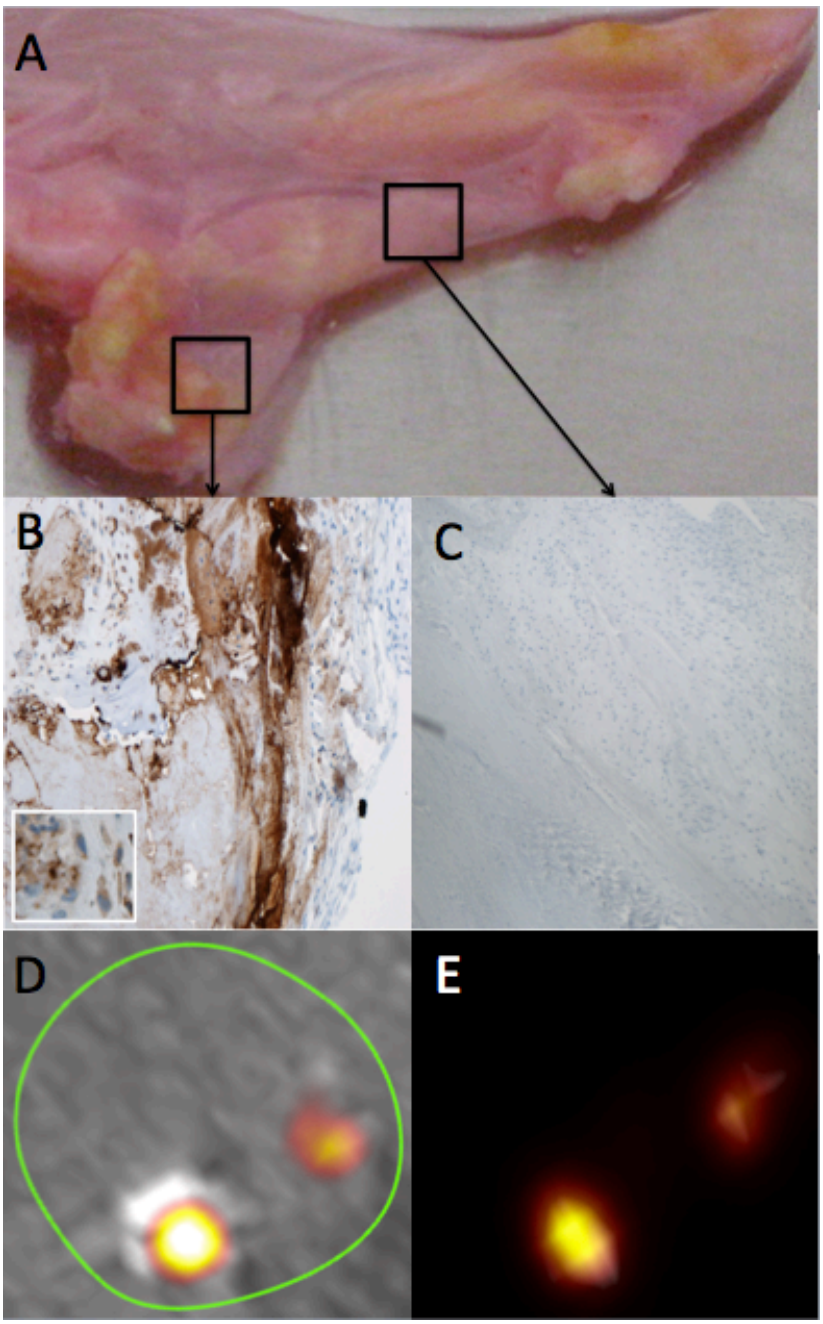

A Excised portion of a stenotic bicuspid aortic valve removed at the time of an aortic valve and root replacement. The aortic side of one of the valve leaflets is shown.
B Immunohistochemistry of the valve for osteocalcin in a region of the valve adjacent to a calcific nodule. Osteocalcin is incorporated in to the bone matrix where it binds to hydroxyapatite during active mineralization. Osteocalcin immunoreactivity can be seen at the periphery of the existing calcified nodule. Inset (black border) shows cytoplasmic staining of cells adjacent to this. **C.** Immunohistochemistry in a region remote from existing calcification with no staining present. This focal distribution of staining matches the pattern of 18F-NaF activity in the valve on both the *in vivo* and *ex vivo* scans described below.
D. *In vivo* 18F-NaF PET/CT scan performed 3 months prior to the operation. Note the focal areas of uptake overlying the area of calcification at the bottom left of the valve and adjacent to the smaller area of calcification in the top right. This closely matches the pattern of uptake observed on the *ex vivo* PET/CT scan performed on the excised valve **(E)**.

Figure 3.5

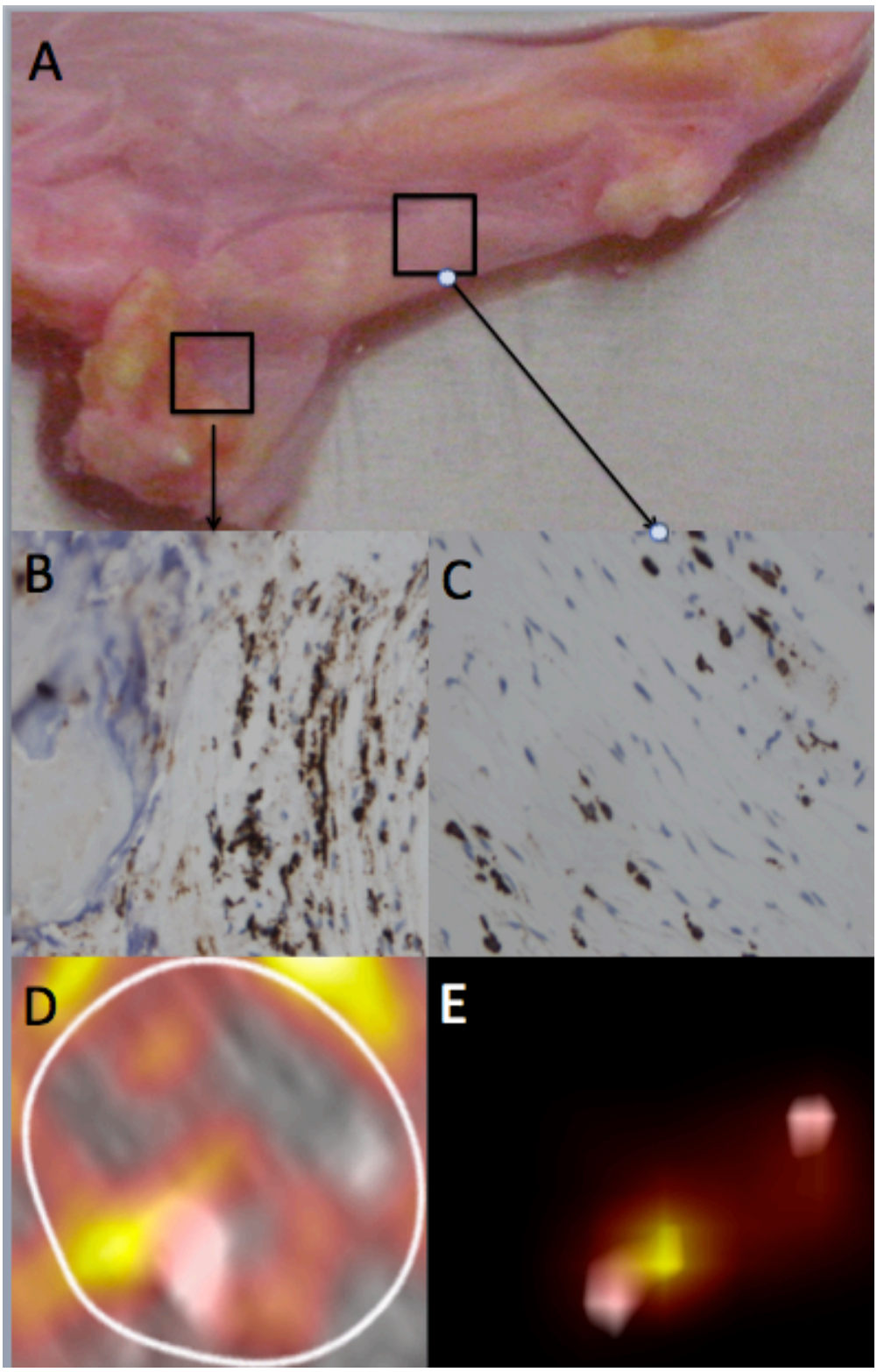

A. Excised portion of the same aortic valve as in Figure 1.
B. Immunohistochemistry for CD 68 in a region of the valve adjacent to a calcific nodule demonstrating the presence of macrophages around the lesion in the fibrosa of the valve leaflet. **C.** Immunohistochemistry in a region remote from existing calcification, which again displays staining for macrophages. **D.** *In vivo* 18F-FDG PET/CT of the valve shows a more diffuse pattern of uptake than for 18F-NaF matching the distribution of macrophages as well as the pattern of uptake observed in the *ex vivo* PET/CT scan of the excised valve tissue **(E)**.

3.5 Discussion

In this PET study, we have established the feasibility of evaluating 18F-NaF and 18F-FDG activity in patients with aortic stenosis. Moreover we have demonstrated excellent reproducibility for the quantification of these tracers in the valve as measures of calcification and inflammation respectively. 18F-NaF and 18F-FDG activity was increased in patients with both aortic sclerosis and stenosis, displaying a progressive rise in uptake with increasing disease severity. However, calcification rather than inflammation appears to be the predominant process affecting the valve particularly in the latter stages of the disease where a more marked progression in 18F-NaF activity was observed that was disproportionate to 18F-FDG.

Valve calcification plays a key role in the development of aortic stenosis. Hydroxyapatite becomes deposited on a bone-like matrix containing collagen, osteopontin and other bone matrix proteins[45, 46, 51] to form nodules that progress until, by the end stage of the disease, lamellar bone, microfractures and haemopoeitic tissue can all be identified.[46] This appears to occur as part of a highly regulated process, coordinated by increased osteoblast activity[43, 44] and the local production of osteopontin, osteocalcin, bone sialoprotein and bone morphogenic protein 2 (BMP-2), all of which are more commonly associated with skeletal bone formation.[44-47] Established aortic valve calcium can be measured accurately using CT[30] but measurement of 18F-NaF uptake offers, for the first time, the possibility of detecting areas of developing calcification within the valve. In this study, 18F-NaF uptake was observed in regions adjacent to, and remote from, existing calcium suggesting expansion of the calcific process to new areas of the valve. In addition, uptake was observed in regions overlapping with that of established calcium, and in these areas, activity is likely to represent calcium remodelling and maturation of the calcific process.

18F-NaF activity was increased in the valves of patients with aortic sclerosis and stenosis compared to control subjects and demonstrated a marked progressive rise with increasing disease severity accounting for more than 50% of the variance associated with valve stenosis. Moreover, increased valvular 18F-NaF activity was observed in 45% of patients with aortic sclerosis, 91% of patients with aortic stenosis and all patients with severe stenosis. Calcium accumulation is the predominant mechanism by which valve cusp rigidity increases and aortic stenosis advances. As such, this technique offers considerable promise as a biomarker of disease activity and as a means of predicting disease progression. Longitudinal studies are now required to determine whether calcification activity quantified by 18F-NaF uptake is an accurate predictor of disease progression and superior to baseline measures of valve severity and calcium scores. If confirmed, these studies would pave the way for mechanistic studies of medical interventions to interrupt progressive calcific disease using 18F-NaF activity as a surrogate biomarker and end-point. Interscan repeatability will however first need to be established in order to power these studies.

In the early stages of aortic stenosis, endothelial damage secondary to mechanical stress and lipid deposition triggers an inflammatory response within the valve. This is characterized by increased macrophage[13] and T-cell activity within the valve leaflets, and the expression of a range of pro-inflammatory cytokines including TGF-β1,[14] TNF-α and interleukin-1β.[15] The inflammatory response is thought to trigger the fibrotic and calcific processes that subsequently drive valve orifice narrowing. Thus, identifying and quantifying valvular inflammation with 18F-FDG has the potential to be critical in the evaluation of aortic stenosis. In the present study, 18F-FDG uptake was higher in patients with aortic sclerosis and stenosis compared to control subjects, and activity again rose with increasing valve severity. However, this association was weaker and the increase in activity more modest than for 18F-NaF. Indeed increased valvular 18F-FDG activity was only observed in 20% of patients with

aortic sclerosis, 35% of patients with aortic stenosis and 52% of patients with severe stenosis. Whilst this may reflect the high cut-off used for increased activity or an insensitivity of 18F-FDG in detecting inflammation, these data would suggest that calcification is the predominant pathogenic process in aortic stenosis and a better target for novel therapeutic strategies. It might also explain the disappointing results of statin therapy in this condition, which has consistently failed to modify vascular calcification even in the coronary circulation despite reducing systemic markers of inflammation.[91-93 94]

A recent retrospective study has described increased 18F-FDG uptake in the valves of 42 patients with cancer who were co-incidentally found to have aortic stenosis.[132] However in contrast to our study, a reduction in activity was observed in patients with severe compared to moderate disease. This difference is likely to reflect the small number of subjects in the severe subgroup (n=8), the retrospective nature of the study analysis as well as the confounding effects of co-existent malignancy. In contrast, we have prospectively recruited a larger well-defined cohort of patients with aortic stenosis who are more likely to be representative of those seen in cardiology practice. Moreover, we studied patients following dietary restriction to minimize effects of myocardial uptake and spillover into the valve. Our data are in keeping with a modest yet sustained and progressive increase in inflammation even in those with advanced disease.

Study Limitations

By excluding a part of the valve, it is possible that the centre-valve technique employed for 18F-FDG analysis may be underestimating valvular inflammation. However, there were no differences in mean uptake values compared to the short-axis technique. This reflects the diffuse nature of 18F-FDG

activity in stenotic valves and the equal distribution of lesions between the base of the valve leaflets (54%), and the mid-portion and tips (46%).[7]

This study has not fully validated 18F-FDG and 18F-NaF activity against histological samples. Whilst the mechanism of uptake for both tracers has been investigated in other tissues, further work is required in the valve to address this issue.

Conclusion

The evaluation of aortic stenosis using PET is feasible and highly reproducible with 18F-FDG and in particular 18F-NaF holding considerable promise as novel biomarkers of disease activity. Both calcification and inflammation are increased in patients with aortic valve disease compared to control subjects and the activity of both steadily rises with increasing disease severity. However, calcification appears to be the predominant pathological process particularly in the latter stages of the disease and would therefore appear to be a better target for future potential medical therapies.

Chapter 4

Coronary Arterial 18F-NaF Uptake: a novel marker of plaque biology

Published by **Dweck MR**, Chow MWL, Joshi N, Williams M, Jones C, Fletcher AM, Richardson H, White A, McKillop G, van Beek EJR, Boon NA, Rudd JHF, Newby DE. Coronary arterial 18F-NaF uptake: a novel marker of plaque biology. **J Am Col. Cardiol** 2012; *59:1539-48*.

4.1 Summary

Objective

Using combined positron emission tomography (PET) and computed tomography (CT), we investigated coronary arterial uptake of 18F-sodium fluoride (18F-NaF) and 18F-fluorodeoxyglucose (18F-FDG) as markers of active plaque calcification and inflammation respectively.

Background

The non-invasive assessment of coronary artery plaque biology would be a major advance particularly in the identification of vulnerable plaques, which are associated with specific pathological characteristics including micro-calcification and inflammation.

Methods

We prospectively recruited 119 volunteers (age 72±8, 68% male) with and without aortic valve disease and measured their coronary calcium score and 18F-NaF and 18F-FDG uptake.

Patients with a calcium score of 0 were used as controls and compared to those with calcific atherosclerosis (ca score >0).

Results

Inter-observer reproducibility of coronary 18F-NaF uptake measurements (maximum tissue-to-background ratio) were excellent (intra-class co-efficient 0.99). Activity was higher in patients with coronary atherosclerosis (n=106) versus controls (1.64±0.49 vs 1.23±0.24; P=0.003) and correlated with the calcium score (r=0.652, p<0.001), although 40% of those with scores >1000 displayed normal uptake. Patients with increased coronary 18F-NaF activity (n=40) had higher rates of prior cardiovascular events (p=0.016) and angina (p=0.023), and higher Framingham risk scores (p=0.011).

Quantification of coronary 18F-FDG uptake was hampered by myocardial activity and was not increased in patients with atherosclerosis versus controls (p=0.498).

Conclusions

18F-NaF is a promising new approach for the assessment of coronary artery plaque biology. Prospective studies with clinical outcomes are now needed to assess whether coronary 18F-NaF uptake represents a novel marker of plaque vulnerability, recent plaque rupture and future cardiovascular risk.

4.2 Introduction

Myocardial infarction (MI) is the foremost cause of death in developed countries[138] and confers a major economic, social and healthcare burden worldwide.[139] The majority of myocardial infarctions result from rupture of atherosclerotic plaque although identifying those at risk of rupture is problematic. The vast majority (86%) of culprit atherosclerotic lesions cause non-flow limiting luminal stenosis[140, 141] that will not be detected by non-invasive stress testing. New methods focusing on plaque pathology are required to identify high-risk lesions so that risk of clinical events can be reduced by appropriate therapy.

Calcification is a key feature of human atherosclerosis and its macroscopic presence in the coronary arteries can be detected by cardiac computed tomography (CT). Coronary artery calcium scoring (CAC) provides a surrogate measure of the atherosclerotic burden and a powerful predictor of cardiovascular risk.[142] Risk prediction can be improved by examining the progression of coronary calcification[143, 144] and by detecting spotty calcification.[145] However CT is unable to measure active calcification directly, nor can it reliably detect microcalcifications that can lead to microfractures and acute thrombosis.[146-148] 18F-NaF is an established PET tracer that detects novel areas of bone formation and remodelling.[149] Uptake has also been described in aortic and carotid atheroma where activity is believed to signal areas of active vascular calcification although this is hypothetical.[111, 112, 150] To date, 18F-NaF uptake has not been measured in the coronary vasculature.

Inflammation is thought to play a key role in plaque rupture. Histologically, the vulnerable plaque is characterized by a lipid-rich pool, infiltration of inflammatory cells and a thin fibrous cap.[141] Macrophages in particular are found in abundance within ruptured plaques and are thought to contribute to a pro-thrombotic state and degradation of the fibrous cap via the action of matrix

metalloproteinases (MMP).[151] Vascular inflammation can be assessed non-invasively in the carotid arteries, aorta, iliac and femoral arteries using uptake of 18F-fluorodeoxyglucose (18F-FDG) as measured by combined positron emission tomography (PET) and computed tomography (CT).[98] 18F-FDG uptake correlates with plaque macrophage burden,[100] symptoms,[99] and Framingham Risk Score [152] and can be lowered with statin and other therapies.[19, 153] Recent *in vitro* and *ex vivo* data have also suggested that 18F-FDG uptake may reflect plaque hypoxia.[154] However, measurement of 18F-FDG uptake within coronary atheroma is challenging because of cardiac and respiratory motion, and the intense myocardial 18F-FDG uptake that can potentially swamp any plaque signal.[106, 155]

The aim of this study was to investigate coronary arterial uptake of 18F-NaF and 18F-FDG as markers of active calcification and inflammation respectively. We hypothesized that the degree of uptake of both tracers would correlate with atherosclerotic disease severity, symptoms, prior cardiovascular events and predictors of future clinical risk. Coronary atherosclerosis and aortic stenosis commonly co-exist and so this study was conducted in a cohort of patients with aortic valve disease originally recruited to study PET uptake in the valve.

4.3 Methods

Study Population

This was a sub-study of the cohort of the 121 patients with and without aortic stenosis described in Chapters 2 and 3.[156] Coronary calcium scoring was not interpretable in 2 of the original cohort who were excluded for the purposes of this present study.

Baseline Clinical Assessment

Baseline clinical assessment was performed on the day of the initial PET/CT scan and included current cardiac symptoms, prior coronary intervention (percutaneous coronary intervention and coronary artery bypass grafting) and past medical history of previous major adverse cardiovascular events (MACE; myocardial infarction, cerebrovascular accident and coronary revascularization). Atherogenic risk factors such as age, sex, smoking habit, history of hypertension, diabetes mellitus, hypercholesterolemia, socioeconomic status and family history of cardiovascular disease were identified. Full external examination was performed, and height and weight measured to determine body mass index (BMI). A 12-lead electrocardiogram was performed and venous blood collected for measurement of serum creatinine, full lipid profile and markers of calcium metabolism. On the basis of this information, Framingham risk scores for coronary heart disease (CHD), CHD death, cardiovascular disease (CVD) and CVD death were calculated.

PET/CT Image Acquisition and Reconstruction

Subjects underwent combined PET/CT imaging of the aorta and coronary arteries with 18F-FDG and 18F-NaF as described in Chapter 2. In addition an ECG-gated breath-hold CT scan (non-contrast enhanced, 40 mAs/rot [CareDose], 100 kV) of the coronary arteries was performed for calculation of the calcium score. Patients observed dietary restrictions prior to their 18F-FDG scan as described in Chapter 2.

Image Analysis: Coronary arteries

Quantification of coronary tracer uptake is described in Chapter 2. Breifly regions of interest drawn around areas of maximal uptake in the left main stem, left anterior descending artery, circumflex artery and the right coronary artery. The maximum SUV and TBR values were recorded from these regions. It was not possible to determine the mean SUV values given the difficulty in identifying the exact borders of the coronary arteries on the non-contrast enhanced scans. Quantification of 18F-FDG uptake was performed as for 18F-NaF but restricted to the proximal and mid-portions of the coronary vessels.[106] Difficulties were still encountered as a result of the pervasive myocardial uptake observed with this tracer and coronary activity was only quantified in areas where myocardial uptake could be confidently avoided. Quantification of the coronary calcium score is described in Chapter 2.

Inter-observer reproducibility of image analysis

Having established the image analysis methodology, PET scans from 20 patients were selected at random from the cohort. All scans from these patients were analyzed independently by two trained observers (MD, NJ). This provided measures of inter-observer reproducibility for maximum TBR values.

Image Analysis: Aorta

The uptake 18F-FDG[157] and 18F-NaF[150] in the ascending and descending aorta was quantified as described in Chapter 2. Mean and maximum SUV and TBR values were derived.

Statistical Analysis

Comparisons of tracer uptake were initially made between those with and without calcific atherosclerosis. Patients with coronary artery calcium scores >0 or a prior history of ischemic heart disease were considered to have underlying calcific coronary atherosclerosis. Patients with a coronary artery calcium score of 0 and no past history of coronary heart disease were considered not to have calcific atherosclerosis and designated as controls. Patients with atherosclerosis were then divided according to well-established cutoffs in the coronary calcium score (0, 1-100, 101-400, 401-1000, >1000)[158] in order of assess the impact of disease severity on tracer activity. Finally comparisons were made between subjects who had normal and increased 18F-NaF uptake. The highest maximum TBR value in the control group was used as the cut-off value above which 18F-NaF was deemed to be elevated. In patients with underlying calcific coronary atherosclerosis, those who had increased 18F-NaF uptake were defined as having active coronary calcification whilst those with normal 18F-NaF uptake were defined as having inactive calcification.

Continuous variables were expressed as mean ± SD and compared using unpaired Student's *t*-test or one-way analysis of variance where appropriate. Categorical variables were expressed as percentages and analyzed using the χ^2-test**.** Correlations between normally distributed data were performed using Pearson's correlation, whilst Spearman's correlation was used for non-parametric data. The 95% confidence interval for differences between sets of SUV and TBR measurements were calculated along with intra-class correlation coefficients.

4.4 Results

Baseline Characteristics

One hundred and nineteen patients were studied (age 72±8 years, 68% male; 66% with aortic stenosis) and had both 18F-NaF (66±6 min after 124±10 MBq) and 18F-FDG (94±7 min after 198±13 MBq) scans of their thorax less than one month apart (median 7 days, interquartile range 1 to 14 days). The effective radiation dose per patient, including all PET and CT scans, was 9.73±1.19 mSv using a CT conversion factor of 0.014 mSv/mGy/cm.

Thirteen patients had no past history of coronary artery disease or evidence of calcific coronary atherosclerosis, and formed the control group (Table 4.1). One hundred and six patients had evidence of coronary atherosclerosis: 41 having a clinical diagnosis of prior coronary artery disease, and a further 65 having calcium scores above zero. One patient had experienced an acute coronary syndrome in the week prior to his 18F-NaF scan; otherwise patients had stable coronary heart disease.

Dietary Restrictions

Average myocardial SUV across the entire cohort was 4.6±3.6 and dietary restrictions effectively suppressed 18F-FDG myocardial uptake (pre-specified as a max SUV <5 measured in the maximal area of uptake in the left ventricular septum) in 67% of patients, similar to that seen in previous studies.[106] Based on dietary diaries, 61% of patients complied with the dietary restrictions and had lower myocardial 18F-FDG uptake than non-compliers (SUV 3.2±2.3 *vs* 6.7±4.2; P<0.001).

Table 4.1. Patient Demographics

	TOTAL	CONTROL	ATHEROSCLEROSIS			
		Ca Score 0	Ca Score 1-100	Ca Score 101-400	Ca Score 401-1000	Ca Score >1000
Number	119	13	19	23	27	37
Age (years)	72 ±8	66 ±7	69 ±8	72 ±8	70 ±9	76 ±7
Male %	68	46	58	61	74	81
BMI	28 ±4	28 ±4	28 ±3	28 ±4	28 ±4	27 ±5
Coronary Heart Disease %	34	0	0	17	48	65
Angina %	24	0	0	13	37	43
MACE %	40	0	0	32	44	75
Previous MI %	12	0	0	9	11	24
Previous CVA / TIA %	6	0	0	14	4	8
Previous PCI %	15	0	0	9	22	27
Previous CABG %	7	0	0	0	7	16
Smokers (ex or current) %	50	38	53	26	59	59
Diabetes %	15	23	5	13	12	22
Hypertension %	60	38	42	65	52	57
Hypercholesterolemia %	49	38	39	39	59	57
Aortic Stenosis %	66	54	58	61	78	73
Aortic Sclerosis %	17	23	11	22	11	19
ACEi / ARB %	49	15	21	39	56	76
Beta-blockers %	39	15	26	48	44	46
Statins %	53	15	21	52	67	73
Total Cholesterol mg/dL	193 ±50	227 ±48	199 ±41	204 ±57	175 ±44	181 ±49
LDL Cholesterol mg/dL	104 ±44	123 ±45	119 ±37	112 ±52	93 ±36	94 ±42
HDL Cholesterol mg/dL	54±20	69 ±42	54 ±12	52 ±15	54 ±18	51 ±12

	TOTAL	CONTROL	ATHEROSLEROSIS			
		Ca Score 0	Ca Score 1-100	Ca Score 101-400	Ca Score 401-1000	Ca Score >1000
Calcium mg/dL	9.30±0.57	9.41 ±0.23	9.41 ±0.97	9.29 ±0.61	9.24 ±0.32	9.24 ±0.49
Phosphate mg/dL	3.55±0.49	3.68 ±0.55	3.57 ±0.55	3.51 ±0.40	3.53 ±0.40	3.54 ±0.48
Alk Phosphatase U/L	84 ±44	93 ±23	83 ±25	79 ±20	80 ±23	77 ±27
Coronary Calcium Score (Ag)*	414	0	19	277	734	1783
	(79-1251)	(0-0)	(2-46)	(125-351)	(448-888)	(1357-3410)
18F-NaF SUV	1.56 ±0.50	1.21 ±0.26	1.28 ±0.27	1.40±0.27	1.49±0.31	1.97 ±0.60
18F-NaF TBR	1.59 ±0.48	1.23 ±0.22	1.33 ±0.32	1.42 ±0.27	1.59 ±0.29	1.97 ±0.58
Patients with increased coronary 18F-NaF %	34%	0%	5%	26%	41%	59%
18F-FDG SUV	1.54 ±0.24	1.43 ±0.30	1.56 ±0.19	1.55 ±0.27	1.46 ±0.24	1.60 ±0.22
18F-FDG TBR	1.22 ±0.21	1.18 ±0.31	1.25 ±0.18	1.19 ±0.16	1.22 ±0.29	1.24 ±0.15
10yr Framingham Risk Scores						
CVD	30 ±13	25 ±17	27 ±13	31 ±10	27 ±12	35 ±13
CVD Death	14 ±10	8 ±9	11 ±8	14 ±8	12 ±10	18 ±11
CHD	19 ±12	16±15	18 ±11	20 ±10	18 ±12	22 ±12
CHD Death	6.3 ±4.7	4.5 ±5.4	5.2 ±3.9	6.3 ±3.6	5.3 ±4.4	8.3 ±5.1

Mean ±SD unless stated. *median ± IQR, Ca score=Agatston Coronary Calcium Score, BMI=Body mass index, MACE=Major Adverse Cardiovascular Events, MI=Myocardial Infarction, CVA=Cerebrovascular accident, TIA=Transient Ischemic Attack, PCI=Percutaneous Coronary Intervention, CABG=Coronary artery bypass graft, ACEi=ACE inhibitors, ARB=Angiotensin Receptor Blocker, LDL=Low Density Lipoprotein, HDL=High Density Lipoprotein, Alk=Alkaline, CVD=Cardiovascular Disease, CHD=Coronary Heart Disease.

18F-NaF Coronary Uptake

Coronary 18F-NaF uptake was quantifiable in 96% of the coronary territories examined. It was not possible to assess the left main stem in 20 patients due to overspill of activity from the aortic valve secondary to calcific aortic stenosis (Table 4.2). Reproducibility studies were excellent for coronary 18F-NaF quantification with no fixed or proportional biases, limits of agreement of ±0.14 for maximum TBR values (Figure 4.1) and an ICC value of 0.99 (0.98-1.00). Limits of agreement for 18F-NaF were in the order ±0.20 when examined in each of the coronary territories (Table 4.2).

18F-NaF activity was observed in areas overlying, adjacent to and remote from existing coronary calcification. Uptake was focal in nature and could be localized to individual calcified coronary plaques. Areas of coronary calcification with no 18F-NaF uptake were also commonly observed (Figure 4.2).

Coronary 18F-NaF uptake was higher in those with coronary atherosclerosis compared to the control group (1.64±0.49 vs 1.23±0.24; p=0.003). The highest maximum TBR value in the control group was 1.61, which was used to divide patients with coronary atherosclerosis into those with increased 18F-NaF uptake (active calcification; TBR maximum >1.61; n=40) and those without (inactive calcification; TBR maximum ≤1.61; n=66; Figure 4.2, Table 4.3).

Patients with increased 18F-NaF uptake were older, more likely to be male, and had higher serum high-density lipoprotein (HDL) cholesterol concentrations than those without increased uptake (Table 4.3). Overall statin use was similar between the groups although atorvastatin use appeared to be double in those with active calcification (28% vs 14%; P=0.077). They also had higher calcium scores, and there was a strong correlation between the coronary artery calcium score and 18F-NaF uptake

(r=0.652, p<0.001). However extensive overlap was observed, with some patients with increased 18F-NaF uptake having relatively little coronary calcification (minimum Agatston score 98) and patients without 18F-NaF uptake having extensive calcium (maximum Agatston score 4636). Indeed 41% of patients with coronary artery calcium scores >1000 had no significant 18F-NaF uptake (Table 4.1).

Sites of increased 18F-NaF uptake were evenly distributed across the coronary vasculature (Table 4.2) and on average activity was 50% higher in these plaques compared to inactive plaques in the same patient (2.14±0.42 *vs* 1.43±0.32; p<0.001). In 25 patients, significant uptake was observed in two or more coronary territories.

Patients with high 18F-NaF uptake were more likely to have a clinical diagnosis of coronary artery disease (60% *vs* 26%; p<0.001), anginal symptoms (40% *vs* 20%; p=0.023), prior revascularization (38% *vs* 11%: p=0.001) and previous major adverse cardiovascular events (45% *vs* 23%; p<0.016: Table 4.3). Furthermore, cardiovascular risk factor burden was increased. Framingham risk prediction scores were higher in those with increased 18F-NaF uptake in terms of Framingham CVD (p=0.043), CVD death (p=0.011), and CHD death (p=0.028, Table 4.4, Figure 4.3). An apparent trend was observed with the Framingham CHD score, but this failed to reach statistical significance. Interestingly 10-year Framingham risk scores for CVD, CVD death and CHD death all displayed a correlation with 18F-NaF coronary uptake but not with the coronary artery calcium score (Table 4.4). Framingham risk scores are not designed for patients with prior cardiovascular events. If these patients were excluded from the analysis, risk scores were higher in those with active calcification for both CHD (inactive calcification 18.1±1.6 vs active calcification 25.6±2.8; p=0.020) and CVD (inactive calcification 28.8±1.9 vs active calcification 36.8±2.7; P=0.017).

One patient was assessed 1 week after sustaining an inferior non-ST elevation myocardial infarction. Intense uptake was observed in the proximal right coronary artery, which had been felt clinically to be the culprit coronary artery (based on dynamic changes on the electrocardiogram and appearances at invasive coronary angiography). Despite having three-vessel coronary artery disease and extensive coronary calcification, relatively little uptake was observed in his other coronary territories (Figure 4.2). This artery had not undergone stenting prior to the PET scan.

18F-FDG Coronary Uptake

18F-FDG uptake was difficult to quantify, particularly in the left main stem and circumflex artery. It was not possible to quantify accurately in 49% of the vessel territories examined (Table 4.2). This was largely the result of myocardial spill over into the coronary arteries, which was observed despite the dietary restrictions imposed in the study. Even when possible, coronary 18F-FDG reproducibility was inferior to that for 18F-NaF, with a fixed bias of 0.22, limits of agreement of ±0.32 and an ICC value of 0.67 (0.31-0.86) (Figure 4.1).

There were no differences in 18F-FDG uptake between the control group and those with atherosclerosis (1.18±0.31 *vs* 1.23±0.20; p=0.498; Table 4.1). Nor was there was a correlation between 18F-FDG activity and the coronary artery calcium score whether in the coronary vasculature as a whole (r=0.063, p=0.538) or on a vessel-by-vessel basis (LAD: r=-0.041, p=0.705; RCA: r=0.039, p=0.726). 18F-FDG coronary uptake was not associated with increased rates of coronary artery disease, anginal symptoms, prior coronary revascularization or previous major adverse cardiovascular events. Neither was there a significant correlation with any of the risk prediction scores (Table 4.4).

Table 4.2. 18F-NaF and 18F-FDG maximum standard uptake values (SUV max) and tissue-to-background ratio (TBR max) values in the coronary arteries, ascending aorta and descending aorta. Inter-observer reproducibility statistics are also provided for TBR max measurements in each of the coronary territories (mean difference ± limits of agreement)

	Coronary Arteries					Ascending	Descending
	LMS	LAD	CX	RCA	ALL VESSELS	**Aorta**	**Aorta**
18F-NaF							
% interpretable	83%	100%	99%	100%	96%	100%	100%
SUV max	1.36 ±0.40	1.32 ±0.46	1.38 ±0.42	1.27 ±0.41	1.56 ±0.50	1.97 ±0.43	2.01 ±0.40
TBR max	1.36 ±0.44	1.35 ±0.46	1.42 ±0.42	1.30 ±0.41	1.59 ±0.48	2.01 ±0.31	2.06 ±0.35
% with increased activity (TBR >1.61)	13%	21%	19%	16%	34%	-	-
Interobserver limits of agreement (mean difference ± 2SD)	0.06 ±0.17	0.01 ±0.20	0.00 ±0.21	0.01 ±0.21	0.03 ±0.14	-	-
18F-FDG							
% interpretable	25%	74%	33%	74%	51%	100%	100%
SUV max	1.55 ±0.25	1.45 ±0.27	1.48 ±0.28	1.34 ±0.22	1.54 ±0.24	2.23 ±0.35	2.24 ±0.31
TBR max	1.20 ±0.23	1.14 ±0.23	1.14 ±0.19	1.05 ±0.24	1.22 ±0.21	1.78 ±0.25	1.79 ±0.25
Inter-observer limits of agreement	-0.09 ±0.28	-0.21 ±0.48	-0.12 ±0.42	-0.23 ±0.30	-0.22 ±0.32	- -	- -

Table 4.3. Baseline characteristics and 10-year Framingham risk scores of patients with coronary atherosclerosis and either normal (SUV≤1.61) or high (SUV>1.61) coronary 18F-NaF uptake.

	Low 18F-NaF uptake (n=66)	High 18F-NaF uptake (n=40)	P value
Age (years)	71 ±8	75 ±8	0.015*
Male %	65	80	0.103
BMI	27 ±4	28 ±5	0.343
Coronary Heart Disease %	26	60	<0.001**
Angina %	20	40	0.023*
Major Adverse Cardiovascular Events %	23	45	0.016*
Previous MI %	11	18	0.324
Previous CVA / TIA %	8	5	0.591
Previous PCI %	9	30	0.005**
Previous CABG %	2	18	0.003**
Smokers (ex/current) %	50	52	0.803
Diabetes %	12	18	0.410
Hypertension %	59	68	0.387
Hypercholesterolaemia %	49	53	0.745
ACEi / ARB %	50	58	0.453
B-blockers %	38	50	0.221
Statin %	52	68	0.107
Atorvastatin %	14	28	0.077

	Low 18F-NaF uptake (n=66)	High 18F-NaF uptake (n=40)	P value
Total Cholesterol mg/dL	196 ±48	174 ±48	0.023*
LDL Cholesterol mg/dL	105 ±43	96 ±43	0.288
HDL Cholesterol mg/dL	55 ±15	48 ±11	0.021*
Creatinine mg/dL	0.90 ±0.14	0.87 ±0.11	0.278
Calcium mg/dL	9.21 ±0.43	9.39 ±0.79	0.125
Phosphate mg/dL	3.55 ±0.52	3.51 ±0.43	0.647
Alkaline Phosphatase U/L	81 ±23	87 ±69	0.473
Coronary Calcium Score[†]	372	1249	<0.001**
	(75-994)	(589-2790)	
Coronary 18F-NaF TBR max	1.34 ±0.17	2.14 ±0.42	<0.001**
Coronary 18F-FDG TBR max	1.23 ±0.20	1.23 ±0.20	0.875
10yr Framingham Risk Scores			
CVD	29 ±13	34 ±12	0.043*
CVD Death	12 ±9	17 ±11	0.011*
CHD	18 ±11	23 ±12	0.058
CHD Death	5.8 ±4.4	7.9 ±4.6	0.028*

BMI=Body mass index, MACE=Major Adverse Cardiovascular Events, MI=Myocardial Infarction, CVA=Cerebrovascular accident, TIA=Transient Ischemic Attack, PCI=Percutaneous Coronary Intervention, CABG=Coronary artery bypass graft, ACEi=ACE inhibitors, ARB=Angiotensin Receptor Blocker, LDL=Low Density Lipoprotein, HDL=High Density Lipoprotein, Alk=Alkaline, CVD=Cardiovascular Disease, CHD=Coronary Heart Disease. *p<0.05, **p<0.01. [†]median (interquartile range)

Table 4.4. Correlation of 10-year Framingham risk scores with the coronary calcium score and 18F-NaF or 18F-FDG uptake in the coronary arteries and aorta.

	10 Year Framingham Risk Scores			
	CVD Events	CVD Death	CHD Events	CHD Death
Coronary Calcium Score	r=0.112 p=0.230	r=0.152 p=0.101	r=0.047 p=0.617	r=0.110 p=0.237
18F-NaF Max TBR				
Coronary Arteries	r=0.196 p=0.035*	r=0.282 p=0.002**	r=0.138, p=0.137	r=0.220 p=0.017*
Ascending Aorta	r=0.208 p=0.024*	r=0.239 p=0.009**	r=0.141 p=0.129	r=0.195 p=0.035*
Descending Aorta	r=0.199 p=0.032*	r=0.231 p=0.012*	r=0.144 p=0.122	r=0.191 p=0.039*
18F-FDG Max TBR				
Coronary Arteries	r=-0.024 p=0.815	r=0.118 p=0.245	r=0.059 P=0.565	r=0.060 p=0.560
Ascending Aorta	r=-0.018 p=0.845	r=-0.047 p=0.618	r=0.031 p=0.741	r=0.012 p=0.899
Descending Aorta	r=-0.043 p=0.645	r=-0.052 p=0.584	r=0.030 P=0.752	r= -0.019 p=0.842

CVD=Cardiovascular Disease, CHD=Coronary Heart Disease, Max TBR=Maximum Tissue-to-Background Ratio. *p<0.05, **p<0.01.

Figure 4.1. Bland Altman Plot of Inter-observer Reproducibility for max TBR values for A) 18F-NaF and B) 18F-FDG

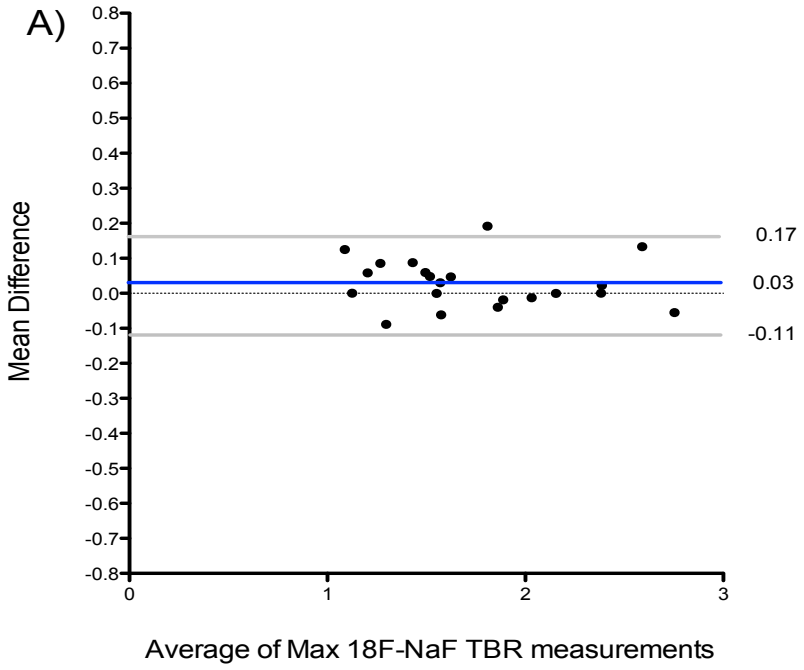

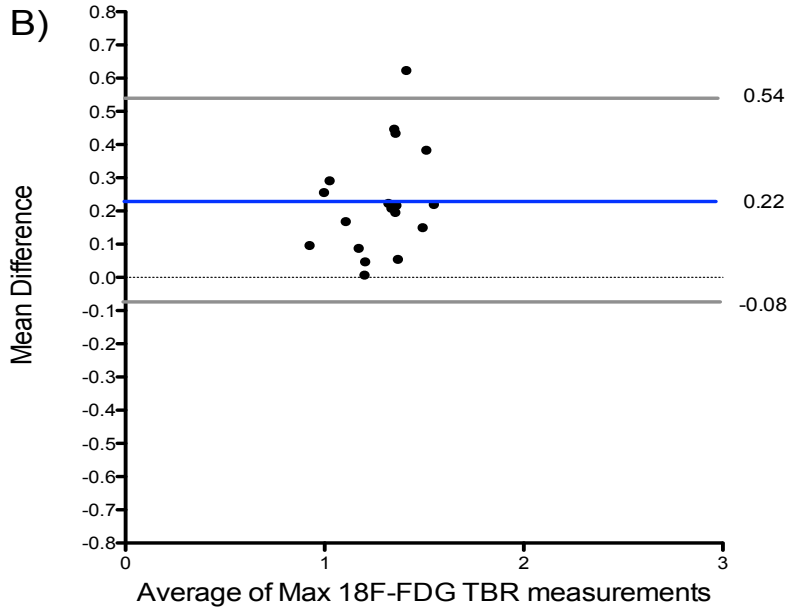

Blue line shows the mean inter-observer difference. Grey lines show the limits of agreement for measurements.

Figure 4.2. Fused PET/CT images of 18F-NaF activity in the coronary arteries

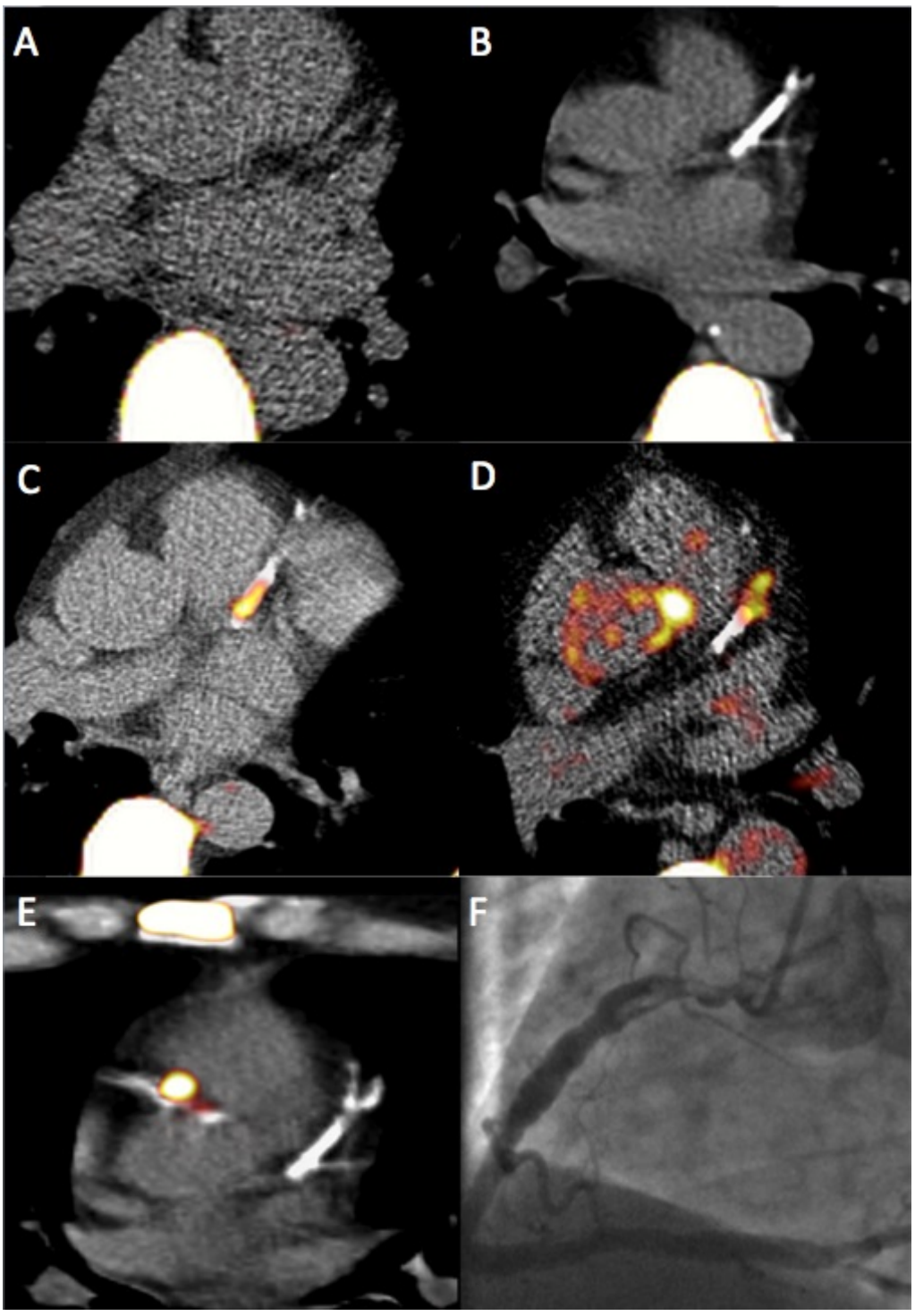

A) Patient in the control group with no coronary calcium and no coronary 18F-NaF uptake. Note the intense uptake in the vertebrae.
B) Patient with extensive calcification in the left anterior descending artery but no 18F-NaF uptake
C) Intense focal 18F-NaF uptake is observed in the proximal LAD overlying existing coronary calcium in this region
D) Increased and focal 18F-NaF uptake is observed in the mid-LAD adjacent to an area of existing coronary calcification.
E) Patient who suffered a recent inferior non-ST segment elevation myocardial infarction showing intense focal uptake of the proximal right coronary artery with sparing of the left anterior descending artery. The proximal right coronary artery was felt to be the culprit artery based on the electrocardiogram and appearances on coronary angiography **(F),** which demonstrated a complex ulcerated plaque with *in situ* thrombus (Supplemental movie file 1).

Figure 4.3. Ten-year Framingham risk scores for control subjects and patients with atherosclerosis who did and did not have increased 18F-NaF uptake

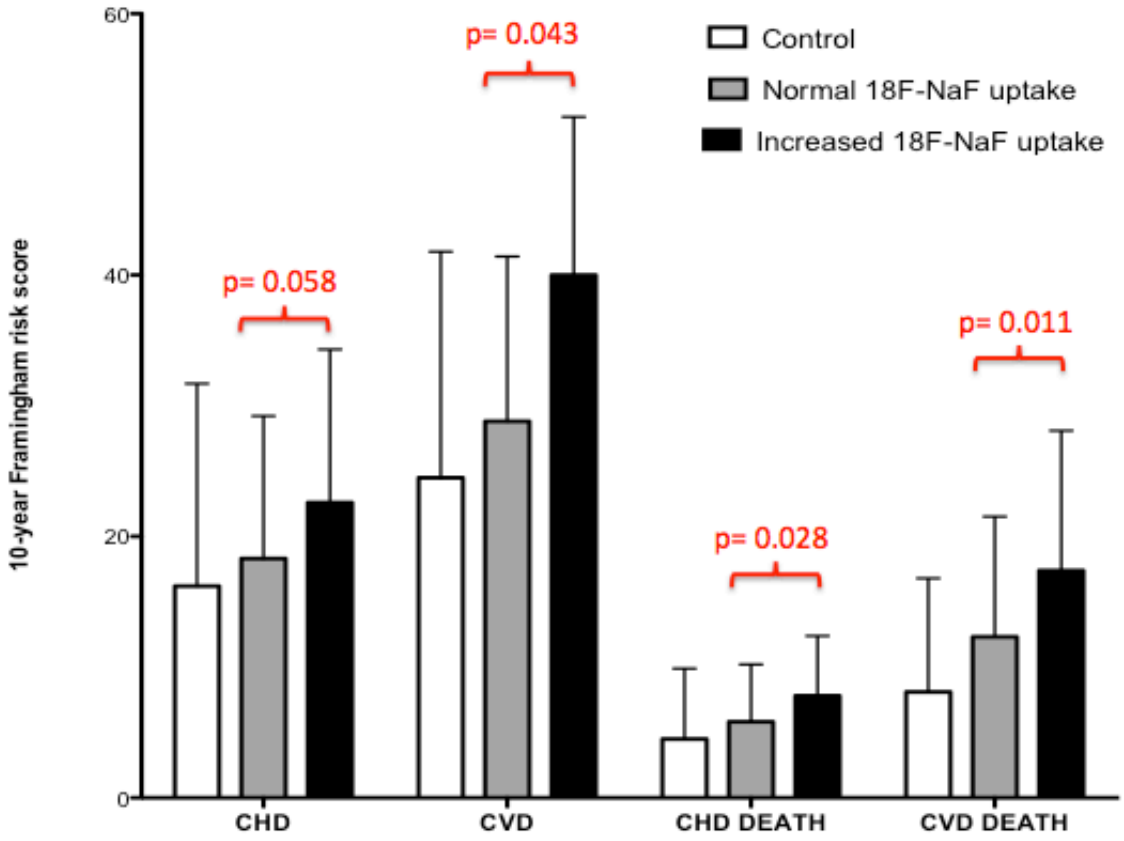

Error bars denote the standard deviation of the mean

Aortic Uptake

18F-NaF uptake in the aorta was observed in a focal distribution most commonly in areas overlying or adjacent to existing aortic calcification (Figure 4.4). Less frequently 18F-NaF uptake occurred in the absence of local calcium (Table 4.2; Figure 4.4). Across the cohort as a whole, 18F-NaF uptake in the aorta was higher than in the coronary arteries (2.01±0.31 *vs* 1.59 ±0.48; p<0.001: Table 4.2). Uptake in the ascending aorta correlated with activity in the descending aorta (r=0.815, p<0.001), the coronary arteries (r=0.525, p<0.001) and with Framingham risk scores (e.g. ascending aorta vs CVD: r=0.208, p=0.024). However, amongst those with increased coronary 18F-NaF activity, a correlation

was no longer observed between activity in the coronary vasculature and the aorta (r=0.157, p=0.333).

18F-FDG uptake was observed in a circumferential pattern around the aortic wall as previously described (Figure 14).[98] Maximum 18F-FDG TBR in the ascending aorta correlated strongly with that in the descending aorta (r=0.824, p<0.001) and the coronary arteries (r=0.543, p<0.001). 18F-FDG activity was higher in the aorta than the coronary arteries (1.78 ±0.25 *vs* 1.22 ±0.21; p<0.001; Table 7). There was no correlation between 18F-NaF and 18F-FDG uptake in the ascending aorta (r=0.043, p=0.647), descending aorta (r=0.124, p=0.183) or the coronary arteries (r=0.127, p=0.21).

Figure 4.4 Vascular PET/CT scans in the coronary arteries and aorta

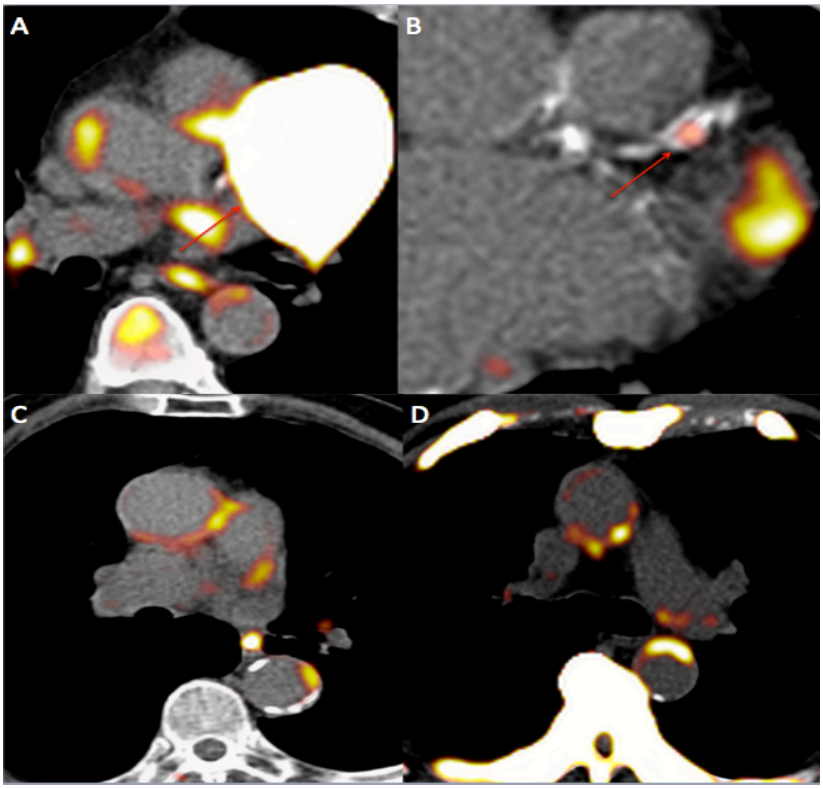

18F-FDG. A) Intense 18F-FDG myocardial uptake is observed that obscures uptake in the coronary arteries, although activity can be observed in the descending aorta. **B)** Effective myocardial suppression has been achieved and a focal area of uptake can be observed in the mid-LAD. **C)** Increased 18F-FDG activity can be observed in a circumferential pattern in both the ascending and descending aortae that rarely overlapped with existing aortic calcium.
18F-NaF. **D)** 18F-NaF uptake is observed in the ascending and descending aortae remote from existing vascular calcification. Also note activity in in the ribs, sternum and vertebra.

4.5 Discussion

This is the first study to describe 18F-NaF uptake in the coronary arteries using PET/CT. We have demonstrated that this technique is both feasible and repeatable, and that it can provide key insights in to coronary artery plaque biology. Activity was higher in patients with atherosclerosis compared to control subjects, displaying a progressive rise with increasing atherosclerotic burden. Furthermore 18F-NaF uptake can be used to discriminate between those patients with active and inactive coronary calcification. Those with active calcification (38%) were more likely to have clinically significant coronary artery disease, have a higher incidence of previous MACE, lower serum HDL cholesterol concentrations and higher Framingham risk prediction scores. 18F-NaF therefore holds promise as a means of identifying high-risk populations and refining the predictive power of coronary artery calcium scoring. Finally, the spatial resolution of PET/CT allows localization of the 18-NaF signal to specific coronary territories and plaques offering the possibility of identifying vulnerable or culprit plaque on an individual basis.

18F-NaF uptake has been described recently in the aorta[111] and carotid arteries,[112] and is believed to reflect active vascular calcification. Although histological validation of this hypothesis is lacking, mechanistic information can be extrapolated from 18F-NaF uptake in bone that has been studied for over thirty years. In that tissue, 18F-NaF is incorporated directly into exposed hydroxyapatite crystal via an exchange mechanism with hydroxyl groups.[113] It therefore detects novel areas of calcification as well as regions of remodelling and is used clinically in Paget's disease,[109] primary osteoblastic tumors and metastatic bone disease.[110] Similarly, we believe that coronary uptake reflects active calcification in atherosclerotic plaque. Certainly coronary 18F-NaF uptake appears to offer information that is additional and complementary to coronary artery calcium scoring. Whilst 18F-NaF activity was most commonly observed overlying existing calcium and a strong correlation was

observed with the coronary artery calcium score, 41% of patients with scores >1000 had no significant 18F-NaF uptake and areas of increased tracer uptake were also found in regions remote from established calcium. This activity potentially relates to developing micro-calcification that is frequently beyond the resolution of CT and believed to be associated with increased mechanical stress and risk of future cardiovascular events.[146,148] 18F-NaF therefore appears to distinguish between patients with dormant calcific disease, established many months or years previously, and subjects with metabolically active disease where the calcification process is ongoing. Importantly this distinction appears to be of clinical relevance, with higher rates of anginal symptoms, prior MACE events and cardiovascular risk factor scores observed in those with active disease.

Calcification plays a key role in the pathophysiology of atherosclerosis although its triggers remain debated. Atherosclerotic plaques with healed rupture almost invariably contain calcium [159, 160] leading to the hypothesis that calcification forms part of a healing response to such events.[144, 161, 162] The spatial resolution of PET/CT is sufficient to localize 18F-NaF activity to specific coronary territories, suggesting that 18F-NaF might be able to identify the presence and location of recent plaque rupture. This is supported by the PET/CT findings in the patient with recent myocardial infarction. Extensive calcification was present in all three vessels yet increased 18F-NaF was only observed in the culprit lesion, which was found to be complex and associated with thrombus at the time of coronary angiography. According to this hypothesis, the increased 18F-NaF activity observed in patients with stable coronary artery disease reflects sub-clinical plaque rupture that has been demonstrated in over 10% of such patients undergoing angioscopy[163,164] and is thought to underlie the step-wise growth of coronary atheroma.

Coronary calcification might occur as a response to intense plaque inflammation. Similar calcific responses can be observed in other inflammatory conditions such as tuberculosis, and intra-vascular ultrasound studies have recently associated micro-calcification with a large necrotic core.[165] However, this theory is not supported by our 18F-FDG data, which failed to show a correlation with 18F-NaF activity in either the coronary arteries or the aorta, indicating that inflammation and calcification occur independently in these regions.

By contrast to 18F-NaF, 18F-FDG activity was not increased in patients with coronary atherosclerosis compared to controls. Our data were however hampered by myocardial uptake that rendered half of the coronary territories uninterpretable. This largely reflected the imperfect dietary compliance that occurred in a third of patients despite the detailed written instructions and verbal reminders provided. Further studies are required in younger cohorts in whom compliance may be improved, although our data do suggest that 18F-FDG may be of limited use in the assessment of stable coronary disease. Inflammation has a more prominent role in acute coronary syndromes and therefore 18-FDG may provide more information in these patients. Indeed a recent study demonstrated increased 18F-FDG uptake in unstable versus stable plaque in the proximal coronary vasculature.[106]

Limitations

PET/CT is expensive especially when compared to circulating biomarkers of calcification activity, and this may limit its clinical use. However, we have demonstrated that amongst those with increased 18F-NaF uptake, activity in the coronaries did not correlate with that in the aorta, suggesting that it is driven by local rather than systemic factors. Blood-based biomarkers are therefore unlikely to provide an accurate indication of coronary calcification activity, and instead will tend to reflect that

within larger vessels or skeletal bone. In our opinion the added costs of PET/CT are therefore justified by its unique ability to measure calcification activity specific to the coronary vasculature. Moreover, 18F-NaF is a very simple and relatively cheap ligand to produce.

The majority of our patients had either concomitant aortic stenosis or aortic sclerosis. Although atherosclerosis and aortic stenosis often co-exist and share many common etiological factors and histopathological similarities, it is nevertheless important to confirm these findings in a cohort of patients more representative of the clinical population with atherosclerosis in the absence of aortic stenosis.

Finally, risk prediction scores are intended to predict events in asymptomatic patients and are therefore not strictly applicable to subjects with an established clinical diagnosis of ischemic heart disease or aortic valve disease. Given these issues, we acknowledge that our data with respect to risk prediction are preliminary and need validation in further prospective clinical trials. However, these scores remained higher in patients with increased coronary NaF uptake even after patients with prior MACE were excluded from the analysis. We therefore believe that this approach has helped to establish an association between 18F-NaF activity and the presence of traditional cardiovascular risk factors, and provides a potential assessment of the risk of future cardiovascular events.

Conclusion

18F-NaF appears to hold promise as a non-invasive method for investigating the role of active calcification in coronary atherosclerosis. There was a strong correlation with established coronary calcium, but 41% of patients with calcium scores >1000 had no significant 18F-NaF uptake. This suggests that 18F-NaF uptake provides different information, relating to metabolically active calcific

plaque, and developing micro-calcification. Moreover, this information appears to be of clinical significance in relation to symptomatic status, prior MACE events and cardiovascular risk scores. Prospective studies to determine the relationship between 18F-NaF uptake, morphological plaque characteristics and future cardiovascular events are now needed in subjects with stable and unstable coronary artery disease.

Chapter 5

Mid-wall fibrosis is an independent predictor of mortality in patients with aortic stenosis

Published by **Dweck MR**, Joshi S, Murigu T, Alpendurada F, Jabbour A, Melina G, Banya W, Gulati A, Roussin I, Raza1 S, Prasad NA, Wage R, Quarto C, Angeloni E, Refice S, Sheppard M, Cook SA, Kilner P, Pennell DJ, Newby DE, Mohiaddin RH, Pepper J, Prasad SK. Mid-wall fibrosis is an independent predictor of mortality in patients with aortic stenosis**. J Am Coll Cardiol** 2011;58: 1271-1279.

5.1 Summary

Objectives: To assess the prognostic significance of mid-wall and infarct patterns of late gadolinium enhancement (LGE) in aortic stenosis.

Background: Myocardial fibrosis occurs in aortic stenosis as part of the hypertrophic response. It can be detected by LGE, which is associated with an adverse prognosis in a range of other cardiac conditions.

Methods: Between January 2003 and October 2008, consecutive patients with moderate or severe aortic stenosis undergoing cardiovascular magnetic resonance with administration of gadolinium contrast were enrolled into a registry. Patients were categorised into absent, mid-wall or infarct patterns of LGE by blinded independent observers. Patients follow-up was completed using, patient questionnaires, source record data and the National Strategic Tracing Scheme.

Results: 143 patients (aged 68±14 years; 97 male) were followed up for 2.0±1.4 years. 72 underwent aortic valve replacement and 27 died (24 cardiac, 3 sudden cardiac deaths). Compared to those with no LGE (n=49), univariate analysis revealed that patients with mid-wall fibrosis (n=54) had an eight-fold increase in all-cause mortality despite similar aortic stenosis severity and coronary artery disease burden. Patients with an infarct pattern (n=40) had a six-fold increase. Mid-wall fibrosis (Hazard Ratio 5.35 [95% confidence interval, 1.16-24.56]; P=0.03) and ejection fraction (Hazard Ratio 0.96 [95% CI, 0.94-0.99]; P=0.01) were independent predictors of all cause mortality by multivariate analysis.

Conclusion: We have shown mid-wall fibrosis to be an independent predictor of mortality in patients with moderate and severe aortic stenosis. It has incremental prognostic value to ejection fraction and may provide a useful method of risk stratification.

5.2 Introduction

Aortic stenosis (AS) is a progressive condition that is characterised by a long and indolent asymptomatic phase followed by a shorter symptomatic stage. The onset of symptoms is associated with an increased morbidity and a high mortality.[166] However there is marked heterogeneity between symptom onset and severity of valvular stenosis. There are several potential explanations for this apparent mismatch but the hypertrophic response of the left ventricle may contribute to the development of symptoms and adverse events.

Aortic stenosis results in increased pressure afterload and ventricular wall stress, thereby stimulating left ventricular hypertrophy (LVH). Initially, increased wall thickness maintains normal wall stress and contraction[52, 53] but ultimately this becomes maladaptive. Indeed, LVH is an independent predictor of cardiac mortality, regardless of etiology.[56-58] Histopathologic studies have demonstrated fibrosis in the left ventricle of patients with aortic stenosis and arterial hypertension.[84, 167] It has been postulated that increasing myocyte size eventually leads to myocyte apoptosis and subsequently replacement fibrosis and that this sequence is responsible for the progression from LVH to heart failure.[168] Myocardial fibrosis has also been linked to the development of arrhythmia and sudden cardiac death in a variety of conditions.[169-172]

Cardiovascular magnetic resonance (CMR) is able to detect replacement myocardial fibrosis non-invasively by late gadolinium enhancement (LGE).[173] Recent studies have demonstrated a mid-wall pattern of enhancement in patients with aortic stenosis in the absence of coronary artery disease.[120, 121] Although the presence of LGE is associated with an adverse prognosis in other cardiac conditions,[124-128] this has not been assessed in aortic stenosis. We sought to determine the prognostic

implications of late gadolinium enhancement in patients with moderate and severe forms of this disease.

5.3 Methods

Patient Population

As described in Chapter 2 all patients referred between January 2003 and October 2009 for CMR at the Royal Brompton Hospital were enrolled into a registry. Patients in whom late gadolinium enhancement was performed were followed up as described below.

Data Collection

Demographic and medical history was documented from source patient record data and patient questionnaires. The presence of coronary artery disease was defined as a prior coronary revascularisation, or the presence of significant coronary artery stenosis as assessed by single photon emission computed tomography, invasive coronary angiography (>50% lumen diameter narrowing), or computed tomography coronary angiography. A patient was considered to have hypertension based on an established clinical diagnosis rather than individual blood pressure readings.

Cardiovascular Magnetic Resonance

CMR including late gadolinium enhancement was performed in each patient as described in Chapter 2. Image analysis included an assessment of the aortic valve area, indexed left ventricular mass and volumes and ejection fraction. The presence and pattern of LGE was assessed by two independent observers and categorised as either no LGE, an infarct pattern or mid-wall LGE. Patients with a mixed pattern of LGE were categorized according to the predominant pattern of fibrosis. LGE was also quantified and expressed as the percentage of total LV mass (Chapter 2).

Clinical End points

The primary end-point of the study was all-cause mortality. The secondary end-point was cardiac mortality. Mortality data was obtained from hospital notes and the National Strategic Tracing Service (NSTS): a national database for all National Health Service patients in the United Kingdom. Cause of death was established from medical notes and / or death certification records and an assessment made as to whether this represented a sudden cardiac death. Data regarding which patients had undergone aortic valve replacement (AVR) during the follow up period was also collected.

Statistical analysis

Continuous variables were expressed as mean ± SD and compared using one-way analysis of variance or unpaired Student's t -test where appropriate. Categorical variables were expressed as percentages and analyzed using the χ^2-test. All continuous variables were tested for normal distribution using the Shapiro-Wilk test. Variables with a skewed distribution were log transformed and the geometric mean with the 95% confidence intervals reported. Where log transformation did not normalize the data, analysis was performed using non-parametric tests: Mann-Whitney rank sum test or the Kruskal-Wallis tests as appropriate.

Kaplan-Meier curves were used to estimate the survival distributions with regard to all cause mortality and cardiac mortality for patients with no LGE, mid-wall LGE and infarct LGE. Differences in the survival patterns of the patients in the 3 groups were assessed using the Log Rank Test. Univariate and multivariate survival analyses (Cox proportional hazard regression) were performed to determine independent predictors of all cause mortality and cardiac mortality. All analyses were performed using Stata statistical package version 10.0 (Stata Corporation, College Station, TX). All authors had full access to and take full responsibility for the integrity of the data.

5.4 Results

CMR was performed on 143 consecutive patients (aged 68 ±14 years; 97 male) with an average aortic valve area of 0.99 ±0.31 cm^2. Overall, 57 patients (40%) had moderate and 86 (60%) severe aortic stenosis. CMR estimation of aortic valve severity correlated closely with echocardiographic data. Coronary artery disease was assessed in all patients (83% had invasive coronary angiography) and was present in eighty-one patients (57%) (Table 5.1).

Patterns of Late Gadolinium Enhancement

Three patterns of LGE were observed: no gadolinium enhancement (no LGE group); localised enhancement consistent with prior myocardial infarction (infarct LGE group); and a mid-wall pattern of enhancement (mid-wall LGE group) (Figure 5.1). Inter-observer agreement in determining the pattern of LGE was very good with a κ value of 0.89.

LGE was absent in 49 (34%) patients. There was a typical pattern of prior myocardial infarction in 40 (28%) patients, and mid-wall fibrosis in 54 (38%) patients (Table 5.1). In eight patients (6%), there was a dual pattern of both myocardial infarction and mid-wall fibrosis. These patients were categorized according to their predominant pattern and the statistical analysis was performed on this basis. Seven were placed in the infarct group and one in to the mid-wall group.

One patient with mid-wall LGE who died underwent autopsy. Assessment of the macroscopic appearance of the cut surface of the heart showed myocardial fibrosis, which was confirmed histologically using Trichome stain (Figure 5.2).

Table 5.1. Baseline characteristics of 143 patients with aortic stenosis according to the pattern of LGE (mid-wall, infarct or no LGE).

	No LGE	Mid-wall LGE	Infarct LGE	P Value
Number of Patients	49	54	40	-
Average Age *yrs*	64±16	70±11	70±13	0.031
Male sex *%*	53	72	80	0.018
Clinical History *%*				
AF	21	18	18	0.915
Diabetes Mellitus	25	19	32	0.378
Hypertension	56	55	50	0.838
Bicuspid Aortic Valve	29	17	23	0.401
Documented CAD *%*	37	42	98	<0.001
1vd	16	17	15	
2vd	2	6	20	<0.001
3vd	2	13	28	
Previous PCI	10	9	30	0.010
Previous CABG	20	8	28	0.040
Medication *%*				
ACE Inhibitor	56	48	61	0.480
Beta Blocker	56	26	49	0.007
Statins	67	60	82	0.079

	No LGE	Mid-wall LGE	Infarct LGE	P Value
CMR DATA				
Aortic Valve Area by CMR *cm^2*	1.05±0.37	1.00±0.31	0.91±0.26	0.111
Peak Aortic Valve Gradient by echo *mmHg*	70±26	70±26	69±16	0.99
Severe Aortic Stenosis *%*	53	50	65	0.353
Ejection Fraction *%*	69±13	58±21	44±18	<0.001
Indexed LA Volume *mL/m^2*	58.9* (53.4, 64.9)	62.9* (56.2, 70.3)	63.3* (57.1, 70.2)	0.560
Indexed LVEDV *mL/m^2*	78.8* (72.1, 86.2)	88.5* (79.4, 98.6)	101.4* (92.6, 111.0)	0.003
Indexed LV Mass *g/m^2*	92.6* (86.0, 99.6)	113.7* (104.5, 123.8)	97.8* (90.9, 105.2)	0.005
Indexed Stroke Volume mL/m^2	54.2±12.9	50.1±18.6	43.2±12.4	0.009
RVEF *%*	58±13	57±12	55±14	0.450
% LGE Mass*%*	0	3.8 (2.3, 5.8)	6.1 (3.2, 11.1)	-

Continuous variables presented as mean ± SD, categorical variables as percentages. LGE- Late Gadolinium Enhancement, LA – Left Atrial, LVED – Left Ventricular End Diastolic, LV – Left Ventricular, RVEF – Right Ventricular Ejection Fraction, CAD – Coronary Artery Disease, AF – Atrial Fibrillation, ACE – Angiotensin Converting Enzyme

Figure 5.1. Patterns of Late Gadolinium Enhancement in Aortic Stenosis

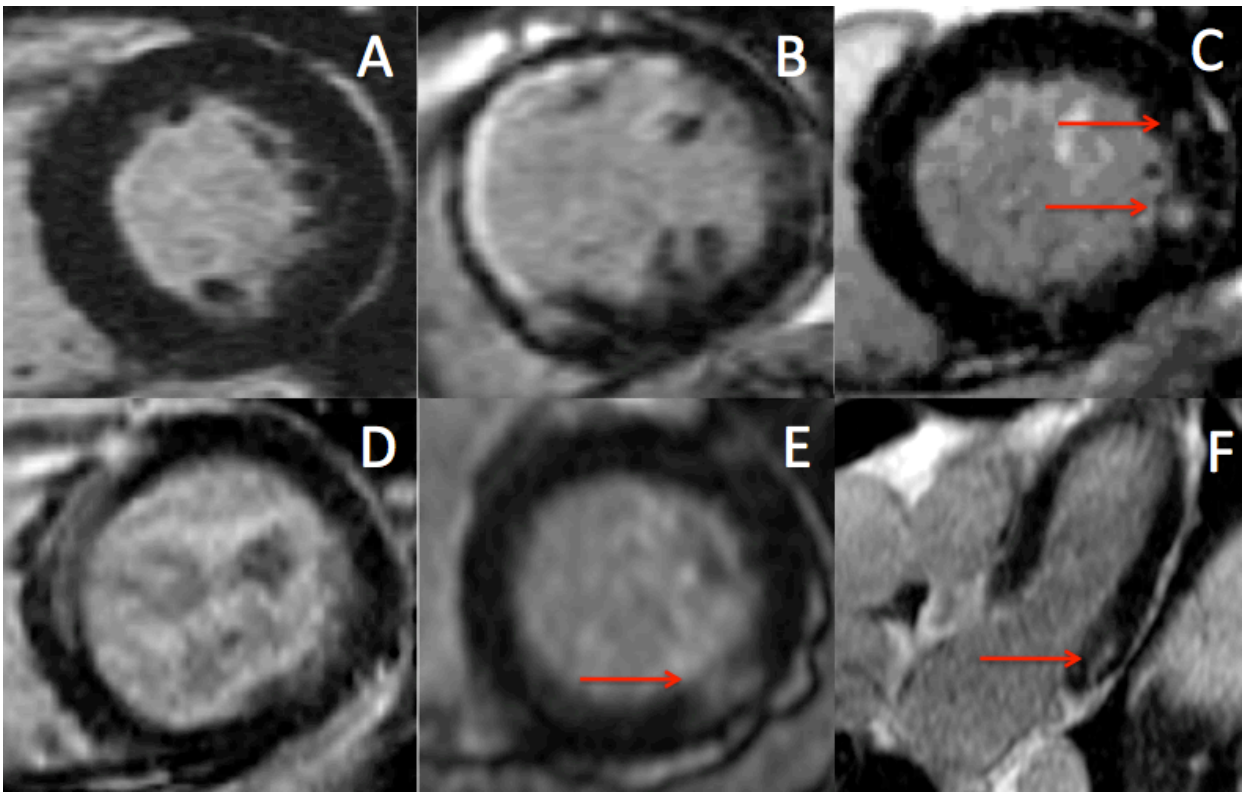

Images show the different patterns of LGE observed in patients with aortic stenosis. A) No LGE. B) Infarct LGE with a subendocardial pattern observed in the septum and anterior wall. C) Two focal areas of mid-wall LGE in the lateral wall of the left ventricle (red arrows); D) Mid-wall LGE in a more linear pattern affecting the septum. E) F) Short and long-axis views of mid-wall LGE (red arrows) of the infero-lateral wall in the same patient.

Figure 5.2. Histology of the myocardium, following Trichome staining, in a patient who had mid-wall LGE

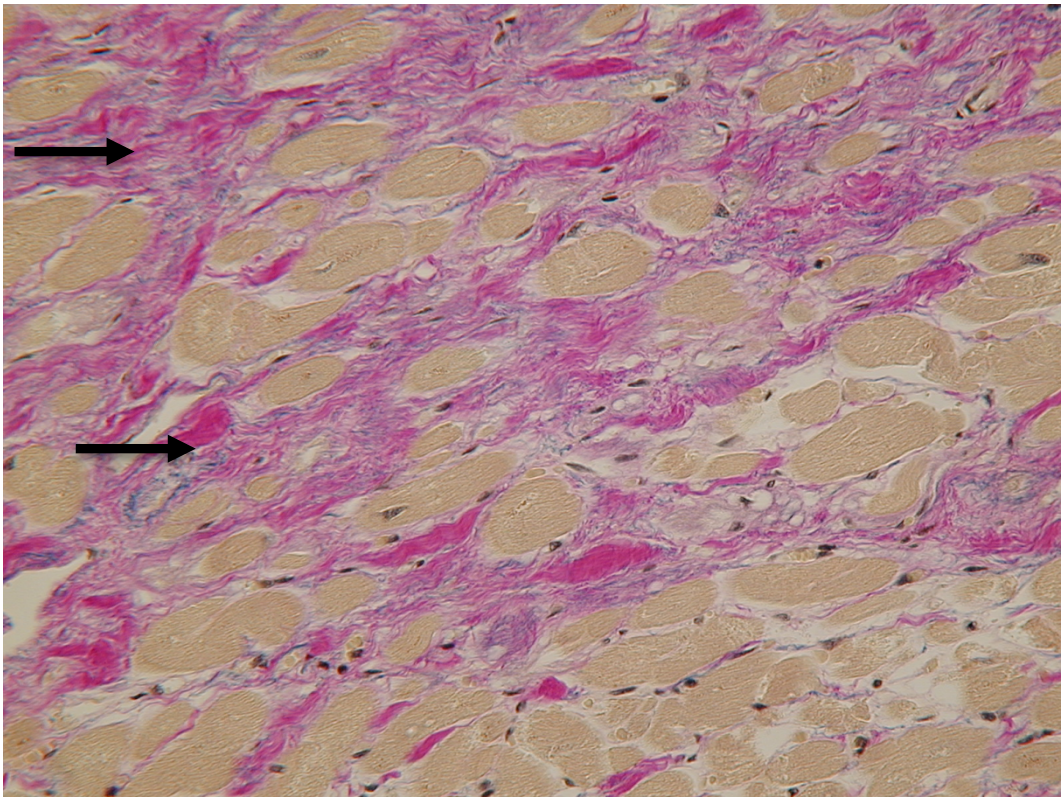

Black arrows demonstrate increased replacement fibrosis in the mid-wall region of the myocardium

Patients with no LGE were younger, more likely to be female and less likely to be on diuretic therapy. The severity of aortic stenosis and prevalence of cardiovascular risk factors were similar to the other groups. As anticipated, patients with an infarct pattern of LGE had more severe coronary artery disease, lower ejection fractions and higher indexed LV volumes than the other groups (Table 5.1).

Patients with mid-wall LGE had the highest indexed LV mass (P=0.005) despite the fact that AS severity and hypertension prevalence were similar between all three groups. Interestingly, ejection fraction (P=0.007) and stroke volume were lower (p=0.01) in patients with mid-wall LGE compared to those with no LGE, even though both groups had a similar degree of coronary artery disease. Whilst there was an apparent trend to a correlation between ejection fraction and the mid-wall LGE burden

(Pearson's: R= -0.26; P=0.08), this did not reach statistical significance. Indexed left atrial volumes were used as a marker of diastolic dysfunction[174] and there was no difference in this variable between the three groups (Table 5.1).

Mortality Data

Patients were followed up for an average of 2.0 ±1.4 years (median 1.7 years). None of the patients were lost to follow-up and overall, 27 patients (19%) died (Table 5.2). Univariate analysis revealed that compared to patients with no LGE, there was an eight-fold increase in all-cause mortality in patients with mid-wall fibrosis (HR 8.59, 95% CI 1.97, 37.38; P=0.004) and a six-fold increase in mortality in those with myocardial infarction (HR 6.46, 95% CI 1.39-30.00; P=0.017) (Table 5.3, Figure 5.3). As fibrosis burden increased, prognosis worsened: with every 1% increase in the percentage LGE mass the risk of mortality appeared to increase by 5% (HR 1.05 [95% CI 1.01-1.09]; P=0.005). A lower ejection fraction and an increased LV end-diastolic volume also predicted an increased all-cause mortality on univariate analysis (Table 5.3). After multivariate analysis, ejection fraction (HR 0.96 [95% CI, 0.94-0.99]; P=0.009) and the mid-wall pattern of LGE (HR, 5.35 [95% CI, 1.16-24.56]; P=0.034) were identified as independent predictors of subsequent all cause mortality (Table 5.4).

Twenty-three of the twenty-seven deaths were from cardiac causes (Table 5.2). There was a five-fold increase in cardiac mortality in the infarct group (HR 5.44, 95% CI 1.15, 25.68; P=0.032) and a six-fold increase in the mid-wall group (HR 6.68, 95% CI 1.51, 29.64; P= 0.012) (Figure 5.4).
Three of the deaths were adjudicated as sudden cardiac deaths and all were in the mid-wall group. Each of these subjects had died suddenly at home with no prior symptoms or signs of heart failure.

Aortic Valve Replacement

During follow-up, 72 (50%) patients underwent AVR (8 patients percutaneously) with no difference in rates between the three groups (Table 5.2). Aortic valve replacement was associated with an improved survival in the univariate analysis (P=0.01) and multivariate analyses (HR 0.32 95% CI 0.13, 0.76 P=0.01) (Tables 5.3 and 5.4). In patients with mid-wall fibrosis, those undergoing AVR had a mortality rate of 54 per 1000 patient years compared to 219 per 1000 patient years in those who did not (Table 5.2). The two groups were well matched with no significant differences in age (P=0.64), aortic valve area (P=0.32), ejection fraction (P=0.24), indexed LVEDV (P=0.29), indexed LV mass (P=0.60), documented CAD (P=0.77), hypertension rates (P=0.10) or diabetes (P=0.23). Two patients were turned down for surgery in the mid-wall group and they were excluded from this analysis.

Table 5.2. Outcome Data

	No LGE	Mid-wall LGE	Infarct LGE	P Value
Subsequent AVR *%*	55	46	53	0.66
Deaths	2	16	9	0.003
Cardiac Deaths	2	13	8	0.016
Sudden Cardiac Deaths	0	3	0	-
All cause Mortality rate*	15.7	142.7	173.1	-
Cardiac Mortality rate*	15.7	130.2	123.2	-
All cause Mortality rate* in AVR patients	13.7	53.8	73.6	-2
All cause Mortality rate* in non-AVR patients	18.2	218.8	190.0	-

Subsequent aortic valve replacement, all-cause mortality, cardiac mortality and sudden cardiac deaths according to the pattern of LGE (mid-wall, infarct or no LGE). In addition all cause mortality rates are displayed for patients who subsequently had an AVR during the period of follow up and for those who did not (patients turned down for surgery have been excluded from this analysis: n=2 in the mid=wall group, n=4 in the infarct group). P values for mortality rates are given in Table 3 and Figures 3 and 4. AVR- Aortic Valve Replacement, LGE- Late Gadolinium Enhancement

Table 5.3. Cox proportional hazards model – Univariate analysis for all-cause mortality

Variable	Dead (n=27)	Alive (n=116)	Hazard Ratio	Confidence Intervals	P value
Age yrs	71.5± 7.8	67.1 ± 14.3	1.03	0.99, 1.07	0.12
Male Sex	69.8%	59.3%	0.68	0.32, 1.47	0.33
Subsequent AVR	25.9%	55.2%	0.32	0.13, 0.75	0.01
Diabetes	23.1%	24.8%	0.94	0.38, 2.35	0.90
Hypertension	53.9%	54.0%	1.02	0.47, 2.21	0.95
Documented CAD	65.4%	53.5%	1.62	0.72, 3.62	0.25
ACE inhibitors	53.9%	54.6%	0.95	0.44, 2.05	0.89
Beta Blockers	42.3%	43.2%	1.00	0.45, 2.18	1.00
Ejection Fraction *%*	45.0 ± 21.6	60.6 ± 18.4	0.96	0.94, 0.98	<0.001
AV Area *cm^2*	0.96 ± 0.31	0.99 ± 0.31	0.68	0.19, 2.40	0.55
Indexed Mass * *g/m2*	116.6 ± 34.5	103.1± 28.3	1.01	1.00, 1.02	0.06
Indexed LVEDV* *g/mL*	99.2* (83.7, 117.7)	86.0* (81.0, 91.3)	3.06	1.03, 9.08	0.04
LGE PATTERN					
No LGE	7.4%	40.5%	1.00	-	-
Infarct LGE	33.3%	26.7%	6.46	1.39, 30.00	0.017
Mid-wall LGE	59.3%	32.8%	8.59	1.97, 37.38	0.004
% LGE Mass	12.6 ± 10.3	6.7 ± 9.1	1.05	1.01, 1.09	0.005

The following were found to be significant predictors of all-cause mortality: subsequent AVR, ejection fraction, indexed LVEDV, an infarct pattern of LGE, mid-wall LGE, and the % LGE mass. AVR- Aortic Valve Replacement, LGE- Late Gadolinium Enhancement, LVEDV- Left ventricular end-diastolic volume.

Table 5.4. Cox regression multivariate analysis for all cause mortality

Variable	Hazard Ratio	Confidence Intervals	P value
Ejection Fraction	0.96	0.94, 0.99	0.01
Indexed LVEDV	0.68	0.18, 2.61	0.57
Mid-wall LGE	5.35	1.16, 24.56	0.03
Infarct LGE	2.56	0.48, 13.64	0.27
Subsequent AVR	0.32	0.13, 0.76	0.01

Ejection fraction, mid-wall LGE and subsequent AVR all emerged as independent predictors of all cause mortality. AVR- Aortic Valve Replacement, LGE- Late Gadolinium Enhancement, LVEDV- Left ventricular end-diastolic volume.

Figure 5.3. Kaplan-Meier survival estimates by pattern of late gadolinium enhancement for all cause mortality in 143 patients with moderate or severe aortic stenosis.

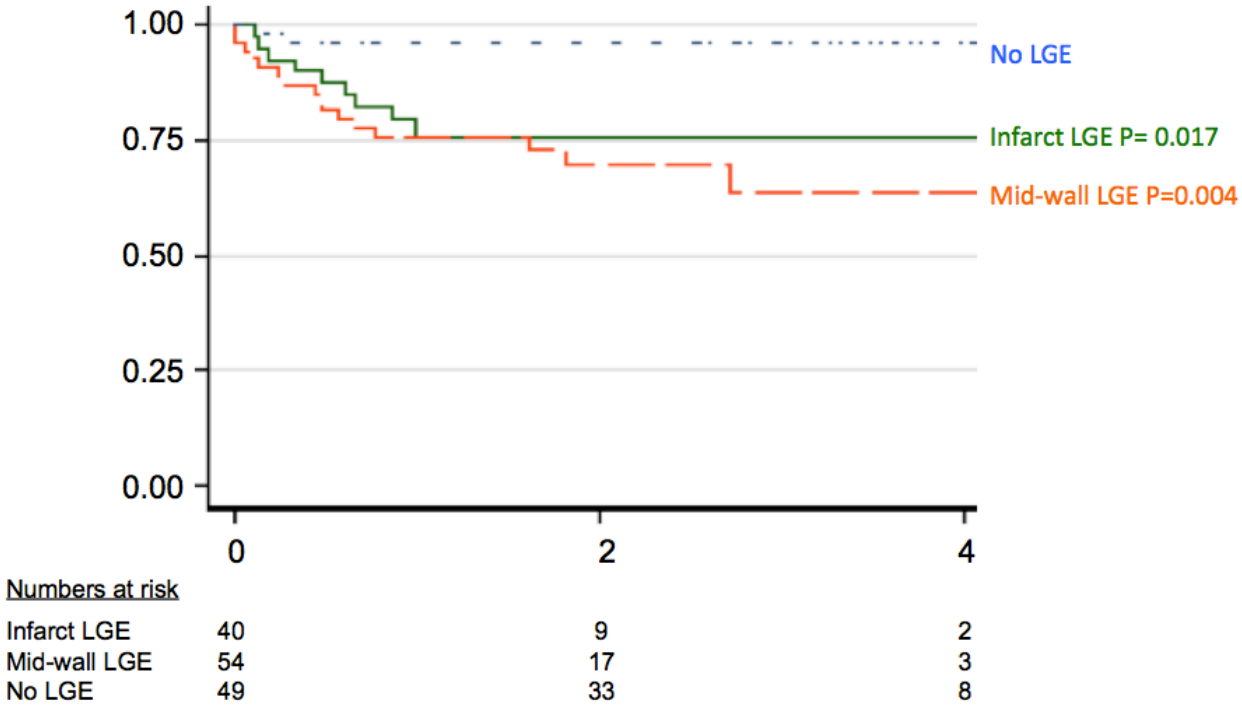

There was a significant increase in all cause mortality in the mid-wall (orange dashed line) and infarct groups (green line) compared to the no-LGE group (blue dotted line). Amongst patients followed up for more than 4 years there were no further deaths.

Figure 5.4. Kaplan-Meier survival estimates by pattern of late gadolinium enhancement (LGE) for cardiac mortality in 143 patients with moderate or severe aortic stenosis

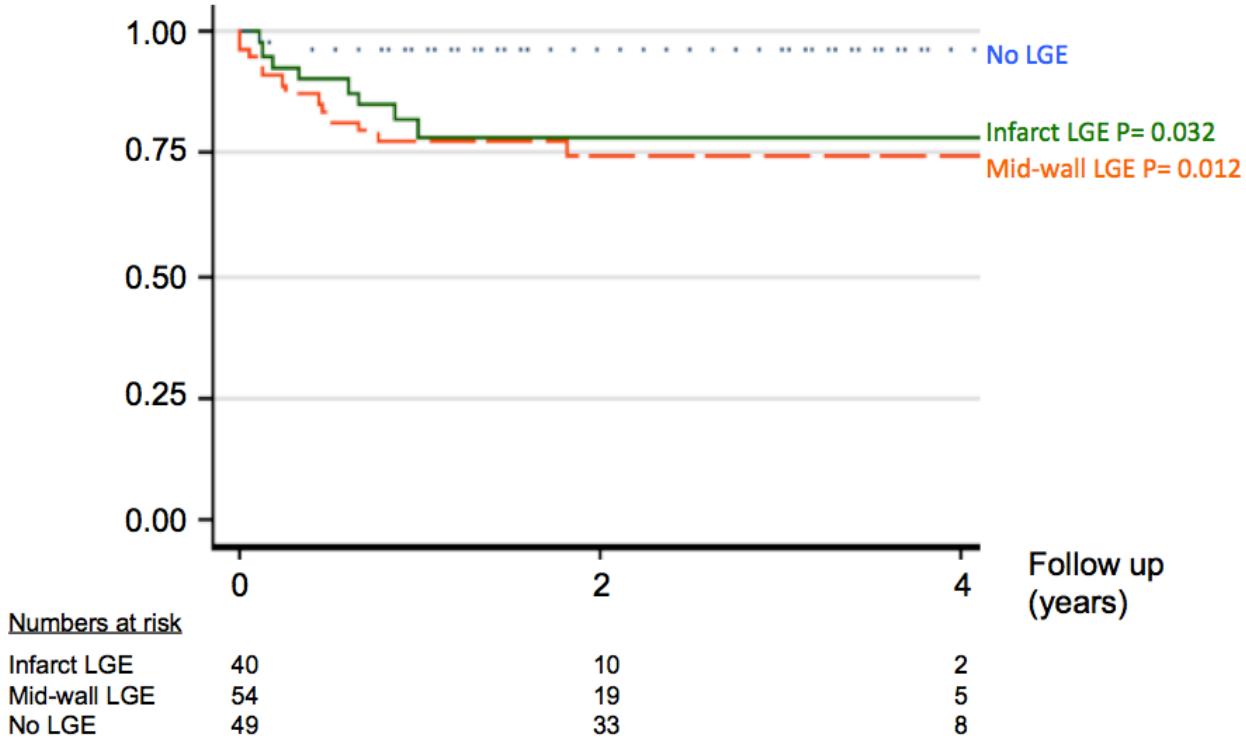

Ejection fraction, mid-wall LGE and subsequent AVR all emerged as independent predictors of all cause mortality. AVR- Aortic Valve Replacement, LGE- Late Gadolinium Enhancement, LVEDV- Left ventricular end-diastolic volume.

5.5 Discussion

Aortic stenosis is the most common indication for valve replacement in Europe and North America [175]. Its clinical importance continues to rise with a progressively ageing population and the expansion of percutaneous valve implantation. Here, we have investigated whether myocardial fibrosis, as assessed by CMR, can predict prognosis in this condition. For the first time, we have demonstrated that mid-wall fibrosis/ LGE is an independent predictor of survival in aortic stenosis and appears to be of incremental prognostic value to ejection fraction.

LGE has been associated with adverse clinical outcomes across a range of different cardiac conditions including hypertrophic cardiomyopathy, dilated cardiomyopathy and myocardial infarction.[124-127] We here extend this to patients with AS. Patients with no LGE had a relatively good prognosis in contrast to those with a mid-wall or infarct pattern of enhancement who experienced an eight- and six-fold increase in mortality respectively.

The poor prognosis associated with prior myocardial infarction is well established in this and other settings,[124, 127] and is thought to be related to arrhythmogenicity and adverse remodelling with progression to heart failure. The findings in relation to mid-wall fibrosis are less expected. Even though patients with prior infarction had a lower ejection fraction and more severe coronary artery disease, patients with mid-wall fibrosis had a higher mortality. With increasing burden of mid-wall LGE, prognosis worsened and in the multivariate survival analysis, mid-wall fibrosis emerged as an independent marker of all-cause mortality. Myocardial infarction was not independently associated probably because of its close association with ejection fraction.

Mid-wall fibrosis in aortic stenosis

Fibrosis is a common pathologic alteration in patients with AS and concurrent LVH.[167] In the hypertrophied myocardium, areas of fibrosis co-localise with areas of myocyte apoptosis [87] and a pathological sequence of myocyte hypertrophy followed by apoptosis and replacement fibrosis has been described.[168] Several possible triggers to this apoptotic process have been postulated including direct mechanical forces [76, 77] and angiotensin II.[77, 78] Ischemia has also been suggested. Increased myocardial mass and afterload leads to increased myocardial oxygen demand. The capillary bed does not expand sufficiently to increase oxygen supply and capillary flow reserve is reduced [80, 176] thereby inducing ischemia. Galiuto et al demonstrated that patients with severe aortic stenosis and no coronary artery disease have impaired myocardial perfusion, and increased cardiomyocyte apoptosis.[81] However the concept that mid-wall fibrosis is due to hypoperfusion remains unproven and one might expect ischemia due to hypertrophy to be greatest in the subendocardium not the mid-wall.

Mid-wall LGE is associated with an increased LV mass,[120, 121] being on average 11g/m^2 higher in our study than in those without fibrosis. The explanation for this increase is not clear given that there were no differences in the severity of aortic valve disease or rates of hypertension between the groups. Other factors are likely to be involved including age, male sex [65, 69, 177] use of beta-blockers [178, 179] and different genotypes.[69, 70, 180] Alternatively it may be explained by differences in the global measure of afterload ZVa, which has not been measured in this study.[73]

It is unlikely that mid-wall fibrosis occurs secondary to coronary artery disease. Previous studies have reported that mid-wall LGE occurs in patients with aortic stenosis and normal coronary arteries.[120, 121] In our study, the presence of coronary artery disease was well characterised, with no difference in its

presence between the mid-wall and the no LGE groups. Furthermore, over half of those with mid-wall LGE had unobstructed coronary arteries.

Mechanism of adverse prognosis

The adverse prognosis associated with mid-wall fibrosis in aortic stenosis appears to be predominantly cardiac in aetiology. Mid-wall LGE predicted a six-fold increase in cardiac mortality compared to no LGE and 81% of deaths in this group were cardiac in nature.

Using CMR we have confirmed that the ejection fraction serves as a powerful prognostic marker in aortic stenosis [181] and shown that it was impaired in the mid-wall group compared to the no LGE group. Previous studies have demonstrated an association between mid-wall fibrosis and low flow severe aortic stenosis.[123] Impaired left ventricular function is therefore likely to be a major contributor to the adverse prognosis in these patients. However, on multivariate analysis, mid-wall fibrosis still predicted an increased mortality after adjustment for the effects of ejection fraction, which suggests the contribution of other factors.

One potential mechanism may be arrhythmogenicity. Fibrosis can serve as a structural substrate for arrhythmia[182] and its detection, using LGE, in patients with dilated cardiomyopathy or previous myocardial infarction has been linked with an increased incidence of arrhythmia and sudden cardiac death.[125, 183] In this study all three patients with aortic stenosis who had a sudden cardiac death were in the mid-wall group. However our study design was not adequately powered to examine this end point and our protocol did not include routine ambulatory monitoring. In addition other patients may have died suddenly without there being sufficient documentation to allow their identification within this study. It is therefore not possible to make any definitive assertions about the contribution

of malignant arrhythmia to the adverse prognosis associated with mid-wall LGE in aortic stenosis. Further work is required to evaluate this question but in our opinion the effect of mid-wall fibrosis on LV function is likely to represent the predominant mechanism.

Aortic valve replacement

Nearly half of our cohort underwent AVR during follow up. The high rates of surgery probably underlie our observation that aortic stenosis severity was not predictive of mortality. AVR is the only available treatment capable of improving the prognosis of patients with symptomatic severe AS, and in our study was predictive of an improved outcome after multivariate analysis.

It is interesting to note that AVR appeared to modulate the poor prognosis associated with mid-wall fibrosis. After excluding patients turned down for surgery patients with mid-wall LGE who had an AVR were four times less likely to die over the course of the follow-up than those who did not undergo AVR (Table 2). This is despite the two groups being well matched in terms of age, indexed LVEDV, ejection fraction, aortic valve area, indexed LV mass, hypertension, diabetes mellitus and concomitant coronary artery disease. Furthermore, over half of the patients with mid-wall fibrosis who died had moderate aortic stenosis and would not have been considered for AVR under conventional management practice. Myocardial fibrosis may therefore have a role in the risk stratification of patients being considered for surgery.

Interestingly it would appear that once established mid-wall fibrosis is not reversible following AVR. Weidemann et al showed no change in the degree of LGE 9-months post AVR.[122] In our study CMR was repeated in one patient a year after surgery. The presence of mid-wall fibrosis and the % LGE mass remained unchanged (4.6% at baseline vs. 4.4% after 1 year).

In accordance the adverse prognosis associated with mid-wall fibrosis also persists to a degree following AVR. The mortality rate amongst patient in the mid-wall group who underwent AVR was 53.8 per 1000 patient-years compared to 13.7 per 1000 patient-years in the no LGE group.

The benefit of AVR in mid-wall fibrosis may instead be related to the prevention of subsequent fibrosis and the further associated increases in left ventricular dysfunction and tendency to arrhythmia.

Limitations

The symptomatic status of our cohort was not assessed. This is an important prognostic marker in aortic stenosis and it would be interesting to investigate its association with the presence of late gadolinium enhancement. Twenty-seven patients died during the course of our study, so that fitting more than three variables in to the multivariate analysis may be problematic. Post-hoc analysis performed using the homoscedastic adjustment inflation factor suggested there was no evidence of over fitting in our model nevertheless a multi-centre study involving a larger cohort with longer follow up is required for confirmation of our findings and definitive conclusions about differential risk based on multivariate analysis. Further attention must also be paid to the mechanisms underlying the increased mortality (including the incidence of arrhythmia, sudden cardiac death and symptoms) and the role of AVR in modulating this risk. Ultimately such studies may pave the way for randomised control trials of anti-fibrotic medications in the treatment of this common clinical condition.

At the Royal Brompton Hospital local guidelines recommend CMR for all patients with severe aortic stenosis. However patients with moderate disease were referred at the discretion of their clinician and therefore there may have been some referral bias in this group. Finally established LGE

techniques detect areas of replacement fibrosis within the myocardium. Diffuse interstitial fibrosis can be detected using T1 mapping techniques [184] and this has not been assessed in our study. Whilst this form of fibrosis predominates in aortic stenosis, T1 mapping has not been validated, whereas LGE is already established in everyday clinical practice.

Conclusions

We have shown that CMR-detected mid-wall fibrosis is an independent predictor of mortality in patients with moderate and severe aortic stenosis and is of incremental value in the prognostic model to ejection fraction. It may prove a useful method of risk stratification in patients with advanced aortic valve disease or as a future target for anti-fibrotic medication.

Chapter 6

Left Ventricular Remodelling and Hypertrophy in Patients with Aortic Stenosis: *Insights from Cardiovascular Magnetic Resonance*

Dweck MR, Joshi S, Murigu T, Gulati A, Gordon R, Roussin I, Northridge DB, Jabbour A, Newby DE, Pennell DJ, Prasad SK. Left ventricular remodelling and hypertrophy in patients with aortic stenosis: insights from cardiovascular magnetic resonance. **Journal of Cardiovascular Magnetic Resonance.** In Press.

6.1 Summary

Background

Cardiovascular magnetic resonance (CMR) is the gold standard non-invasive method for determining left ventricular (LV) mass and volume but has not been used previously to characterise the LV remodelling response in aortic stenosis. We sought to investigate the degree and patterns of hypertrophy in aortic stenosis using CMR.

Methods

Patients with moderate/ severe aortic stenosis, normal coronary arteries and no other significant valve lesions or cardiomyopathy were scanned by CMR with valve severity assessed by planimetry and velocity mapping. The extent and patterns of hypertrophy were investigated based upon measurements of indexed LV mass, indexed LV volume and the relative wall mass. Asymmetric forms of remodelling and hypertrophy were defined as a ventricular wall thickening >12mm that was >1.5-fold the thickness of the opposing myocardial segment.

Results

Ninety-one patients (61±21 years; 57 male) with aortic stenosis (aortic valve area 0.93±0.32cm^2) were studied. The degree of hypertrophy was unrelated to aortic stenosis severity (r=0.068, P=0.53). Furthermore there was wide variation in LV morphology comprising normal ventricular geometry (n=11), concentric remodelling (n=11), asymmetric remodelling (n=11), concentric hypertrophy (n=34), asymmetric hypertrophy (n=14) and LV decompensation (n=10). Asymmetric forms of remodelling and hypertrophy displayed considerable overlap in appearance (wall thickness 17±2mm) to patients with hypertrophic cardiomyopathy.

Conclusions

We have characterised six patterns of LV adaption in response to aortic stenosis and have demonstrated that the degree of hypertrophy is independent of the severity of valve narrowing. This variation is likely to be of clinical relevance given the adverse prognosis associated with increasing hypertrophy.

6.2 INTRODUCTION

Aortic stenosis is characterised by progressive narrowing of the aortic valve and can be considered the paradigm for left ventricular pressure overload. The ventricle responds to this pressure overload by triggering a hypertrophic response, leading to an increase in myocyte size, left ventricular wall thickness and mass. Initially this response restores wall stress[52, 53] but ultimately proves maladaptive and predicts an adverse prognosis in both hypertension and aortic stenosis.[4, 56, 58]

There is wide individual variation in both the degree and pattern of hypertrophy observed in aortic stenosis. Indeed, four different patterns of anatomic adaption have been categorized using echocardiographic measurements of left ventricular mass, volumes and the relative wall thickness.[185, 186] These patterns are: *normal ventricular geometry*, c*oncentric remodelling*, c*oncentric hypertrophy,* and *eccentric hypertrophy. A*symmetric patterns have also been reported,[187 188] however they have not been included in the above or other definitions.

The assessment of left ventricular remodelling and hypertrophy by echocardiography has several limitations when compared to cardiovascular magnetic resonance (CMR). This technique offers the more precise measurements of left ventricular mass, volume and wall thickness[189-191] but has not previously been used to characterise the hypertrophic response of the left ventricle to aortic stenosis. The aim of this study was to use CMR to investigate both the different morphological patterns of LV adaption observed in this condition and the factors affecting the magnitude of the hypertrophic response.

6.3 METHODS

Patients with Aortic Stenosis

As described in Chapters 2 and 5 patients with aortic stenosis who were referred to the Royal Brompton Hospital for CMR were enrolled into a registry. Briefly patients with moderate or severe disease were considered for this study regardless of whether late gadolinium enhancement had been performed. In order to study the effects of aortic stenosis on the ventricle in isolation, the patient group was carefully selected to avoid those with confounding drivers of left ventricular remodelling. Stringent exclusion criteria were therefore employed as described in Chapter 2. Briefly patients with other forms of cardiac disease were excluded with the exception of those with mild or moderate hypertension (based on an established clinical diagnosis). Comprehensive baseline clinical characteristics and history were obtained using a standardised structured proforma and were completed from source clinic record data and patient questionnaires.

CMR Protocol

CMR was performed on Avanto 1.5T magnetic resonance scanners and analysed as described in Chapters 2 and 5. Left ventricular dilatation and hypertrophy were defined as an indexed left ventricular end-diastolic volume and mass above the 95th percentile respectively after correcting for age and gender according to the widely used normal ranges published Maceira et al.[134] Similarly left ventricular ejection fraction was reduced if <95th percentile.[134] Wall thickness measurements were made as described in Chapter 3. Asymmetric left ventricular wall thickening was defined as a regional wall thickening of greater than 12 mm that was >1.5-fold the thickness of the opposing myocardial segment. Criteria had to be fulfilled on two adjacent short-axis slices.

The Relative Wall Mass

The relative wall mass is the conceptual equivalent of the echocardiogram-derived relative wall thickness[192-194] and is calculated by dividing the left ventricular mass by the left ventricular end diastolic volume. Both index wall thickness to cavity size, but the relative wall mass is based on the geometry of the ventricle as a whole and not 2-dimensional measurements of wall thickness. However, because the relative wall mass lacks a well-defined normal reference range, age and sex-matched healthy volunteers without co-existent coronary artery disease, hypertension, aortic stenosis or other forms of heart disease were recruited and scanned contemporaneously in order to facilitate its quantification.

Definition of the Patterns of Left Ventricular Hypertrophy and Remodelling

Patients were subsequently categorised into six, pre-defined patterns of left ventricular anatomic adaption according to the indexed LV mass, indexed LV volume and the relative wall mass. Normal ventricular structure, characterised by normal relative wall mass and normal LV indexed mass and volume. Concentric remodelling, characterised by an increased relative wall mass but normal indexed LV mass. Asymmetric remodelling, similar to concentric remodelling but with evidence of asymmetric wall thickening. Concentric Hypertrophy, characterised by an increased relative wall mass and indexed LV mass. Asymmetric hypertrophy, similar to concentric hypertrophy but with evidence of asymmetric wall thickening. Eccentric hypertrophy, characterised by a normal relative wall mass and a dilated left ventricle.

Statistical analysis

Continuous variables were expressed as mean ± standard deviation, and compared using unpaired Student's *t*-test or one-way analysis of variance where appropriate. Categorical variables were

expressed as percentages and analyzed using the chi-squared test. Correlation between normally distributed data was performed using Pearson's correlation. All statistical analysis was performed using Stata 10.1 software (StataCorp, Texas, USA).

6.4 RESULTS

Study Population

Ninety-one patients (61±21 years; 57 male) were assessed and had moderate (31%) or severe (69%) aortic stenosis and a mean aortic valve area (AVA) of 0.93±0.32 cm^2 (Table 6.1). Ninety-one healthy control subjects were identified and matched for age and sex (mean age 61±10 years, 61% male). Relative wall mass in this group was 0.88±0.14 (95% confidence intervals: 0.60 to 1.16) g/mL and displayed an apparent weak association with age (r=0.189, P=0.073). M/V was higher in males than females but this difference was small (0.91±0.13 vs 0.84±0.15; P=0.02) and there was little difference in the upper 95% confidence interval. The relative wall mass was subsequently calculated for each patient in the aortic stenosis group and values above 1.16 g/mL were considered elevated.

Determinants of Left Ventricular Hypertrophy

Indexed left ventricular mass was unrelated to aortic stenosis severity both in terms of the aortic valve area (r=0.068 P=0.53, Figure 6.1) and the aortic valve area indexed to body surface area (r= -0.046, P=0.666). There was no difference in the degree of hypertrophy between patients with moderate and severe disease (mean difference in mass 3.9 g/m^2; 95% CI, -7.6 to 15.5 g/m^2, P=0.50). Male sex was the only variable associated with an increased indexed LV mass, being 13.8 g/m^2 (95% CI, 2.8 to 24.7 g/m^2, P=0.02) higher in men (Table 6.2). There was also an apparent trend to an increased mass with co-existent hypertension (mean difference 9.9 g/m^2; 95% CI, -1.1 to 20.9 g/m^2, P=0.08).

Table 6.1. Characteristics of patients with different forms of remodelling and hypertrophy

	Normal Ventricle	Concentric Remodelling	Asymmetric Remodelling	Concentric Hypertrophy	Asymmetric Hypertrophy	LV Decompensation
Number	11	11	11	34	14	10
Male sex (%)	45	55	82	65	64	60
Age (years)	52±26	54±21	70±12	57±18	75±11	69±18
CMR DATA						
Indexed LVEDV (mL/m^2)	76±9	55±12	56±9	77±19	78±24	126±34
Indexed Mass (g/m^2)	63±11	75±10	78±7	113±21	110±24	106±18
Relative wall mass (g/mL)	0.84±0.16	1.39±0.31	1.43±0.28	1.51±0.28	1.47±0.33	0.88±0.19
Maximal wall thickness (mm)	11±2	13±3	17±2	15±2	17±2	13±2
Ejection Fraction (%)	73±5	77±9	76±15	70±13	67±14	42 (30-48)
Impaired Ejection Fraction (%)	0	0	0	15	14	100
Aortic valve area (cm^2)	0.85±0.30	0.90±0.43	1.10±0.32	0.98±0.34	0.86±0.25	0.80±0.16
Peak Velocity (m/s)	3.6±0.4	3.6±0.8	3.42±0.67	4.0±0.97	3.80±0.76	3.8±0.8
Severe AS (%)	73	64	45	65	78	100
Bicuspid valve (%)	55	45	27	41	29	40
Hypertension (%)	9	18	64	38	64	50
Diabetes Mellitus (%)	18	0	18	15	7	30
ACEi / ARB (%)	20	10	55	39	36	22
Beta blocker (%)	20	10	37	18	18	20

Demographic, CMR and Clinical data for patients with normal LV structure, LV remodelling, LV hypertrophy and eccentric hypertrophy

Figure 6.1. Correlation between aortic valve area and left ventricular mass index r=0.068, P=0.53)

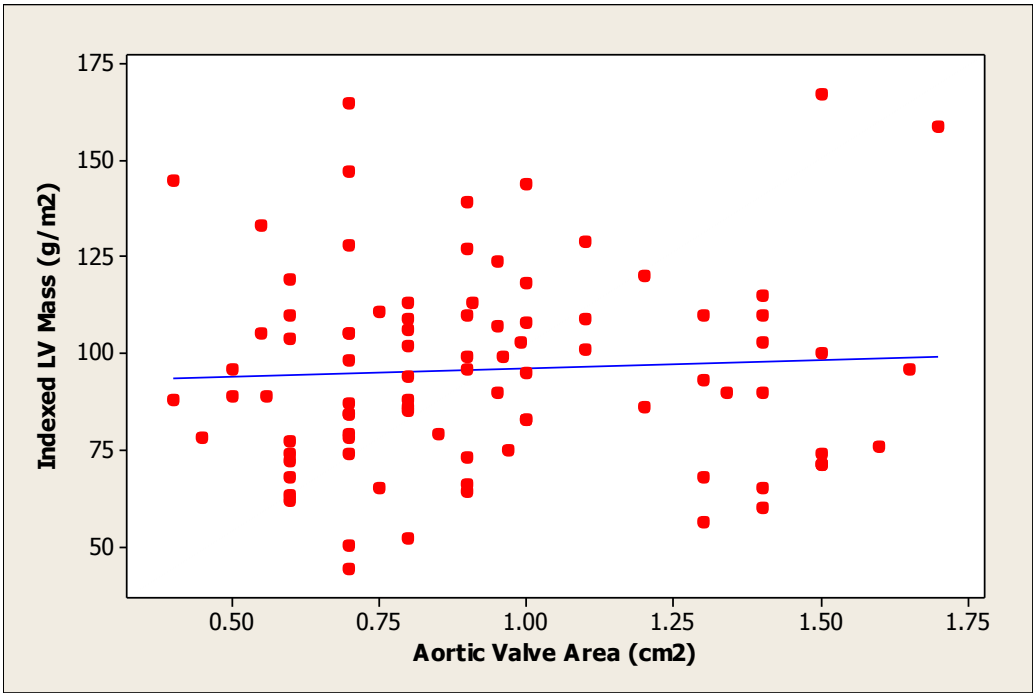

Table 6.2. The association between the indexed left ventricular mass and different independent variables

Variable	Mean difference in Indexed Mass (g)	Confidence Intervals	p value
Age >66 years	7.5	-3.4 – 18.4	0.17
Male	13.8	2.8 – 24.7	0.02
Moderate Aortic Stenosis	3.9	-7.6 – 15.5	0.50
Bicuspid	-7.3	-18.4 – 3.9	0.20
Hypertension	9.9	-1.1 – 20.9	0.08
Diabetes mellitus	11.9	-3.6 – 27.4	0.13
ACE Inhibitor / ARB	11.2	-1.00 – 23.3	0.07
β-Blocker	3.2	-11.2 – 17.6	0.66

Male sex was the only variable associated with a significant increase in the indexed LV mass, being 13.8g/m^2 higher in males than females. There was no difference in LV mass between patients with moderate and severe aortic stenosis

Left Ventricular Characteristics of Patients with Aortic Stenosis

Twelve per cent (n=11) of subjects had normal left ventricular structure and 24% left ventricular remodelling (n=22; 11 asymmetric and 11 concentric) (Table 6.1, Figure 6.2). Left ventricular hypertrophy was the most prevalent pattern and occurred in 53% (n=48) of subjects (concentric 71%; asymmetric 29%). Absolute wall thickness was similar between patients with remodelling and hypertrophy (15±3 *vs* 16±2mm; P=0.16) but the indexed mass was significantly higher in those with hypertrophy (112±22 vs 76±9 g/m^2; P<0.001) and the LVEDV lower in those with remodelling (78±20 v*s* 56±10 ml/m^2; P<0.001). In the majority of patients with hypertrophy, left ventricular ejection fraction was preserved but it was impaired in 15% (n=7; mean ejection fraction of 48%). Criteria for eccentric hypertrophy was met in 11% (n=10). However, each patient in this group had impaired systolic function and a reduced ejection fraction (45±16%; p<0.001 *vs* normal group). This is different from the classical definition of eccentric hypertrophy, observed in athletes and aortic regurgitation in whom ejection fraction is preserved. This group was therefore reclassified as having LV decompensation (Figure 6.2).

Figure 6.2. CMR definitions of the six patterns of left ventricular hypertrophy and remodelling in aortic stenosis.

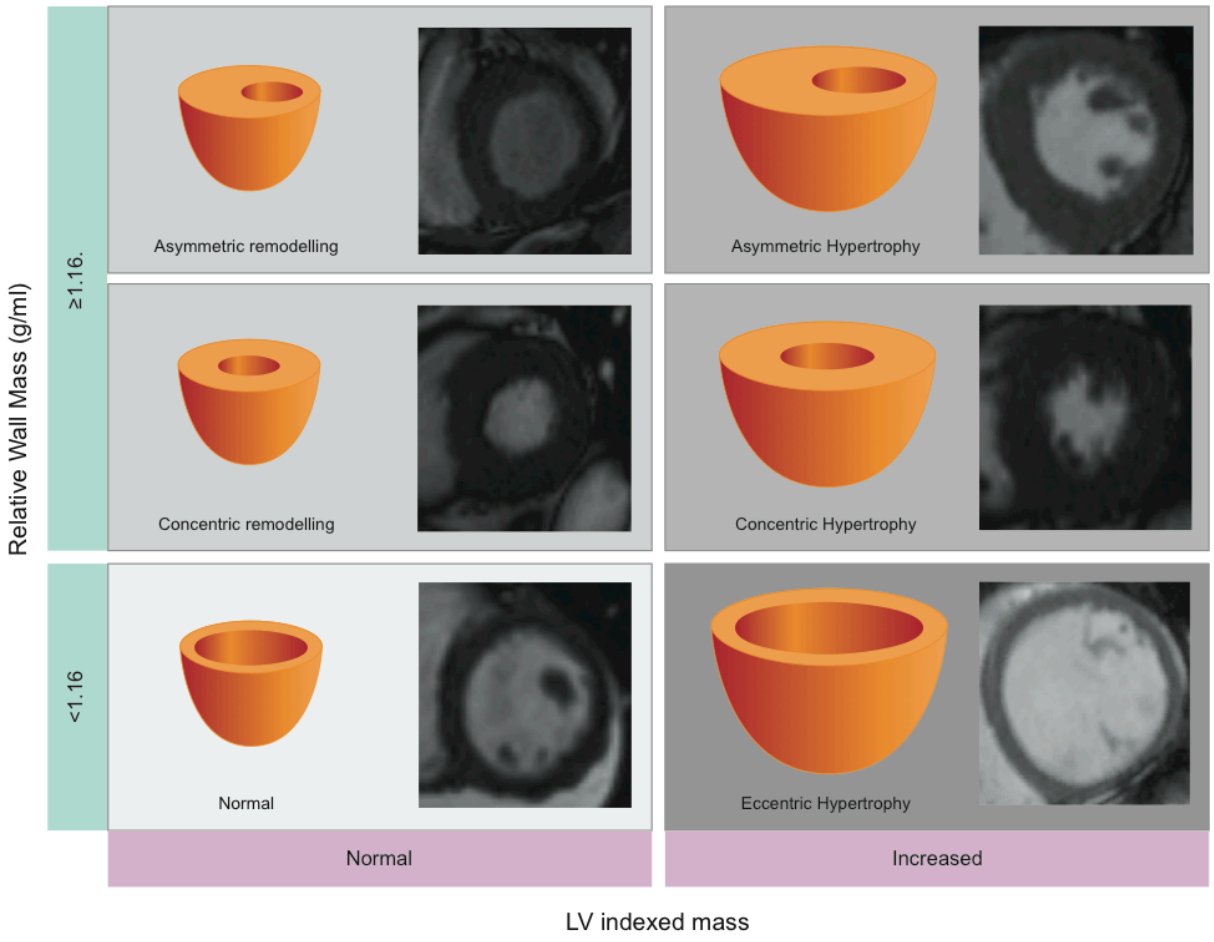

	Indexed LV Mass	Indexed LV Volume	Relative wall mass	Asymmetric wall thickening	Ejection Fraction
Normal	=	=	=	✖	=
Concentric Remodelling	=	ê	é	✖	=/é
Asymmetric Remodelling	=	ê	é	✔	=/é
Concentric Hypertrophy	é	=	é	✖	=/ê
Asymmetric Hypertrophy	é	=	é	✔	=/ê
LV Decompensation	é	é	=	✖	ê

Schematic representation of the left ventricular structure alongside CMR short-axis images of the left ventricle in end-diastole. *Normal ventricular structure,* characterised by a normal LV indexed mass and volume, and a normal relative wall mass. *Concentric remodelling,* characterised by an increased relative wall mass and normal indexed LV mass. *Asymmetric remodelling,* similar to concentric remodelling except that in addition there is evidence of asymmetric wall thickening. *Concentric Hypertrophy,* characterised by an increased relative wall mass and indexed LV mass. *Asymmetric hypertrophy,* similar to concentric hypertrophy except that in addition there is evidence of asymmetric wall thickening. *Left Ventricular Decompensation,* characterised by a dilated left ventricle and normal relative wall mass. The LV mass is increased primarily due to LV dilatation. é increased; ê decreased; = normal; ✔ present; ✖ absent.

There was no clear relationship between aortic stenosis severity and the pattern of LV remodelling/hypertrophy except that those with LV decompensation appeared to have the most severe disease. However, our study was not powered to detect differences between these groups.

Asymmetric versus Concentric Patterns of Wall Thickness

An asymmetric pattern of left ventricular wall thickness was observed in 25 patients with remodelling or hypertrophy (Table 6.3). Compared to concentric patterns, patients were older (72±11 *vs* 56±19 years, P<0.001), more likely to have hypertension (64 *vs* 33%, P=0.01) and had a greater maximal wall thickness (17±2 *vs* 15±3mm, P<0.001). The site of asymmetry was most often in the basal septum (Figure 6.3) and affected two segments of the 17-segment model in 72% of subjects (1 segment in 24%; 3 segments in 4%). In 7%, it affected the basal anterior wall but otherwise focal wall thickening was not observed outwith the septum.

Figure 6.3. Site of maximal wall thickening in asymmetric hypertrophy and remodelling based on the 17-segment model of the left ventricle. (This often involved more than one segment)

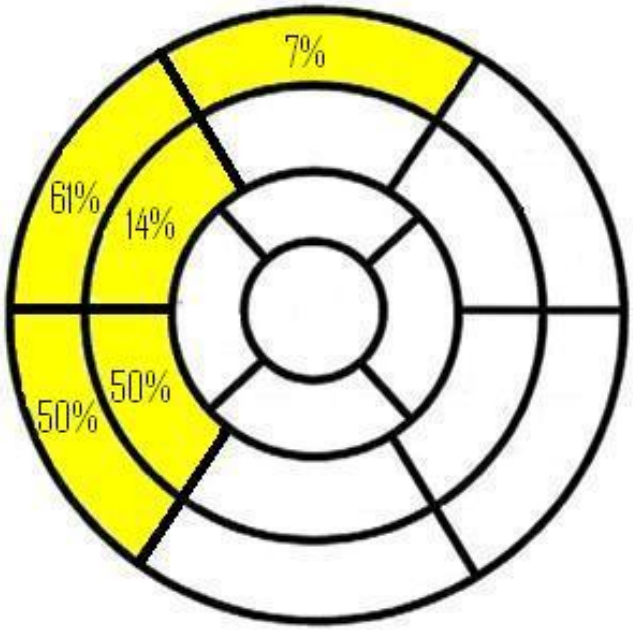

Table 6.3. Comparison of characteristics of patients with asymmetric and concentric forms of hypertrophy/remodelling in aortic stenosis.

	Concentric	Asymmetric	p-value
Number	45	25	-
Age (years)	56±19	72±11	<0.01
Male sex (%)	62	68	0.41
Indexed Mass (g/m^2)	103±25	96±25	0.23
Max wall thickness (mm)	15±3	17±2	<0.01
Remodelling (%)	24	44	0.09
Aortic valve area (cm^2)	0.96±0.36	0.96±0.30	0.83
Ejection Fraction	72±12	71±15	0.79
Indexed LVEDV (mL/m^2)	72±20	69±22	0.57
Hypertension (%)	33	64	0.01
Diabetes Mellitus (%)	11	12	0.91
ACE inhibitor / ARB use (%)	33	45	0.45
Beta-blocker (%)	16	27	0.32

6.5 DISCUSSION

This is the first study to use CMR to investigate both the magnitude of the hypertrophic response and the different morphological patterns of remodelling/ hypertrophy observed in patients with aortic stenosis. We have demonstrated that the degree of hypertrophy is independent of the severity of valve stenosis severity and have categorized patients into six distinct patterns of left ventricular adaption. These patterns provide a more detailed description of the left ventricular myocardial response to pressure overload in this condition and they include a high prevalence of asymmetric forms of remodelling and hypertrophy. Furthermore in the absence of other triggers to remodelling no patients fulfilled criteria for eccentric hypertrophy. Instead a decompensated form of remodelling associated with left ventricular dilatation, wall thinning and systolic impairment was observed.

Magnitude of the Hypertrophic Response

The magnitude of left ventricular hypertrophy varied widely but was unrelated to the severity of aortic stenosis, such that patients with severe valve narrowing were observed to have normal ventricular structure whilst patients with moderate disease often had extensive hypertrophy. This observation is important because increased LV mass is associated with the presence of mid-wall late gadolinium enhancement, which is associated with an increased mortality.[195] Indeed, left ventricular hypertrophy is an independent predictor of cardiac mortality, regardless of aetiology.[4, 56-58] There is therefore a strong rationale for considering the hypertrophic response alongside the degree of valvular narrowing when making an assessment of the overall disease severity. Further studies are required to assess whether, for example, patients with moderate disease but an advanced hypertrophic response would benefit from earlier intervention.

Male gender was the only variable associated with an increased left ventricular mass [69, 196] although an apparent trend was observed with concomitant hypertension. The latter is consistent with an analysis of the Simvastatin and Ezetimibe in Aortic Stenosis (SEAS) trial showing that hypertension together with aortic stenosis predicted increased left ventricular mass independent of other known confounders.[71] Strict blood pressure control may therefore provide an important clinical means of blunting the hypertrophic response. Finally genetic factors may have a role. They modulate the magnitude of hypertrophy in response to a number of physiological and pathological triggers.[67, 68, 180] Indeed, polymorphisms of the angiotensin-converting enzyme I/D genotype have been associated with different degrees of wall thickening and hypertrophy[69] and regression of this process after aortic valve replacement.[70]

Six Patterns of Remodelling and Hypertrophy in Aortic Stenosis

In line with previous echocardiographic definitions, we have observed normal left ventricular structure, concentric remodelling, and concentric hypertrophy, in a cohort of patients with aortic stenosis. However, no patient in our cohort met criteria for eccentric hypertrophy, rather those with a dilated left ventricle had a decompensated form of LV remodelling associated with significant impairment of left ventricular function. Furthermore we have confirmed that two additional geometric patterns also occur commonly, namely asymmetric remodelling and asymmetric hypertrophy. An asymmetric pattern of wall thickening was in fact observed in 27% of our cohort being particularly prevalent amongst the elderly and in those with hypertension. This confirms the findings of Tuseth et al who described asymmetric patterns of wall thickening in 22% of patients in aortic stenosis using echocardiography.[188] We therefore propose that there are six and not four common geometric patterns of LV adaption in aortic stenosis (Figure 6.1).

Asymmetric wall thickening was most frequently observed in the septum at the basal and mid-cavity levels with a mean of 17 mm and a maximum of 22 mm. Current guidelines recommend consideration of the diagnosis of hypertrophic cardiomyopathy if regional wall thickness exceeds 15 mm.[197] Our data therefore suggests considerable overlap in the appearances of asymmetric wall thickening in these two conditions and underlines the fact that the morphological diagnosis of hypertrophic cardiomyopathy may be challenging or impossible in the context of an increased afterload. It should be noticed that the guidelines also indicate that hypertrophic cardiomyopathy should be diagnosed only in the absence of another condition, which could explain the hypertrophic responses. Nevertheless in clinical practice the question often arises as to whether patients with an increased afterload might also have HCM. Furthermore it is plausible that specific genotypes, related to those causing hypertrophic cardiomyopathy, predispose to an asymmetric rather than concentric remodelling response to an increased afterload. In line with this theory, patients with hypertension and asymmetric thickening have a higher familial incidence of hypertrophic cardiomyopathy and more myocardial disarray.[198]

Left Ventricular Remodelling

Recent studies have suggested that Identification of left ventricular remodelling is of importance because it can be associated with paradoxical low flow aortic stenosis, in which the small cavity size and resultant low stroke volume results in a paradoxically low transvalvular aortic valve gradient.[199] Left ventricular remodelling, in both its concentric and asymmetric forms, was characterized by a normal LV mass. This was despite an increased relative wall mass and absolute wall thickness measurements that were similar to patients with hypertrophy. This apparent contradiction is explained by the small cavity size associated with remodelling. This ensures that increases in wall

thickness have a much less profound effect on LV mass than in patients with hypertrophy, who have a normal volume ventricle.

Ejection Fraction

Left ventricular decompensation can be considered as the end-stage of the hypertrophic process in which the left ventricle has failed in the face of an increased afterload. Although ejection fraction was impaired in all patients in this group, not all patients with a reduction in ejection fraction conformed to this phenotype: 41% had either concentric or asymmetric hypertrophy. It is likely that these patients are in the early stages of left ventricular decompensation but have not yet proceeded to overt LV dilatation. They represent an important group to identify because prompt surgery might avoid a further deterioration in ejection fraction, which is associated with poorer post-operative recovery [181], and may prove irreversible.

The Relative Wall Mass

CMR is widely accepted as the gold standard investigation for the measurement of left ventricular mass and volume,[190, 191] and affords more accurate measurement of wall thickness through improved contrast between the blood pool and myocardium, and the ability to image in multiple planes.[189] We believe that the CMR-derived relative wall mass is superior to the relative wall thickness, as a means of indexing wall thickness to cavity size, because it is based upon the geometry of the left ventricle as a whole and is not limited by the echocardiographic windows obtained. In addition, the relative wall mass is easily calculated as left ventricular mass and volumes are routinely quantified by CMR. Buchner *et al* have previously published measurements for this variable in 30 health volunteers

reporting values of 0.76±0.18 g/mL and an upper limit of normal of 1.12 g/mL.[193] This is very similar to the findings in our larger control cohort, and demonstrates consistency of this measurement. The apparent trend to a modest rise in the relative wall mass with increasing age, may reflect the higher arterial blood pressure and stiffness seen in older individuals.

Study Limitations

In our institution local guidelines recommend CMR for all patients with severe aortic stenosis. However patients with moderate disease were referred at the discretion of their clinician and therefore there may have been some referral bias in this group. In addition, we had incomplete data on the duration of aortic stenosis. In practice, this is difficult to adjudicate because the majority of patients will have subclinical disease for many years before a murmur is detected and the diagnosis established. The symptomatic status of our cohort was not assessed and it would be interesting to investigate its association with the pattern of remodeling.

Multi-centre longitudinal trials are required to provide prognostic information and specifically to determine whether and how patients transition between these various geometric patterns. In the era of transcatheter aortic valve implantation (TAVI), where earlier treatment may have benefit, it will also be important to assess if the different patterns of remodelling and hypertrophy show variable potential for reverse remodelling following intervention.

In clinical practice aortic stenosis is often associated with aortic or mitral regurgitation, coronary artery disease and myocardial infarction[200] that result in a composite form of ventricular adaption in many patients. In our study, we rigorously excluded patients with these co-morbidities so that the patterns of left ventricular remodelling and hypertrophy observed can be considered the direct result

of aortic valve narrowing and the associated increase in afterload. However, this has resulted in a selection bias against more elderly patients and does limit the generalizability of our findings.

In patients with left ventricular hypertrophy the ejection fraction may over estimate LV systolic function. Other measures such the corrected mid-wall shortening may better reflect myocardial contractility but were not measured in this study.

Conclusions

There is marked variation in the hypertrophic response of the LV to aortic stenosis. The degree of hypertrophy is independent of the severity of valve narrowing and it can be characterised into six distinct patterns of LV adaption, including asymmetric patterns that show considerable overlap with hypertrophic cardiomyopathy. This variation highlights the importance of detailing the left ventricular remodelling response in all patients with aortic stenosis, particularly given the adverse prognosis associated with increased levels of hypertrophy.

CONCLUSIONS

7.1 SUMMARY OF FINDINGS

The studies in this thesis have successfully applied PET/CT to the study of inflammation and calcification within the valves of patients with aortic stenosis and used CMR to study the left ventricular hypertrophic response and myocardial fibrosis. In so doing they have provided some key insights in to the pathogenesis of this common cardiac condition.

Uptake of 18F-NaF and 18F-FDG in the aortic valve

In this study the assessment of valvular calcification and inflammation using PET/CT was shown to be feasible and its quantification reproducible. Indeed measures of inter-observer and intra-observer reproducibility were excellent for both 18F-NaF and 18F-FDG. However the PET/CT scans were not performed a second time in our patients and so further studies are required to assess inter-scan reproducibility. In addition satisfactory reproducibility was only achieved for 18F-FDG measurements when peripheral regions of the valve were excluded (the centre-valve technique). Myocardial uptake of 18F-FDG presents a major challenge in assessing tracer activity in both the valve and the coronary vessels. This reflects the non-specific nature of 18F-FDG due to the central role that glucose plays in the body's metabolism. More specific tracers for inflammation are keenly awaited and these include ligands targeted to the macrophage peripheral benzodiazepine[201, 202] and somatostatin receptors.[203] Indeed improved tracer development will be the key to unlocking the potential of PET/CT as both a clinical and research tool. By contrast 18F-NaF is not routinely taken up by the myocardium or indeed other structures lying in close proximity to the heart. This allows activity in the valve, myocardium and aorta to be measured without the problem of spill-over and adds greatly to the potential to this tracer as a means of studying calcification in the cardiovascular system.

Uptake of both 18F-NaF and 18F-FDG was increased in patients with aortic sclerosis and stenosis compared to controls, displaying a progressive rise with increasing valve severity. However, calcification appears to be the predominant pathological process particularly in the latter stages of the disease and would therefore appear to be a better target for future medical therapies.

These observations further support the growing opinion that whilst similar, aortic stenosis and atherosclerosis are in fact different disease processes. Aortic stenosis appears to be established in a manner akin to atherosclerosis, with the increased 18F-FDG activity observed in the early stages reflecting the role of lipid deposition and inflammation. However, the pathogenesis of these two conditions appears to diverge once osteoblast activity has been established in the valve. Thereafter progressive calcification predominates in a manner that is quite distinct from the pathogenesis of atherosclerosis and appears to be independent and disproportionate to the degree of valvular inflammation. Consequently disease progression in these patients is more likely to be regulated by the mediators of calcium homeostasis than atherogenesis. In support of this concept, whilst atherosclerotic risk factors and serum C-reactive protein concentrations predict the development of aortic stenosis, they do not predict subsequent disease progression.[204, 205] Rather this is best predicted by the degree of valvular calcification at baseline.[205]

Uptake of 18F-NaF and 18F-FDG in the coronary arteries

Current risk stratification of patients with coronary artery disease relies on the detection of flow limiting coronary lesions that are capable of inducing myocardial ischaemia. However, contrary to this approach, studies have consistently shown that the majority of heart attacks occur on the basis on non-flow limiting lesions,[140, 141] due primarily to their increased prevalence. However, vulnerable plaques are known to be associated with certain pathological processes such as inflammation[141,151]

and microcalcification,[145] which has aroused interest in using PET/CT as a means of improving their identification. Based upon this rationale, the uptake of both 18F-NaF and 18-FDG was assessed in the coronary arteries of our aortic stenosis cohort. This was a pre-defined aim of this thesis and as such we included CT calcium scoring of the coronary arteries in our original protocol to serve as a marker of atherosclerotic burden.

18F-NaF in particular appeared to show promise as a novel pathological biomarker in atherosclerosis. Whilst a strong correlation was observed between uptake of this tracer and the coronary calcium score, 41% of patients with scores >1000 had no significant 18F-NaF uptake. This suggests that 18F-NaF uptake provides complementary information to the calcium score, relating to metabolic activity and developing micro-calcification. Indeed on the basis of these two parameters, patients could be divided in to three groups: those without calcific coronary artery disease and those with active and inactive calcific coronary atherosclerosis. Importantly increased metabolic activity of the calcific plaque appears to be of clinical significance being associated with anginal symptoms, a higher incidence of prior MACE events and elevated Framingham risk scores. Further work is required to establish whether increased 18F-NaF can truly identify plaques at risk of rupture (see Future Directions) but this study has raised hope that this technique might prove useful as a non-invasive means of studying plaque pathology and improving patient risk-stratification.

Interest has surrounded the use of 18F-FDG as a measure of coronary inflammation for many years but convincing data as to its efficacy in this role is still lacking. Again this is likely to reflect the non-specific nature of its uptake. In our studies, intense myocardial uptake of 18F-FDG was observed in a third of patients (even despite the strict dietary restrictions), which frequently resulted in spill-over in to the coronary vessels and rendered half of these territories uninterpretable. Furthermore when the

interpretable regions were analysed, there was no significant difference in coronary 18F-FDG activity between those with and without atherosclerosis. Whilst our cohort was largely made up of patient with stable coronary disease, this result is somewhat surprising given the central role that inflammation is known to play in the development and progression of atherosclerosis. This calls in to doubt the ability of this technique to measure inflammation within the coronary vessels, which are much smaller than the aortic and carotid vessels in which 18F-FDG PET has been established. However it remains possible that better results might be achieved in a younger cohort in whom dietary compliance is likely to be better and in those with unstable coronary disease in whom the inflammatory signal will be greater.

Prognostic Role of myocardial fibrosis in aortic stenosis

Using a second cohort of patients, this thesis has gone on to investigate the hypertrophic response of the left ventricle in aortic stenosis. Previous studies have generally used echocardiography for this purpose. Cardiovascular magnetic resonance offers several advantages in the assessment of left ventricular structure including improved estimation of left ventricular mass, volume and wall thickness in addition to its ability to non-invasively identify regions of replacement fibrosis and prior myocardial infarction. The late gadolinium enhancement technique has been used to identify such regions in a range of cardiac conditions and its presence has been linked to an adverse prognosis in dilated cardiomyopathy, hypertrophic cardiomyopathy and myocardial infarction.[124-128]

Both mid-wall and infarct patterns of late gadolinium enhancement have previously been reported in aortic stenosis[120, 121] and the aim of this study was to assess their prevalence and prognostic importance in a large cohort of these patients. The results demonstrated that both infarct and mid-wall patterns of LGE are common in patients with moderate and severe disease occurring in 28% and

38% of our population respectively. Mid-wall fibrosis was observed in patients with an increased left ventricular mass and in those with both moderate and severe valve narrowing. The association of fibrosis with an advanced hypertrophic response has been described before[120, 121] and suggests that mid-wall LGE might act as an early marker of ventricular decompensation. Certainly it appears to be associated with an adverse prognosis. Univariate analysis revealed that patients with mid-wall fibrosis had an eight-fold increase in all-cause mortality despite similar aortic stenosis severity and coronary artery disease burden. Patients with an infarct pattern had a six-fold increase. Moreover multivariate analysis demonstrated for the first time that CMR-detected mid-wall fibrosis was an independent predictor of mortality in aortic stenosis and had incremental value in the prognostic model to ejection fraction.

Differences in the magnitude and patterns of the hypertrophic response

The subsequent study aimed to assess the relationship between the degree of aortic valve narrowing and the magnitude of the hypertrophic response. As far as possible patients with concomitant triggers to remodelling were excluded so that assessment of left ventricular geometry could be attributed to aortic valve disease. Based upon this cohort, the study demonstrated significant individual variation in the degree of left ventricular hypertrophy, which was poorly related to the degree of valve narrowing and more closely linked to gender and concomitant hypertension. This is an important observation because it underlines the fact that the progression of valve narrowing and left ventricular hypertrophy do not necessarily go hand in hand. Given the prognostic importance associated with myocardial fibrosis and its link with advanced hypertrophy, this indicates that the ventricular response should be carefully considered along side the degree of valve narrowing when assessing patients with aortic stenosis.

Finally this same cohort was used to examine the patterns of remodelling and hypertrophy in aortic stenosis and demonstrated that asymmetric patterns of wall thickening are common, with important potential implications for the diagnosis of hypertrophic cardiomyopathy in patients with an increased afterload.

7.2 FUTURE DIRECTIONS

A number of questions have arisen from the results of this thesis and the peer review it has generated.[206, 207] As described below our research group hopes to explore these in future studies, indeed they have formed the basis of several major research grant applications.

Positron Emission Tomography

Follow up studies

Having established the feasibility and reproducibility of quantifying 18F-NaF and 18F-FDG uptake in the aortic valve, the key question is whether this technique can truly provide a measure of disease activity. In order to answer this issue, we plan to follow our PET/CT cohort over the next two years and assess whether tracer activity predicts the progression of valve narrowing. Each patient will undergo repeat echocardiography performed by the same technician on the same machine using the same protocol after both 1 and 2 years. Furthermore we shall repeat CT calcium scoring of the aortic valve after 2 years have elapsed. If it can be established that this technique predicts changes in aortic valve gradient or calcium score then this will pave the way for its use as a clinical tool and end-point in clinical trials of novel therapies.[207]

Histology studies

18F-NaF is believed to localise to areas of exposed hydroxyapatite crystal, which is an important component of both vascular calcification and skeletal bone. However this is based upon studies conducted on bone.[113] Histological validation and kinetic modeling of vascular 18F-NaF is lacking and required to establish with certainty its mechanism of uptake in the valve and coronary arteries. We have ethical permission to examine the valves of patients who participated in our PET/CT study

should they undergo subsequent aortic valve replacement, and this will provide the opportunity for histological correlation. By contrast histological validation of coronary uptake is not straightforward. However we have submitted a grant to perform kinetic modeling of carotid 18F-NaF uptake in patients undergoing endarterectomy, in whom atherosclerotic tissue will subsequently be available for pathological comparison.

Randomised control trial of anti-calcific medication in aortic stenosis

To date, there are no effective medical treatments for aortic stenosis. These are urgently required as they might avoid the need for invasive cardiac surgery in patients that are often elderly and not ideally suited to a major operation. Treatment strategies to date have focused upon targeting lipid deposition and inflammation without success. The data from this thesis suggests that calcification is in fact the dominant pathological process and therefore the better target for therapeutic intervention.

Patients with osteoporosis have an increased incidence of aortic stenosis and display more rapid rates of disease progression.[34 208] Both conditions are characterized by abnormalities in calcium metabolism and are governed by common systemic regulatory systems. These pathways help co-ordinate calcium homeostasis via the action of osteoblasts and osteoclasts and include the OPG/RANK/ RANKL axis.[40] OPG is a decoy receptor for RANKL: a potent stimulator of osteoclast differentiation and bone resorption.[209] Increased expression of RANKL and reduced levels of OPG have been observed in osteoporosis and have led to the development of denusomab, a novel anti-RANKL monoclonal antibody, as a highly efficacious and well-tolerated osteoporosis treatment.[210] Interestingly the OPG/RANK/RANKL axis also appears to regulate vascular and aortic valve calcification (Figure 2). Mice with targeted inactivation of OPG develop high-turnover osteoporosis

and extensive vascular calcification,[211 212] whilst increased expression of RANKL and reduced levels of OPG have been observed within stenotic aortic valves.[41]

We therefore believe that there is a strong rationale for investigating RANKL inhibition as a treatment strategy for aortic stenosis.[213] Indeed we have recently submitted a grant for a double blind randomised placebo-controlled trial of denosumab to assess its effect of on aortic jet velocity in 230 patients with aortic stenosis. Patients with an aortic jet velocity of ≥2.5 m/s will be recruited into the trial and randomised to denosumab 60 mg subcutaneous or matched placebo every 6 months for up to 3 years. They will undergo baseline assessments of Doppler echocardiography, computed tomography and sodium 18-fluoride positron emission tomography, and be followed up 6-monthly for Doppler echocardiography, annually for computed tomography, and at 3 and 12 months for sodium 18-fluoride PET. Disease progression will be determined by the rate of change in aortic jet velocity and the aortic valve calcium score. If successful, this study will pave the way for a larger and definitive multicentre randomised controlled trial of this therapeutic approach.

Coronary studies

We have provided preliminary data that indicates 18F-NaF may prove to be a useful tool in the study of coronary artery pathology and as a means of improving risk prediction. The next step is to identify the exact mechanism for the increased PET signal in the coronary vasculature. It is possible that active calcification may reflect a healing response to plaque rupture or alternatively a response to chronic inflammation within the necrotic plaque core. We have received a grant to investigate this issue. We will study 40 patients with stable coronary artery disease and 40 following acute coronary syndromes. All patients will undergo 18F-NaF PET/CT in addition to CT coronary angiography (to give us additional data with respect to soft plaque), invasive angiography and virtual histology intra-

vascular ultrasound (VH-IVUS). This multi-modal imaging protocol should allow us to identify accurately the plaque characteristics associated with 18F-NaF uptake. If we confirm its relationship to either recent plaque rupture or a large necrotic core then this tracer would hold considerable promise as a clinical tool in predicting future adverse cardiac events. In addition it might provide a novel biomarker that could be used to assess the numerous anti-atherosclerotic drug targets currently being developed by the pharmaceutical industry.

ECG and Respiratory Gating

Whilst the heart spends much of its time still in diastole, significant motion occurs in the aortic valve and coronary arteries during the course of the cardiac cycle. Furthermore these structures move as a result of the changes in intra-thoracic pressure that accompany respiration. The attenuation correction CT and PET scans will be affected equally by these processes nevertheless, motion artifact may limit the ability of PET/CT to localise uptake to specific coronary plaques or regions of the valve. However this problem can be overcome using ECG and respiratory gating. In collaboration with the imaging research group at Cedars-Sinai Medical Center in Los Angeles and Siemens we intend to use such gating to minimize the effects of motion in our future PET/CT projects. The basis for our approach is to only include diastolic PET data (when the coronary arteries and valve are still), which can then be refined by adjusting for respiratory motion. We anticipate that this strategy will improve the resolution with which we are able to detect PET uptake within the heart.

Cardiovascular Magnetic Resonance and Late Gadolinium Enhancement

We have established that mid-wall LGE is associated with an adverse prognosis in a prospective registry. However, there is some potential referral bias in this population given their requirement for a CMR scan. Furthermore the mechanism for the adverse prognosis remains unclear, potentially being related to impaired left ventricular function and increased arrhythmogenicity.[206]

We have been awarded a research grant in order to address these issues. As part of the study we will recruit a population of 240 adults, comprising control subjects, and patients with the full spectrum of aortic stenosis disease including a group about to undergo aortic valve replacement. This will include a large proportion of patients who originally took part in the PET studies. At baseline all subjects will undergo a standardised clinical assessment including a quality of life questionnaire, a six-minute walk test and 72-hour Holter monitoring. In addition CMR scanning will be performed with LGE of the myocardium and valve. Clinical assessment will be repeated after 1 and 2 years of follow-up and patients will also be contacted by phone and mail after 3, 4 and 5 years. We hope that this study will confirm the prognostic role of mid-wall LGE in a prospectively recruited population of aortic stenosis and provide explanation for its adverse prognosis.

T1 mapping

The late gadolinium enhancement technique is limited by the fact that it only identifies regional differences in replacement myocardial fibrosis. In patients with aortic stenosis, the predominant form is in fact diffuse interstitial fibrosis that is evenly distributed throughout the myocardium and therefore not detected. CMR T1 mapping systems have recently been developed that can identify and quantify this form of fibrosis. This technique is therefore likely to become the preferred assessment of myocardial fibrosis in aortic stenosis, having already undergone histological validation

and been shown to correlate with symptomatic status and exercise tolerance.[214, 215] However to date no study has confirmed the prognostic importance of T1 mapping in aortic stenosis. In collaboration with Siemens, who have provided us with a novel T1 mapping sequence for use at 3T, and the Royal Brompton Hospital, we shall therefore perform this technique in all the patients recruited in to the above study.

7.3 CLINICAL PERSPECTIVE

Aortic stenosis is the most common form of valve disease in the western world yet we lack any effective medical therapies capable of halting its progression. In part this reflects our incomplete understanding of the pathological mechanisms, which underlie this condition. Histopathological studies are limited by the availability of valves in the earlier stages of the disease and by an inability to monitor disease progression.

Non-invasive imaging modalities offer us the opportunity to study the pathophysiology in all stages of the disease process and have provided us with some important insights during the course of this thesis. We have demonstrated that calcification and inflammation are both active within the valve at all stages of the disease and increase as the disease advances. However calcification appears to be the dominant process particularly in the latter stages and is therefore likely to be a more effective therapeutic target.

In addition we have shown that the effects of valve narrowing on the left ventricular myocardium are also of importance. In particular there appears to be considerable variation in both the magnitude and pattern of left ventricular hypertrophy and that decompensation of this process, as detected by mid-wall late gadolinium enhancement, heralds an adverse prognosis. Given that the degree of hypertrophy is poorly related to the severity of valve narrowing, it is our opinion that the left ventricular remodeling response should be considered carefully alongside standard measures of valve narrowing when assessing overall valve severity.

These insights pave the way for larger multi-centre trials to assess whether PET/CT and CMR might allow for better prediction of aortic stenosis progression and decompensation and act as surrogate

end-points in trials of novel therapeutic strategies, in particular of anti-calcific and anti-fibrotic medication.

References

1. Nkomo VT, Gardin JM, Skelton TN, Gottdiener JS, Scott CG, Enriquez-Sarano M. Burden of valvular heart diseases: A population-based study. *Lancet*. 2006;368:1005-1011
2. Otto CM. Calcific aortic stenosis--time to look more closely at the valve. *N Engl J Med*. 2008;359:1395-1398
3. Pellikka PA, Sarano ME, Nishimura RA, Malouf JF, Bailey KR, Scott CG, Barnes ME, Tajik AJ. Outcome of 622 adults with asymptomatic, hemodynamically significant aortic stenosis during prolonged follow-up. *Circulation*. 2005;111:3290-3295
4. Cioffi G, Faggiano P, Vizzardi E, Tarantini L, Cramariuc D, Gerdts E, de Simone G. Prognostic effect of inappropriately high left ventricular mass in asymptomatic severe aortic stenosis. *Heart*. 2011;97:301-307
5. Thubrikar MJ, Nolan SP, Aouad J, Deck JD. Stress sharing between the sinus and leaflets of canine aortic valve. *Ann Thorac Surg*. 1986;42:434-440
6. Freeman RV, Otto CM. Spectrum of calcific aortic valve disease: Pathogenesis, disease progression, and treatment strategies. *Circulation*. 2005;111:3316-3326
7. Otto CM, Kuusisto J, Reichenbach DD, Gown AM, O'Brien KD. Characterization of the early lesion of 'degenerative' valvular aortic stenosis. Histological and immunohistochemical studies. *Circulation*. 1994;90:844-853
8. Pachulski RT, Chan KL. Progression of aortic valve dysfunction in 51 adult patients with congenital bicuspid aortic valve: Assessment and follow up by doppler echocardiography. *Br Heart J*. 1993;69:237-240
9. Beppu S, Suzuki S, Matsuda H, Ohmori F, Nagata S, Miyatake K. Rapidity of progression of aortic stenosis in patients with congenital bicuspid aortic valves. *Am J Cardiol*. 1993;71:322-327
10. O'Brien KD, Reichenbach DD, Marcovina SM, Kuusisto J, Alpers CE, Otto CM. Apolipoproteins b, (a), and e accumulate in the morphologically early lesion of 'degenerative' valvular aortic stenosis. *Arterioscler Thromb Vasc Biol*. 1996;16:523-532
11. Olsson M, Thyberg J, Nilsson J. Presence of oxidized low density lipoprotein in nonrheumatic stenotic aortic valves. *Arterioscler Thromb Vasc Biol*. 1999;19:1218-1222
12. Parhami F, Morrow AD, Balucan J, Leitinger N, Watson AD, Tintut Y, Berliner JA, Demer LL. Lipid oxidation products have opposite effects on calcifying vascular cell and bone cell differentiation. A possible explanation for the paradox of arterial calcification in osteoporotic patients. *Arterioscler Thromb Vasc Biol*. 1997;17:680-687
13. Ghaisas NK, Foley JB, O'Briain DS, Crean P, Kelleher D, Walsh M. Adhesion molecules in nonrheumatic aortic valve disease: Endothelial expression, serum levels and effects of valve replacement. *J Am Coll Cardiol*. 2000;36:2257-2262
14. Jian B, Narula N, Li QY, Mohler ER, 3rd, Levy RJ. Progression of aortic valve stenosis: Tgf-beta1 is present in calcified aortic valve cusps and promotes aortic valve interstitial cell calcification via apoptosis. *Ann Thorac Surg*. 2003;75:457-465; discussion 465-456
15. Kaden JJ, Dempfle CE, Grobholz R, Tran HT, Kilic R, Sarikoc A, Brueckmann M, Vahl C, Hagl S, Haase KK, Borggrefe M. Interleukin-1 beta promotes matrix metalloproteinase expression and cell proliferation in calcific aortic valve stenosis. *Atherosclerosis*. 2003;170:205-211
16. Galante A, Pietroiusti A, Vellini M, Piccolo P, Possati G, De Bonis M, Grillo RL, Fontana C, Favalli C. C-reactive protein is increased in patients with degenerative aortic valvular stenosis. *J Am Coll Cardiol*. 2001;38:1078-1082

17. Skowasch D, Schrempf S, Preusse CJ, Likungu JA, Welz A, Luderitz B, Bauriedel G. Tissue resident c reactive protein in degenerative aortic valves: Correlation with serum c reactive protein concentrations and modification by statins. *Heart*. 2006;92:495-498
18. Toutouzas K, Drakopoulou M, Synetos A, Tsiamis E, Agrogiannis G, Kavantzas N, Patsouris E, Iliopoulos D, Theodoropoulos S, Yacoub M, Stefanadis C. In vivo aortic valve thermal heterogeneity in patients with nonrheumatic aortic valve stenosis the: First in vivo experience in humans. *J Am Coll Cardiol*. 2008;52:758-763
19. Fayad ZA, Mani V, Woodward M, Kallend D, Abt M, Burgess T, Fuster V, Ballantyne CM, Stein EA, Tardif JC, Rudd JH, Farkouh ME, Tawakol A. Safety and efficacy of dalcetrapib on atherosclerotic disease using novel non-invasive multimodality imaging (dal-plaque): A randomised clinical trial. *Lancet*. 2011; 378: 1547-1549
20. Marincheva-Savcheva G, Subramanian S, Qadir S, Figueroa A, Truong Q, Vijayakumar J, Brady TJ, Hoffmann U, Tawakol A. Imaging of the aortic valve using fluorodeoxyglucose positron emission tomography increased valvular fluorodeoxyglucose uptake in aortic stenosis. *J Am Coll Cardiol*. 2011;57:2507-2515
21. Mazzone A, Epistolato MC, De Caterina R, Storti S, Vittorini S, Sbrana S, Gianetti J, Bevilacqua S, Glauber M, Biagini A, Tanganelli P. Neoangiogenesis, t-lymphocyte infiltration, and heat shock protein-60 are biological hallmarks of an immunomediated inflammatory process in end-stage calcified aortic valve stenosis. *J Am Coll Cardiol*. 2004;43:1670-1676
22. Mazzone A, Epistolato MC, Gianetti J, Castagnini M, Sassi C, Ceravolo R, Bevilacqua S, Glauber M, Biagini A, Tanganelli P. Biological features (inflammation and neoangiogenesis) and atherosclerotic risk factors in carotid plaques and calcified aortic valve stenosis: Two different sites of the same disease? *Am J Clin Pathol*. 2006;126:494-502
23. Akahori H, Tsujino T, Naito Y, Matsumoto M, Lee-Kawabata M, Ohyanagi M, Mitsuno M, Miyamoto Y, Daimon T, Hao H, Hirota S, Masuyama T. Intraleaflet haemorrhage is associated with rapid progression of degenerative aortic valve stenosis. *Eur Heart J*. 2011;32:888-896
24. Liu AC, Joag VR, Gotlieb AI. The emerging role of valve interstitial cell phenotypes in regulating heart valve pathobiology. *Am J Pathol*. 2007;171:1407-1418
25. Sun Y, Weber KT. Infarct scar: A dynamic tissue. *Cardiovasc Res*. 2000;46:250-256
26. Kaden JJ, Dempfle CE, Grobholz R, Fischer CS, Vocke DC, Kilic R, Sarikoc A, Pinol R, Hagl S, Lang S, Brueckmann M, Borggrefe M. Inflammatory regulation of extracellular matrix remodeling in calcific aortic valve stenosis. *Cardiovasc Pathol*. 2005;14:80-87
27. Soini Y, Satta J, Maatta M, Autio-Harmainen H. Expression of mmp2, mmp9, mt1-mmp, timp1, and timp2 mrna in valvular lesions of the heart. *J Pathol*. 2001;194:225-231
28. O'Brien KD, Shavelle DM, Caulfield MT, McDonald TO, Olin-Lewis K, Otto CM, Probstfield JL. Association of angiotensin-converting enzyme with low-density lipoprotein in aortic valvular lesions and in human plasma. *Circulation*. 2002;106:2224-2230
29. Zhou G, Kandala JC, Tyagi SC, Katwa LC, Weber KT. Effects of angiotensin ii and aldosterone on collagen gene expression and protein turnover in cardiac fibroblasts. *Mol Cell Biochem*. 1996;154:171-178
30. Cowell SJ, Newby DE, Burton J, White A, Northridge DB, Boon NA, Reid J. Aortic valve calcification on computed tomography predicts the severity of aortic stenosis. *Clin Radiol*. 2003;58:712-716
31. Davies SW, Gershlick AH, Balcon R. Progression of valvar aortic stenosis: A long-term retrospective study. *Eur Heart J*. 1991;12:10-14

32. Rosenhek R, Binder T, Porenta G, Lang I, Christ G, Schemper M, Maurer G, Baumgartner H. Predictors of outcome in severe, asymptomatic aortic stenosis. *N Engl J Med*. 2000;343:611-617
33. Strickberger SA, Schulman SP, Hutchins GM. Association of paget's disease of bone with calcific aortic valve disease. *Am J Med*. 1987;82:953-956
34. Skolnick AH, Osranek M, Formica P, Kronzon I. Osteoporosis treatment and progression of aortic stenosis. *Am J Cardiol*. 2009;104:122-124
35. Ortlepp JR, Hoffmann R, Ohme F, Lauscher J, Bleckmann F, Hanrath P. The vitamin d receptor genotype predisposes to the development of calcific aortic valve stenosis. *Heart*. 2001;85:635-638
36. Urena P, Malergue MC, Goldfarb B, Prieur P, Guedon-Rapoud C, Petrover M. Evolutive aortic stenosis in hemodialysis patients: Analysis of risk factors. *Nephrologie*. 1999;20:217-225
37. Cosmi JE, Kort S, Tunick PA, Rosenzweig BP, Freedberg RS, Katz ES, Applebaum RM, Kronzon I. The risk of the development of aortic stenosis in patients with "benign" aortic valve thickening. *Arch Intern Med*. 2002;162:2345-2347
38. Osman L, Yacoub MH, Latif N, Amrani M, Chester AH. Role of human valve interstitial cells in valve calcification and their response to atorvastatin. *Circulation*. 2006;114:I547-552
39. Rajamannan NM. Calcific aortic stenosis: Lessons learned from experimental and clinical studies. *Arterioscler Thromb Vasc Biol*. 2009;29:162-168
40. Caira FC, Stock SR, Gleason TG, McGee EC, Huang J, Bonow RO, Spelsberg TC, McCarthy PM, Rahimtoola SH, Rajamannan NM. Human degenerative valve disease is associated with up-regulation of low-density lipoprotein receptor-related protein 5 receptor-mediated bone formation. *J Am Coll Cardiol*. 2006;47:1707-1712
41. Kaden JJ, Bickelhaupt S, Grobholz R, Haase KK, Sarikoc A, Kilic R, Brueckmann M, Lang S, Zahn I, Vahl C, Hagl S, Dempfle CE, Borggrefe M. Receptor activator of nuclear factor kappab ligand and osteoprotegerin regulate aortic valve calcification. *J Mol Cell Cardiol*. 2004;36:57-66
42. Kaden JJ, Kilic R, Sarikoc A, Hagl S, Lang S, Hoffmann U, Brueckmann M, Borggrefe M. Tumor necrosis factor alpha promotes an osteoblast-like phenotype in human aortic valve myofibroblasts: A potential regulatory mechanism of valvular calcification. *Int J Mol Med*. 2005;16:869-872
43. Mohler ER, 3rd, Chawla MK, Chang AW, Vyavahare N, Levy RJ, Graham L, Gannon FH. Identification and characterization of calcifying valve cells from human and canine aortic valves. *J Heart Valve Dis*. 1999;8:254-260
44. Rajamannan NM, Subramaniam M, Rickard D, Stock SR, Donovan J, Springett M, Orszulak T, Fullerton DA, Tajik AJ, Bonow RO, Spelsberg T. Human aortic valve calcification is associated with an osteoblast phenotype. *Circulation*. 2003;107:2181-2184
45. O'Brien KD, Kuusisto J, Reichenbach DD, Ferguson M, Giachelli C, Alpers CE, Otto CM. Osteopontin is expressed in human aortic valvular lesions. *Circulation*. 1995;92:2163-2168
46. Mohler ER, 3rd, Gannon F, Reynolds C, Zimmerman R, Keane MG, Kaplan FS. Bone formation and inflammation in cardiac valves. *Circulation*. 2001;103:1522-1528
47. Kaden JJ, Bickelhaupt S, Grobholz R, Vahl CF, Hagl S, Brueckmann M, Haase KK, Dempfle CE, Borggrefe M. Expression of bone sialoprotein and bone morphogenetic protein-2 in calcific aortic stenosis. *J Heart Valve Dis*. 2004;13:560-566
48. Ix JH, Chertow GM, Shlipak MG, Brandenburg VM, Ketteler M, Whooley MA. Association of fetuin-a with mitral annular calcification and aortic stenosis among persons with coronary heart disease: Data from the heart and soul study. *Circulation*. 2007;115:2533-2539

49. Moe SM, Reslerova M, Ketteler M, O'Neill K, Duan D, Koczman J, Westenfeld R, Jahnen-Dechent W, Chen NX. Role of calcification inhibitors in the pathogenesis of vascular calcification in chronic kidney disease (ckd). *Kidney Int*. 2005;67:2295-2304
50. Wang AY, Woo J, Lam CW, Wang M, Chan IH, Gao P, Lui SF, Li PK, Sanderson JE. Associations of serum fetuin-a with malnutrition, inflammation, atherosclerosis and valvular calcification syndrome and outcome in peritoneal dialysis patients. *Nephrol Dial Transplant*. 2005;20:1676-1685
51. Mohler ER, 3rd, Adam LP, McClelland P, Graham L, Hathaway DR. Detection of osteopontin in calcified human aortic valves. *Arterioscler Thromb Vasc Biol*. 1997;17:547-552
52. Grossman W JD, McLaurin L. Wall stress and patterns of hypertrophy in the human left ventricle. . *J Clin Invest* 1975;56:56-64
53. Carabello BA. The relationship of left ventricular geometry and hypertrophy to left ventricular function in valvular heart disease. . *J Heart Valve Dis* 1995;4 Suppl 2:S132–138, discussion S138–139
54. Kupari M, Turto H, Lommi J. Left ventricular hypertrophy in aortic valve stenosis: Preventive or promotive of systolic dysfunction and heart failure? *Eur Heart J*. 2005;26:1790-1796
55. Levy D, Garrison RJ, Savage DD, Kannel WB, Castelli WP. Prognostic implications of echocardiographically determined left ventricular mass in the framingham heart study. *N Engl J Med*. 1990;322:1561-1566
56. Gosse P. Left ventricular hypertrophy as a predictor of cardiovascular risk. *J Hypertens Suppl*. 2005;23:S27-33
57. Spirito P, Bellone P, Harris KM, Bernabo P, Bruzzi P, Maron BJ. Magnitude of left ventricular hypertrophy and risk of sudden death in hypertrophic cardiomyopathy. *N Engl J Med*. 2000;342:1778-1785
58. Gradman AH AF. From left ventricular hypertrophy to congestive heart failure: Management of hypertensive heart disease. *Prog Cardiovasc Dis* 2006;48:326-341
59. Schillaci G, Verdecchia P, Porcellati C, Cuccurullo O, Cosco C, Perticone F. Continuous relation between left ventricular mass and cardiovascular risk in essential hypertension. *Hypertension*. 2000;35:580-586
60. Esposito G, Rapacciuolo A, Naga Prasad SV, Takaoka H, Thomas SA, Koch WJ, Rockman HA. Genetic alterations that inhibit in vivo pressure-overload hypertrophy prevent cardiac dysfunction despite increased wall stress. *Circulation*. 2002;105:85-92
61. Salcedo EE, Korzick DH, Currie PJ, Stewart WJ, Lever HM, Goormastic M. Determinants of left ventricular hypertrophy in patients with aortic stenosis. *Cleve Clin J Med*. 1989;56:590-596
62. Gunther S, Grossman W. Determinants of ventricular function in pressure-overload hypertrophy in man. *Circulation*. 1979;59:679-688
63. Lavie CJ, Milani RV, Ventura HO, Cardenas GA, Mehra MR, Messerli FH. Disparate effects of left ventricular geometry and obesity on mortality in patients with preserved left ventricular ejection fraction. *Am J Cardiol*. 2007;100:1460-1464
64. Lavie CJ, Milani RV, Patel D, Artham SM, Ventura HO. Disparate effects of obesity and left ventricular geometry on mortality in 8088 elderly patients with preserved systolic function. *Postgrad Med*. 2009;121:119-125
65. Lavie CJ, Milani RV, Messerli FH. Prevention and reduction of left ventricular hypertrophy in the elderly. *Clin Geriatr Med*. 1996;12:57-68
66. Schunkert H, Brockel U, Hengstenberg C, Luchner A, Muscholl MW, Kurzidim K, Kuch B, Doring A, Riegger GA, Hense HW. Familial predisposition of left ventricular hypertrophy. *J Am Coll Cardiol*. 1999;33:1685-1691

67. Montgomery HE CP, Dollery C, Prasad K, Losi MA. Association of angiotensin-converting enzyme gene i/d polymorphism with change in left ventricular mass in response to physical training. *Circulation*. 1997;96:741-747
68. Marian AJ. Genetic determinants of cardiac hypertrophy. *Curr Opin Cardiol* 2008;115:199-205
69. Orlowska-Baranowska E, Placha G, Gaciong Z, Baranowski R, Zakrzewski D, Michalek P, Hoffman P, Rawczynska-Englert I. Influence of ace i/d genotypes on left ventricular hypertrophy in aortic stenosis: Gender-related differences. *J Heart Valve Dis*. 2004;13:574-581
70. Dellgren G, Eriksson MJ, Blange I, Brodin LA, Radegran K, Sylven C. Angiotensin-converting enzyme gene polymorphism influences degree of left ventricular hypertrophy and its regression in patients undergoing operation for aortic stenosis. *Am J Cardiol*. 1999;84:909-913
71. Rieck AE, Cramariuc D, Staal EM, Rossebo AB, Wachtell K, Gerdts E. Impact of hypertension on left ventricular structure in patients with asymptomatic aortic valve stenosis (a seas substudy). *J Hypertens*. 2010;28:377-383
72. Briand M, Dumesnil JG, Kadem L, Tongue AG, Rieu R, Garcia D, Pibarot P. Reduced systemic arterial compliance impacts significantly on left ventricular afterload and function in aortic stenosis: Implications for diagnosis and treatment. *J Am Coll Cardiol*. 2005;46:291-298
73. Hachicha Z, Dumesnil JG, Pibarot P. Usefulness of the valvuloarterial impedance to predict adverse outcome in asymptomatic aortic stenosis. *J Am Coll Cardiol*. 2009;54:1003-1011
74. Hein S AE, Kostin S, Schönburg M, Elsässer W et al Progression from compensated hypertrophy to failure in the pressure-overloaded human heart structural deterioration and compensatory mechanisms. *Circulation*. 2003;107:984-991
75. Bishopric NH, Andreka P, Slepak T, Webster KA. Molecular mechanisms of apoptosis in the cardiac myocyte. *Curr Opin Pharmacol*. 2001;1:141-150
76. Cheng W, Li B, Kajstura J, Li P, Wolin MS, Sonnenblick EH, Hintze TH, Olivetti G, Anversa P. Stretch-induced programmed myocyte cell death. *J Clin Invest*. 1995;96:2247-2259
77. Leri A, Claudio PP, Li Q, Wang X, Reiss K, Wang S, Malhotra A, Kajstura J, Anversa P. Stretch-mediated release of angiotensin ii induces myocyte apoptosis by activating p53 that enhances the local renin-angiotensin system and decreases the bcl-2-to-bax protein ratio in the cell. *J Clin Invest*. 1998;101:1326-1342
78. Gonzalez A, Lopez B, Ravassa S, Querejeta R, Larman M, Diez J, Fortuno MA. Stimulation of cardiac apoptosis in essential hypertension: Potential role of angiotensin ii. *Hypertension*. 2002;39:75-80
79. Schluter KD, Wenzel S. Angiotensin ii: A hormone involved in and contributing to pro-hypertrophic cardiac networks and target of anti-hypertrophic cross-talks. *Pharmacol Ther*. 2008;119:311-325
80. Marcus ML, Koyanagi S, Harrison DG, Doty DB, Hiratzka LF, Eastham CL. Abnormalities in the coronary circulation that occur as a consequence of cardiac hypertrophy. *Am J Med*. 1983;75:62-66
81. Galiuto L, Lotrionte M, Crea F, Anselmi A, Biondi-Zoccai GG, De Giorgio F, Baldi A, Baldi F, Possati G, Gaudino M, Vetrovec GW, Abbate A. Impaired coronary and myocardial flow in severe aortic stenosis is associated with increased apoptosis: A transthoracic doppler and myocardial contrast echocardiography study. *Heart*. 2006;92:208-212
82. Steadman CD, Jerosch-Herold M, Grundy B, Rafelt S, Ng LL, Squire IB, Samani NJ, McCann GP. Determinants and functional significance of myocardial perfusion reserve in severe aortic stenosis. *JACC Cardiovasc Imaging*. 2012;5:182-189

83. Rajappan K, Rimoldi OE, Camici PG, Bellenger NG, Pennell DJ, Sheridan DJ. Functional changes in coronary microcirculation after valve replacement in patients with aortic stenosis. *Circulation*. 2003;107:3170-3175
84. Anderson KR, Sutton MG, Lie JT. Histopathological types of cardiac fibrosis in myocardial disease. *J Pathol*. 1979;128:79-85
85. Krayenbuehl HP HO, Monrad ES, et al. Left ventricular myocardial structure in aortic valve disease before, intermediate, and late after aortic valve replacement. *Circulation*. 1989;79:744-755
86. Weber KT. Fibrosis in hypertensive heart disease: Focus on cardiac fibroblasts. *J Hypertens*. 2004;22:47-50
87. Bing OH, Ngo HQ, Humphries DE, Robinson KG, Lucey EC, Carver W, Brooks WW, Conrad CH, Hayes JA, Goldstein RH. Localization of alpha1(i) collagen mrna in myocardium from the spontaneously hypertensive rat during the transition from compensated hypertrophy to failure. *J Mol Cell Cardiol*. 1997;29:2335-2344
88. Lindsay MM, Maxwell P, Dunn FG. Timp-1: A marker of left ventricular diastolic dysfunction and fibrosis in hypertension. *Hypertension*. 2002;40:136-141
89. Heymans S, Schroen B, Vermeersch P, Milting H, Gao F, Kassner A, Gillijns H, Herijgers P, Flameng W, Carmeliet P, Van de Werf F, Pinto YM, Janssens S. Increased cardiac expression of tissue inhibitor of metalloproteinase-1 and tissue inhibitor of metalloproteinase-2 is related to cardiac fibrosis and dysfunction in the chronic pressure-overloaded human heart. *Circulation*. 2005;112:1136-1144
90. Polyakova V, Hein S, Kostin S, Ziegelhoeffer T, Schaper J. Matrix metalloproteinases and their tissue inhibitors in pressure-overloaded human myocardium during heart failure progression. *J Am Coll Cardiol*. 2004;44:1609-1618
91. Rossebo AB, Pedersen TR, Boman K, Brudi P, Chambers JB, Egstrup K, Gerdts E, Gohlke-Barwolf C, Holme I, Kesaniemi YA, Malbecq W, Nienaber CA, Ray S, Skjaerpe T, Wachtell K, Willenheimer R. Intensive lipid lowering with simvastatin and ezetimibe in aortic stenosis. *N Engl J Med*. 2008;359:1343-1356
92. Cowell SJ, Newby DE, Prescott RJ, Bloomfield P, Reid J, Northridge DB, Boon NA. A randomized trial of intensive lipid-lowering therapy in calcific aortic stenosis. *N Engl J Med*. 2005;352:2389-2397
93. Chan KL, Teo K, Dumesnil JG, Ni A, Tam J. Effect of lipid lowering with rosuvastatin on progression of aortic stenosis: Results of the aortic stenosis progression observation: Measuring effects of rosuvastatin (astronomer) trial. *Circulation*.2010. 121:306-314
94. Houslay ES, Cowell SJ, Prescott RJ, Reid J, Burton J, Northridge DB, Boon NA, Newby DE. Progressive coronary calcification despite intensive lipid-lowering treatment: A randomised controlled trial. *Heart*. 2006;92:1207-1212
95. Arad Y, Spadaro LA, Roth M, Newstein D, Guerci AD. Treatment of asymptomatic adults with elevated coronary calcium scores with atorvastatin, vitamin c, and vitamin e: The st. Francis heart study randomized clinical trial. *J Am Coll Cardiol*. 2005;46:166-172
96. Raggi P, Davidson M, Callister TQ, Welty FK, Bachmann GA, Hecht H, Rumberger JA. Aggressive versus moderate lipid-lowering therapy in hypercholesterolemic postmenopausal women: Beyond endorsed lipid lowering with ebt scanning (belles). *Circulation*. 2005;112:563-571
97. Lin E.C AA. *Pet and pet/ct. A clinical guide*. Thieme, New York Stuttgart; 2005.
98. Rudd JH, Narula J, Strauss HW, Virmani R, Machac J, Klimas M, Tahara N, Fuster V, Warburton EA, Fayad ZA, Tawakol AA. Imaging atherosclerotic plaque inflammation by fluorodeoxyglucose with positron emission tomography: Ready for prime time? *J Am Coll Cardiol*.2010. 55:2527-2535

99. Rudd JH, Warburton EA, Fryer TD, Jones HA, Clark JC, Antoun N, Johnstrom P, Davenport AP, Kirkpatrick PJ, Arch BN, Pickard JD, Weissberg PL. Imaging atherosclerotic plaque inflammation with [18f]-fluorodeoxyglucose positron emission tomography. *Circulation*. 2002;105:2708-2711
100. Tawakol A, Migrino RQ, Bashian GG, Bedri S, Vermylen D, Cury RC, Yates D, LaMuraglia GM, Furie K, Houser S, Gewirtz H, Muller JE, Brady TJ, Fischman AJ. In vivo 18f-fluorodeoxyglucose positron emission tomography imaging provides a noninvasive measure of carotid plaque inflammation in patients. *J Am Coll Cardiol*. 2006;48:1818-1824
101. Folco EJ SY, Rocha VZ, Christen T, Shvartz E, Sukhova GK, Di Carli MF, Libby P Hypoxia but not inflammation augments glucose uptake in human macrophages. *Journal of the American College of Cardiology*. 2011;58:603-614
102. Rudd JH, Myers KS, Bansilal S, Machac J, Rafique A, Farkouh M, Fuster V, Fayad ZA. (18)fluorodeoxyglucose positron emission tomography imaging of atherosclerotic plaque inflammation is highly reproducible: Implications for atherosclerosis therapy trials. *J Am Coll Cardiol*. 2007;50:892-896
103. Rudd JH, Myers KS, Bansilal S, Machac J, Pinto CA, Tong C, Rafique A, Hargeaves R, Farkouh M, Fuster V, Fayad ZA. Atherosclerosis inflammation imaging with 18f-fdg pet: Carotid, iliac, and femoral uptake reproducibility, quantification methods, and recommendations. *J Nucl Med*. 2008;49:871-878
104. Paulmier B, Duet M, Khayat R, Pierquet-Ghazzar N, Laissy JP, Maunoury C, Hugonnet F, Sauvaget E, Trinquart L, Faraggi M. Arterial wall uptake of fluorodeoxyglucose on pet imaging in stable cancer disease patients indicates higher risk for cardiovascular events. *J Nucl Cardiol*. 2008;15:209-217
105. Rominger A, Saam T, Wolpers S, Cyran CC, Schmidt M, Foerster S, Nikolaou K, Reiser MF, Bartenstein P, Hacker M. 18f-fdg pet/ct identifies patients at risk for future vascular events in an otherwise asymptomatic cohort with neoplastic disease. *J Nucl Med*. 2009;50:1611-1620
106. Rogers IS, Nasir K, Figueroa AL, Cury RC, Hoffmann U, Vermylen DA, Brady TJ, Tawakol A. Feasibility of fdg imaging of the coronary arteries: Comparison between acute coronary syndrome and stable angina. *JACC Cardiovasc Imaging*. 2010; 3:388-397
107. Cheng VY, Slomka PJ, Ahlen M, Thomson LE, Waxman AD, Berman DS. Impact of carbohydrate restriction with and without fatty acid loading on myocardial (18)f-fdg uptake during pet: A randomized controlled trial. *J Nucl Cardiol*. 2010;17:286-291
108. Wykrzykowska J, Lehman S, Williams G, Parker JA, Palmer MR, Varkey S, Kolodny G, Laham R. Imaging of inflamed and vulnerable plaque in coronary arteries with 18f-fdg pet/ct in patients with suppression of myocardial uptake using a low-carbohydrate, high-fat preparation. *J Nucl Med*. 2009;50:563-568
109. Installe J, Nzeusseu A, Bol A, Depresseux G, Devogelaer JP, Lonneux M. (18)f-fluoride pet for monitoring therapeutic response in paget's disease of bone. *J Nucl Med*. 2005;46:1650-1658
110. Grant FD, Fahey FH, Packard AB, Davis RT, Alavi A, Treves ST. Skeletal pet with 18f-fluoride: Applying new technology to an old tracer. *J Nucl Med*. 2008;49:68-78
111. Derlin T, Richter U, Bannas P, Begemann P, Buchert R, Mester J, Klutmann S. Feasibility of 18f-sodium fluoride pet/ct for imaging of atherosclerotic plaque. *J Nucl Med*. 2010; 51:862-865
112. Derlin T, Wisotzki C, Richter U, Apostolova I, Bannas P, Weber C, Mester J, Klutmann S. In vivo imaging of mineral deposition in carotid plaque using 18f-sodium fluoride pet/ct: Correlation with atherogenic risk factors. *J Nucl Med*. 2011; 52:362-368
113. Blau M, Ganatra R, Bender MA. 18 f-fluoride for bone imaging. *Semin Nucl Med*. 1972;2:31-37

114. Foldager CB, Bendtsen M, Bunger C. Pet scanning for evaluation of bone metabolism. *Acta Orthop*. 2009;80:737-738; author reply 738-739
115. Hawkins RA, Choi Y, Huang SC, Hoh CK, Dahlbom M, Schiepers C, Satyamurthy N, Barrio JR, Phelps ME. Evaluation of the skeletal kinetics of fluorine-18-fluoride ion with pet. *J Nucl Med*. 1992;33:633-642
116. Toegel S, Hoffmann O, Wadsak W, Ettlinger D, Mien LK, Wiesner K, Nguemo J, Viernstein H, Kletter K, Dudczak R, Mitterhauser M. Uptake of bone-seekers is solely associated with mineralisation! A study with 99mtc-mdp, 153sm-edtmp and 18f-fluoride on osteoblasts. *Eur J Nucl Med Mol Imaging*. 2006;33:491-494
117. Massimo Lombardi CC. *Mri of the heart and vessels*. Springer Milan Berlin Heidelberg New York; 2004.
118. Hundley WG, Bluemke DA, Finn JP, Flamm SD, Fogel MA, Friedrich MG, Ho VB, Jerosch-Herold M, Kramer CM, Manning WJ, Patel M, Pohost GM, Stillman AE, White RD, Woodard PK. Accf/acr/aha/nasci/scmr 2010 expert consensus document on cardiovascular magnetic resonance: A report of the american college of cardiology foundation task force on expert consensus documents. *J Am Coll Cardiol*. 2010;55:2614-2662
119. John AS, Dill T, Brandt RR, Rau M, Ricken W, Bachmann G, Hamm CW. Magnetic resonance to assess the aortic valve area in aortic stenosis: How does it compare to current diagnostic standards? *J Am Coll Cardiol*. 2003;42:519-526
120. Debl K, Djavidani B, Buchner S, Lipke C, Nitz W, Feuerbach S, Riegger G, Luchner A. Delayed hyperenhancement in magnetic resonance imaging of left ventricular hypertrophy caused by aortic stenosis and hypertrophic cardiomyopathy: Visualisation of focal fibrosis. *Heart*. 2006;92:1447-1451
121. Rudolph A, Abdel-Aty H, Bohl S, Boye P, Zagrosek A, Dietz R, Schulz-Menger J. Noninvasive detection of fibrosis applying contrast-enhanced cardiac magnetic resonance in different forms of left ventricular hypertrophy relation to remodeling. *J Am Coll Cardiol*. 2009;53:284-291
122. Weidemann F, Herrmann S, Stork S, Niemann M, Frantz S, Lange V, Beer M, Gattenlohner S, Voelker W, Ertl G, Strotmann JM. Impact of myocardial fibrosis in patients with symptomatic severe aortic stenosis. *Circulation*. 2009;120:577-584
123. Herrmann S, Stork S, Niemann M, Lange V, Strotmann JM, Frantz S, Beer M, Gattenlohner S, Voelker W, Ertl G, Weidemann F. Low-gradient aortic valve stenosis myocardial fibrosis and its influence on function and outcome. *J Am Coll Cardiol*. 2011;58:402-412
124. Kwong RY, Chan AK, Brown KA, Chan CW, Reynolds HG, Tsang S, Davis RB. Impact of unrecognized myocardial scar detected by cardiac magnetic resonance imaging on event-free survival in patients presenting with signs or symptoms of coronary artery disease. *Circulation*. 2006;113:2733-2743
125. Assomull RG, Prasad SK, Lyne J, Smith G, Burman ED, Khan M, Sheppard MN, Poole-Wilson PA, Pennell DJ. Cardiovascular magnetic resonance, fibrosis, and prognosis in dilated cardiomyopathy. *J Am Coll Cardiol*. 2006;48:1977-1985
126. Moon JC MW, McCrohon JA, Elliott PM, Smith GC, Pennell DJ. Toward clinical risk assessment in hypertrophic cardiomyopathy with gadolinium cardiovascular magnetic resonance. . *J Am Coll Cardiol* 2003;41:1561-1567
127. Cheong BY, Muthupillai R, Wilson JM, Sung A, Huber S, Amin S, Elayda MA, Lee VV, Flamm SD. Prognostic significance of delayed-enhancement magnetic resonance imaging: Survival of 857 patients with and without left ventricular dysfunction. *Circulation*. 2009;120:2069-2076
128. O'Hanlon R, Grasso A, Roughton M, Moon JC, Clark S, Wage R, Webb J, Kulkarni M, Dawson D, Sulaibeekh L, Chandrasekaran B, Bucciarelli-Ducci C, Pasquale F, Cowie MR, McKenna

WJ, Sheppard MN, Elliott PM, Pennell DJ, Prasad SK. Prognostic significance of myocardial fibrosis in hypertrophic cardiomyopathy. *J Am Coll Cardiol*.2010. 56:867-874
129. Bonow RO, Carabello BA, Chatterjee K, de Leon AC, Jr., Faxon DP, Freed MD, Gaasch WH, Lytle BW, Nishimura RA, O'Gara PT, O'Rourke RA, Otto CM, Shah PM, Shanewise JS, Smith SC, Jr., Jacobs AK, Adams CD, Anderson JL, Antman EM, Fuster V, Halperin JL, Hiratzka LF, Hunt SA, Nishimura R, Page RL, Riegel B. Acc/aha 2006 guidelines for the management of patients with valvular heart disease: A report of the american college of cardiology/american heart association task force on practice guidelines (writing committee to revise the 1998 guidelines for the management of patients with valvular heart disease) developed in collaboration with the society of cardiovascular anesthesiologists endorsed by the society for cardiovascular angiography and interventions and the society of thoracic surgeons. *J Am Coll Cardiol*. 2006;48:e1-148
130. Williams G, Kolodny GM. Suppression of myocardial 18f-fdg uptake by preparing patients with a high-fat, low-carbohydrate diet. *AJR Am J Roentgenol*. 2008;190:W151-156
131. Shankar LK, Hoffman JM, Bacharach S, Graham MM, Karp J, Lammertsma AA, Larson S, Mankoff DA, Siegel BA, Van den Abbeele A, Yap J, Sullivan D. Consensus recommendations for the use of 18f-fdg pet as an indicator of therapeutic response in patients in national cancer institute trials. *J Nucl Med*. 2006;47:1059-1066
132. Marincheva-savcheva G, Subramanian S, Qadir S, Truong Q, Vijayakumar J, Brady TJ, Hoffmann U, Tawakol A. Imaging of the aortic valve using fluorodeoxyglucose positron emission tomography increased valvular fluorodeoxyglucose uptake in aortic stenosis. *Journal of the American College of Cardiology*. 2011;57:2507-2515
133. Agatston AS, Janowitz WR, Hildner FJ, Zusmer NR, Viamonte M, Jr., Detrano R. Quantification of coronary artery calcium using ultrafast computed tomography. *J Am Coll Cardiol*. 1990;15:827-832
134. Maceira AM, Prasad SK, Khan M, Pennell DJ. Normalized left ventricular systolic and diastolic function by steady state free precession cardiovascular magnetic resonance. *J Cardiovasc Magn Reson*. 2006;8:417-426
135. Cerqueira MD, Weissman NJ, Dilsizian V, Jacobs AK, Kaul S, Laskey WK, Pennell DJ, Rumberger JA, Ryan T, Verani MS. Standardized myocardial segmentation and nomenclature for tomographic imaging of the heart: A statement for healthcare professionals from the cardiac imaging committee of the council on clinical cardiology of the american heart association. *Circulation*. 2002;105:539-542
136. Friedrich M S-MJ, Dietz R. Magnetic resonance to assess the aortic valve area in aortic stenosis. *J Am Coll Cardiol* 2004;43:2148, author reply 2148-2149
137. Weber WA, Ziegler SI, Thodtmann R, Hanauske AR, Schwaiger M. Reproducibility of metabolic measurements in malignant tumors using fdg pet. *J Nucl Med*. 1999;40:1771-1777
138. Roger VL, Go AS, Lloyd-Jones DM, Adams RJ, Berry JD, Brown TM, Carnethon MR, Dai S, de Simone G, Ford ES, Fox CS, Fullerton HJ, Gillespie C, Greenlund KJ, Hailpern SM, Heit JA, Ho PM, Howard VJ, Kissela BM, Kittner SJ, Lackland DT, Lichtman JH, Lisabeth LD, Makuc DM, Marcus GM, Marelli A, Matchar DB, McDermott MM, Meigs JB, Moy CS, Mozaffarian D, Mussolino ME, Nichol G, Paynter NP, Rosamond WD, Sorlie PD, Stafford RS, Turan TN, Turner MB, Wong ND, Wylie-Rosett J. Heart disease and stroke statistics--2011 update: A report from the american heart association. *Circulation*.2010; 123:e18-e209
139. Gaziano TA. Cardiovascular disease in the developing world and its cost-effective management. *Circulation*. 2005;112:3547-3553
140. Davies MJ. The pathophysiology of acute coronary syndromes. *Heart*. 2000;83:361-366

141. Kolodgie FD, Burke AP, Farb A, Gold HK, Yuan J, Narula J, Finn AV, Virmani R. The thin-cap fibroatheroma: A type of vulnerable plaque: The major precursor lesion to acute coronary syndromes. *Curr Opin Cardiol*. 2001;16:285-292
142. Budoff MJ, Gul KM. Expert review on coronary calcium. *Vasc Health Risk Manag*. 2008;4:315-324
143. Raggi P, Callister TQ, Shaw LJ. Progression of coronary artery calcium and risk of first myocardial infarction in patients receiving cholesterol-lowering therapy. *Arterioscler Thromb Vasc Biol*. 2004;24:1272-1277
144. McEvoy JW, Blaha MJ, Defilippis AP, Budoff MJ, Nasir K, Blumenthal RS, Jones SR. Coronary artery calcium progression: An important clinical measurement? A review of published reports. *J Am Coll Cardiol*.2010. 56:1613-1622
145. Motoyama S, Kondo T, Sarai M, Sugiura A, Harigaya H, Sato T, Inoue K, Okumura M, Ishii J, Anno H, Virmani R, Ozaki Y, Hishida H, Narula J. Multislice computed tomographic characteristics of coronary lesions in acute coronary syndromes. *J Am Coll Cardiol*. 2007;50:319-326
146. Huang H, Virmani R, Younis H, Burke AP, Kamm RD, Lee RT. The impact of calcification on the biomechanical stability of atherosclerotic plaques. *Circulation*. 2001;103:1051-1056
147. Ehara S, Kobayashi Y, Yoshiyama M, Shimada K, Shimada Y, Fukuda D, Nakamura Y, Yamashita H, Yamagishi H, Takeuchi K, Naruko T, Haze K, Becker AE, Yoshikawa J, Ueda M. Spotty calcification typifies the culprit plaque in patients with acute myocardial infarction: An intravascular ultrasound study. *Circulation*. 2004;110:3424-3429
148. Vengrenyuk Y, Carlier S, Xanthos S, Cardoso L, Ganatos P, Virmani R, Einav S, Gilchrist L, Weinbaum S. A hypothesis for vulnerable plaque rupture due to stress-induced debonding around cellular microcalcifications in thin fibrous caps. *Proc Natl Acad Sci U S A*. 2006;103:14678-14683
149. Even-Sapir E, Metser U, Mishani E, Lievshitz G, Lerman H, Leibovitch I. The detection of bone metastases in patients with high-risk prostate cancer: 99mtc-mdp planar bone scintigraphy, single- and multi-field-of-view spect, 18f-fluoride pet, and 18f-fluoride pet/ct. *J Nucl Med*. 2006;47:287-297
150. Derlin T, Toth Z, Papp L, Wisotzki C, Apostolova I, Habermann CR, Mester J, Klutmann S. Correlation of inflammation assessed by 18f-fdg pet, active mineral deposition assessed by 18f-fluoride pet, and vascular calcification in atherosclerotic plaque: A dual-tracer pet/ct study. *J Nucl Med*. 2011;52:1020-1027
151. Libby P. The molecular mechanisms of the thrombotic complications of atherosclerosis. *J Intern Med*. 2008;263:517-527
152. Kim TN, Kim S, Yang SJ, Yoo HJ, Seo JA, Kim SG, Kim NH, Baik SH, Choi DS, Choi KM. Vascular inflammation in patients with impaired glucose tolerance and type 2 diabetes: Analysis with 18f-fluorodeoxyglucose positron emission tomography. *Circ Cardiovasc Imaging*. 2010;3:142-148
153. Tahara N, Kai H, Ishibashi M, Nakaura H, Kaida H, Baba K, Hayabuchi N, Imaizumi T. Simvastatin attenuates plaque inflammation: Evaluation by fluorodeoxyglucose positron emission tomography. *J Am Coll Cardiol*. 2006;48:1825-1831
154. Folco EJ, Sheikine Y, Rocha VZ, Christen T, Shvartz E, Sukhova GK, Di Carli MF, Libby P. Hypoxia but not inflammation augments glucose uptake in human macrophages implications for imaging atherosclerosis with (18)fluorine-labeled 2-deoxy-d-glucose positron emission tomography. *J Am Coll Cardiol*. 2011;58:603-614
155. Izquierdo-Garcia D, Davies JR, Graves MJ, Rudd JH, Gillard JH, Weissberg PL, Fryer TD, Warburton EA. Comparison of methods for magnetic resonance-guided [18-f]fluorodeoxyglucose positron emission tomography in human carotid arteries:

Reproducibility, partial volume correction, and correlation between methods. *Stroke*. 2009;40:86-93
156. Dweck MR, Jones C, Joshi N, Fletcher AM, Richardson H, White A, Marsden M, Pessotto R, Clark JC, Wallace WA, Salter DM, McKillop G, van Beek EJ, Boon NA, Rudd JH, Newby DE. Assessment of valvular calcification and inflammation by positron emission tomography in patients with aortic stenosis. *Circulation*. 2011; 125: 76-86
157. Rudd JH, Myers KS, Bansilal S, Machac J, Woodward M, Fuster V, Farkouh ME, Fayad ZA. Relationships among regional arterial inflammation, calcification, risk factors, and biomarkers: A prospective fluorodeoxyglucose positron-emission tomography/computed tomography imaging study. *Circ Cardiovasc Imaging*. 2009;2:107-115
158. Taylor AJ, Cerqueira M, Hodgson JM, Mark D, Min J, O'Gara P, Rubin GD, Kramer CM, Berman D, Brown A, Chaudhry FA, Cury RC, Desai MY, Einstein AJ, Gomes AS, Harrington R, Hoffmann U, Khare R, Lesser J, McGann C, Rosenberg A, Schwartz R, Shelton M, Smetana GW, Smith SC, Jr. Accf/scct/acr/aha/ase/asnc/nasci/scai/scmr 2010 appropriate use criteria for cardiac computed tomography. A report of the american college of cardiology foundation appropriate use criteria task force, the society of cardiovascular computed tomography, the american college of radiology, the american heart association, the american society of echocardiography, the american society of nuclear cardiology, the north american society for cardiovascular imaging, the society for cardiovascular angiography and interventions, and the society for cardiovascular magnetic resonance. *J Am Coll Cardiol*. 2010;56:1864-1894
159. Virmani R, Burke AP, Farb A, Kolodgie FD. Pathology of the vulnerable plaque. *J Am Coll Cardiol*. 2006;47:C13-18
160. Burke AP, Weber DK, Kolodgie FD, Farb A, Taylor AJ, Virmani R. Pathophysiology of calcium deposition in coronary arteries. *Herz*. 2001;26:239-244
161. Stary HC, Chandler AB, Dinsmore RE, Fuster V, Glagov S, Insull W, Jr., Rosenfeld ME, Schwartz CJ, Wagner WD, Wissler RW. A definition of advanced types of atherosclerotic lesions and a histological classification of atherosclerosis. A report from the committee on vascular lesions of the council on arteriosclerosis, american heart association. *Arterioscler Thromb Vasc Biol*. 1995;15:1512-1531
162. Ueda M. [clinical relevance of coronary artery calcification, as a risk factor for plaque rupture: Viewpoint from pathology]. *Clin Calcium*. 2010. 20:1656-1662
163. de Feyter PJ, Ozaki Y, Baptista J, Escaned J, Di Mario C, de Jaegere PP, Serruys PW, Roelandt JR. Ischemia-related lesion characteristics in patients with stable or unstable angina. A study with intracoronary angioscopy and ultrasound. *Circulation*. 1995;92:1408-1413
164. Thieme T, Wernecke KD, Meyer R, Brandenstein E, Habedank D, Hinz A, Felix SB, Baumann G, Kleber FX. Angioscopic evaluation of atherosclerotic plaques: Validation by histomorphologic analysis and association with stable and unstable coronary syndromes. *J Am Coll Cardiol*. 1996;28:1-6
165. Wu X, Maehara A, Mintz GS, Kubo T, Xu K, Choi SY, He Y, Guo N, Moses JW, Leon MB, De Bruyne B, Serruys PW, Stone GW. Virtual histology intravascular ultrasound analysis of non-culprit attenuated plaques detected by grayscale intravascular ultrasound in patients with acute coronary syndromes. *Am J Cardiol*. 2010;105:48-53
166. Otto CM, Burwash IG, Legget ME, Munt BI, Fujioka M, Healy NL, Kraft CD, Miyake-Hull CY, Schwaegler RG. Prospective study of asymptomatic valvular aortic stenosis. Clinical, echocardiographic, and exercise predictors of outcome. *Circulation*. 1997;95:2262-2270
167. Krayenbuehl HP, Hess OM, Monrad ES, Schneider J, Mall G, Turina M. Left ventricular myocardial structure in aortic valve disease before, intermediate, and late after aortic valve replacement. *Circulation*. 1989;79:744-755

168. Hein S, Arnon E, Kostin S, Schonburg M, Elsasser A, Polyakova V, Bauer EP, Klovekorn WP, Schaper J. Progression from compensated hypertrophy to failure in the pressure-overloaded human heart: Structural deterioration and compensatory mechanisms. *Circulation*. 2003;107:984-991
169. Emoto R, Yokota Y, Miki T, Nomura H, Usuki S, Chou HT, Kurozumi H, Seo T, Fukuzaki H. [prognosis of hypertrophic cardiomyopathy: Echocardiographic and postmortem histopathologic study of 30 patients]. *J Cardiol*. 1988;18:695-703
170. Fujiwara H TM, Onodera T, Kawai C. Hypertrophic cardiomyopathy: Mode of death and pathological findings. *J Cardiol* 1987;16:3-8
171. Fabre A SM. Sudden adult death syndrome and other non-ischaemic causes of sudden cardiac death. *Heart*. 2006;92:316-320
172. Brandenburg RO. Cardiomyopathies and their role in sudden death. *J Am Coll Cardiol*. 1985;5:185B-189B
173. Moon JC PS. Cardiovascular magnetic resonance and the evaluation of heart failure. *Curr Cardiol Rep* 2005;7:39-44
174. Tsang TS, Barnes ME, Gersh BJ, Bailey KR, Seward JB. Left atrial volume as a morphophysiologic expression of left ventricular diastolic dysfunction and relation to cardiovascular risk burden. *Am J Cardiol*. 2002;90:1284-1289
175. Vahanian A, Otto CM. Risk stratification of patients with aortic stenosis. *Eur Heart J*. 2010;31:416-423
176. Gosse P, Clementy J. Coronary reserve in experimental myocardial hypertrophy. *Eur Heart J*. 1995;16 Suppl I:22-25
177. Artham SM, Lavie CJ, Milani RV, Patel DA, Verma A, Ventura HO. Clinical impact of left ventricular hypertrophy and implications for regression. *Prog Cardiovasc Dis*. 2009;52:153-167
178. Keating GM, Jarvis B. Carvedilol: A review of its use in chronic heart failure. *Drugs*. 2003;63:1697-1741
179. Oka T, Komuro I. Molecular mechanisms underlying the transition of cardiac hypertrophy to heart failure. *Circ J*. 2008;72 Suppl A:A13-16
180. Petretto E, Sarwar R, Grieve I, Lu H, Kumaran MK, Muckett PJ, Mangion J, Schroen B, Benson M, Punjabi PP, Prasad SK, Pennell DJ, Kiesewetter C, Tasheva ES, Corpuz LM, Webb MD, Conrad GW, Kurtz TW, Kren V, Fischer J, Hubner N, Pinto YM, Pravenec M, Aitman TJ, Cook SA. Integrated genomic approaches implicate osteoglycin (ogn) in the regulation of left ventricular mass. *Nat Genet*. 2008;40:546-552
181. Lund O, Flo C, Jensen FT, Emmertsen K, Nielsen TT, Rasmussen BS, Hansen OK, Pilegaard HK, Kristensen LH. Left ventricular systolic and diastolic function in aortic stenosis. Prognostic value after valve replacement and underlying mechanisms. *Eur Heart J*. 1997;18:1977-1987
182. Jin H, Lyon AR, Akar FG. Arrhythmia mechanisms in the failing heart. *Pacing Clin Electrophysiol*. 2008;31:1048-1056
183. Bello D, Fieno DS, Kim RJ, Pereles FS, Passman R, Song G, Kadish AH, Goldberger JJ. Infarct morphology identifies patients with substrate for sustained ventricular tachycardia. *J Am Coll Cardiol*. 2005;45:1104-1108
184. Iles L, Pfluger H, Phrommintikul A, Cherayath J, Aksit P, Gupta SN, Kaye DM, Taylor AJ. Evaluation of diffuse myocardial fibrosis in heart failure with cardiac magnetic resonance contrast-enhanced t1 mapping. *J Am Coll Cardiol*. 2008;52:1574-1580
185. Ganau A, Devereux RB, Roman MJ, de Simone G, Pickering TG, Saba PS, Vargiu P, Simongini I, Laragh JH. Patterns of left ventricular hypertrophy and geometric remodeling in essential hypertension. *J Am Coll Cardiol*. 1992;19:1550-1558

186. Cioffi G, Stefenelli C. Comparison of left ventricular geometry and left atrial size and function in patients with aortic stenosis versus those with pure aortic regurgitation. *Am J Cardiol*. 2002;90:601-606
187. Hess OM, Schneider J, Turina M, Carroll JD, Rothlin M, Krayenbuehl HP. Asymmetric septal hypertrophy in patients with aortic stenosis: An adaptive mechanism or a coexistence of hypertrophic cardiomyopathy? *J Am Coll Cardiol*. 1983;1:783-789
188. Tuseth N, Cramariuc D, Rieck AE, Wachtell K, Gerdts E. Asymmetric septal hypertrophy - a marker of hypertension in aortic stenosis (a seas substudy). *Blood Press*. 2010;19:140-144
189. Maron MS, Maron BJ, Harrigan C, Buros J, Gibson CM, Olivotto I, Biller L, Lesser JR, Udelson JE, Manning WJ, Appelbaum E. Hypertrophic cardiomyopathy phenotype revisited after 50 years with cardiovascular magnetic resonance. *J Am Coll Cardiol*. 2009;54:220-228
190. Myerson SG, Bellenger NG, Pennell DJ. Assessment of left ventricular mass by cardiovascular magnetic resonance. *Hypertension*. 2002;39:750-755
191. Hudsmith LE, Petersen SE, Francis JM, Robson MD, Neubauer S. Normal human left and right ventricular and left atrial dimensions using steady state free precession magnetic resonance imaging. *J Cardiovasc Magn Reson*. 2005;7:775-782
192. Rodriguez CJ, Diez-Roux AV, Moran A, Jin Z, Kronmal RA, Lima J, Homma S, Bluemke DA, Barr RG. Left ventricular mass and ventricular remodeling among hispanic subgroups compared with non-hispanic blacks and whites: Mesa (multi-ethnic study of atherosclerosis). *J Am Coll Cardiol*. 2010;55:234-242
193. Buchner S, Debl K, Haimerl J, Djavidani B, Poschenrieder F, Feuerbach S, Riegger GA, Luchner A. Electrocardiographic diagnosis of left ventricular hypertrophy in aortic valve disease: Evaluation of ecg criteria by cardiovascular magnetic resonance. *J Cardiovasc Magn Reson*. 2009;11:18
194. Lamb HJ, Beyerbacht HP, de Roos A, van der Laarse A, Vliegen HW, Leujes F, Bax JJ, van der Wall EE. Left ventricular remodeling early after aortic valve replacement: Differential effects on diastolic function in aortic valve stenosis and aortic regurgitation. *J Am Coll Cardiol*. 2002;40:2182-2188
195. Dweck M, Joshi S, Murigu T, Gulati A et al. Mid-wall fibrosis is an independent predictor of mortality in aortic stenosis. *J Amer Coll Cardiol*. 2011; 58: 1271-9.
196. Carroll JD, Carroll EP, Feldman T, Ward DM, Lang RM, McGaughey D, Karp RB. Sex-associated differences in left ventricular function in aortic stenosis of the elderly. *Circulation*. 1992;86:1099-1107
197. Maron BJ, McKenna WJ, Danielson GK, Kappenberger LJ, Kuhn HJ, Seidman CE, Shah PM, Spencer WH, 3rd, Spirito P, Ten Cate FJ, Wigle ED. American college of cardiology/european society of cardiology clinical expert consensus document on hypertrophic cardiomyopathy. A report of the american college of cardiology foundation task force on clinical expert consensus documents and the european society of cardiology committee for practice guidelines. *J Am Coll Cardiol*. 2003;42:1687-1713
198. Yokota Y, Teng SS, Emoto R, Miki T, Takarada A, Seo T, Sano H, Fukuzaki H. Mechanism of development of asymmetric septal hypertrophy in patients with essential systemic hypertension. *Jpn Circ J*. 1989;53:1173-1184
199. Hachicha Z, Dumesnil JG, Bogaty P, Pibarot P. Paradoxical low-flow, low-gradient severe aortic stenosis despite preserved ejection fraction is associated with higher afterload and reduced survival. *Circulation*. 2007;115:2856-2864
200. Peltier M, Trojette F, Sarano ME, Grigioni F, Slama MA, Tribouilloy CM. Relation between cardiovascular risk factors and nonrheumatic severe calcific aortic stenosis among patients with a three-cuspid aortic valve. *Am J Cardiol*. 2003;91:97-99

201. Schroeter M, Dennin MA, Walberer M, Backes H, Neumaier B, Fink GR, Graf R. Neuroinflammation extends brain tissue at risk to vital peri-infarct tissue: A double tracer [11c]pk11195- and [18f]fdg-pet study. *J Cereb Blood Flow Metab*. 2009;29:1216-1225
202. Fujita M, Imaizumi M, Zoghbi SS, Fujimura Y, Farris AG, Suhara T, Hong J, Pike VW, Innis RB. Kinetic analysis in healthy humans of a novel positron emission tomography radioligand to image the peripheral benzodiazepine receptor, a potential biomarker for inflammation. *Neuroimage*. 2008;40:43-52
203. Rominger A, Saam T, Vogl E, Ubleis C, la Fougere C, Forster S, Haug A, Cumming P, Reiser MF, Nikolaou K, Bartenstein P, Hacker M. In vivo imaging of macrophage activity in the coronary arteries using 68ga-dotatate pet/ct: Correlation with coronary calcium burden and risk factors. *J Nucl Med*.51:193-197
204. Novaro GM, Katz R, Aviles RJ, Gottdiener JS, Cushman M, Psaty BM, Otto CM, Griffin BP. Clinical factors, but not c-reactive protein, predict progression of calcific aortic-valve disease: The cardiovascular health study. *J Am Coll Cardiol*. 2007;50:1992-1998
205. Messika-Zeitoun D, Bielak LF, Peyser PA, Sheedy PF, Turner ST, Nkomo VT, Breen JF, Maalouf J, Scott C, Tajik AJ, Enriquez-Sarano M. Aortic valve calcification: Determinants and progression in the population. *Arterioscler Thromb Vasc Biol*. 2007;27:642-648
206. Nazarian S. Is ventricular arrhythmia a possible mediator of the association between aortic stenosis-related midwall fibrosis and mortality? *J Am Coll Cardiol*. 2011;58:1280-1282
207. Aikawa E, Otto CM. Look more closely at the valve: Imaging calcific aortic valve disease. *Circulation*. 2012;125:9-11
208. Aksoy Y, Yagmur C, Tekin GO, Yagmur J, Topal E, Kekilli E, Turhan H, Kosar F, Yetkin E. Aortic valve calcification: Association with bone mineral density and cardiovascular risk factors. *Coron Artery Dis*. 2005;16:379-383
209. Sattler AM, Schoppet M, Schaefer JR, Hofbauer LC. Novel aspects on rank ligand and osteoprotegerin in osteoporosis and vascular disease. *Calcif Tissue Int*. 2004;74:103-106
210. Cummings SR, San Martin J, McClung MR, Siris ES, Eastell R, Reid IR, Delmas P, Zoog HB, Austin M, Wang A, Kutilek S, Adami S, Zanchetta J, Libanati C, Siddhanti S, Christiansen C. Denosumab for prevention of fractures in postmenopausal women with osteoporosis. *N Engl J Med*. 2009;361:756-765
211. Bucay N, Sarosi I, Dunstan CR, Morony S, Tarpley J, Capparelli C, Scully S, Tan HL, Xu W, Lacey DL, Boyle WJ, Simonet WS. Osteoprotegerin-deficient mice develop early onset osteoporosis and arterial calcification. *Genes Dev*. 1998;12:1260-1268
212. Bennett BJ, Scatena M, Kirk EA, Rattazzi M, Varon RM, Averill M, Schwartz SM, Giachelli CM, Rosenfeld ME. Osteoprotegerin inactivation accelerates advanced atherosclerotic lesion progression and calcification in older apoe-/- mice. *Arterioscler Thromb Vasc Biol*. 2006;26:2117-2124
213. Goldstein RE. Bone modifiers and the quest to slow progression of aortic stenosis. *Am J Cardiol*. 2009;104:125-127
214. Flett AS, Hayward MP, Ashworth MT, Hansen MS, Taylor AM, Elliott PM, McGregor C, Moon JC. Equilibrium contrast cardiovascular magnetic resonance for the measurement of diffuse myocardial fibrosis: Preliminary validation in humans. *Circulation*. 2010;122:138-144
215. Flett AS SD, Quarta G, Huttin O, Hausenloy D, Banypersad SM, Lawrence D, Pellerin D, McGregor C, Taylor AM, Moon JC. Beyond late gadolinium enhancement: The key role of diffuse myocardial fibrosis in severe aortic stenosis- an equilibrium contrast cmr study. *Journal of Cardiovascular Magnetic Resonance*. 2011;13(Suppl 1):O39

Appendix

Awards arising from this thesis

- 2012 William W. Parmley Young Author Award, Journal of the American College of Cardiology
- 2012 Winner Young Investigator Award, American College of Cardiology, USA
- 2012 Winner Presidents Medal, Royal Society of Medicine, London
- 2012 Runner up Young Investigator Award, British Cardiac Society
- 2011 Winner Research Worker's Prize, Radiology Society North America, Chicago, USA
- 2010 Gold-medal award for best abstract at EURO-CMR conference, Florence, 2010

Research Grants related to this thesis

- 2010 British Heart Foundation Clinical PhD Training Fellowship FS/10/026. Role of inflammation and calcification in the progression of aortic stenosis: the ring of fire. £280,048. 3 years

- 2011 British Heart Foundation Supplement to Clinical PhD Training Fellowship. The Role of Fibrosis in Aortic Stenosis. £119,200. 2 years

- 2011 Chief Scientist Office Project Grant ETM/160. Novel imaging approaches to identify unstable atherosclerotic coronary plaques. £225,001. 3 years.

- 2012 British Heart Foundation Project Grant PG/12/8/29371. Role of 18F- Fluoride imaging as a novel marker of plaque instability. £251,525. 3 years.

Publications arising from this thesis

• **Dweck MR,** Boon NA, Newby DE. Calcific aortic stenosis: a disease of the valve and the myocardium. **J Am Coll Cardiol.** In press.

• **Dweck MR**, Newby DE. Osteoporosis is a major confounder in observational studies investigating bisphosphonates therapy in aortic stenosis. **J Am Coll Cardiol.** In press

• **Dweck MR**, Joshi S, Murigu T, Gulati A, Gordon R, Roussin I, Northridge DB, Jabbour A, Newby DE, Pennell DJ, Prasad SK. Left ventricular remodelling and hypertrophy in patients with aortic stenosis: insights from cardiovascular magnetic resonance. **Journal of Cardiovascular Magnetic Resonance**. In press

• **Dweck MR**, Chow MWL, Joshi N, Williams M, Jones C, Fletcher AM, Richardson H, White A, McKillop G, van Beek EJR, Boon NA, Rudd JHF, Newby DE. Coronary arterial 18F-NaF uptake: a novel marker of plaque biology. **J. Am. Coll. Cardiol**. 2012; 59: 1539-1548. [Appended]

• **Dweck MR**, Jones C, Joshi N, Fletcher AM, Richardson H, White A, Marsden M, Pessotto R, Clark JC, Wallace WA, Salter DM, McKillop G, van Beek EJR, Boon NA, Rudd JHF, Newby DE. Assessment of valvular calcification and inflammation by positron emission tomography in patients with aortic stenosis. **Circulation.** 2012;125(1):76-86. [Appended]

• **Dweck MR**, Joshi S, Murigu T, Gulati A, Alpendurado F, Jabbour A, Mohaiaddin, Pepper J, Pennell D, Newby DE, Prasad S. Mid-wall fibrosis is an independent predictor of mortality in patients with aortic stenosis. **J. Am. Coll. Cardiol.** 2011;58;1271-1279. [Appended]

Publications related to this thesis

• **Dweck MR**, Quarto C, Murigu T, Joshi S, Melina G, Angeloni E, Prasad SK, Pepper JR. Late gadolinium enhancement as a potential marker of increased peri-operative risk in aortic valve replacement. **Interactive Cardiovascular and Thoracic Surgery.** 2012 Apr 17. [Epub ahead of print]